Hyperfine fields in rare-earth compounds

Joseph Theophilus Christopher

H Y P E R F I N E F I E L D S

in

R A R E - E A R T H C O M P O U N D S

by

Joseph Theophilus Christopher, B.Sc.(McGill)

Presented in candidature for the Degree of
Doctor of Philosophy

Durham University

May, 1969.

To

My Mother, Ismay

And

My Wife, Marlene

HYPERFINE FIELDS IN RARE-EARTH COMPOUNDS

Ph.D. Thesis
by J.T. Christopher

A B S T R A C T

The hyperfine field at the cobalt nucleus in $GdCo_2$, $Gd_{1-x}Y_xCo_2$, $Gd_{1-x}Dy_xCo_2$, and $Gd(Co_{1-x}Ni_x)_2$ were studied using the technique of "Spin-Echo" N.M.R. At $4.2^{o}K$ cobalt has a negative hyperfine field of 60.8 Koe with a line width of 1.94 Koe. This field is composed of contributions from two main sources;

a) from conduction electron (C.E.) polarization and core polarization of the cobalt electron configuration by the cobalt sublattice;

b) from C.E. polarization of the cobalt electron configuration by the gadolinium sublattice.

The spin of the gadolinium sublattice is decreased in the yttrium substituted series. This

is accompanied by a slight decrease in the hyperfine field and a simultaneous increase in the line width of the resonance. An analysis of the variation in H_{Co}, taking into account the induced change in cobalt sublattice magnetization, indicates that the contribution from the gadolinium sublattice is approximately 10 Koe per unpaired 4f electron. In addition, line width measurements show that the R.E. - T.M. interaction is long range in character.

Magnetization measurements on the nickel substituted series show that the T.M. moment remains constant initially; indicating that the cobalt-nickel sublattice has an itinerant electron configuration. The variation in H_{Co} along this series is ascribed to a decrease in C.E. concentration with nickel substitution. A T.M. - T.M. interaction of short range is indicated by the line width variation.

C O N T E N T S

		Page No.
CHAPTER I	INTRODUCTION	1
1.1	The Rare Earths	1
1.2	Rare Earth Transition Metal Compounds	6
1.3	Hyperfine Interactions	8
1.3.1	Specific Heat	12
1.3.2	The Mossbauer Effect	14
1.3.3	Angular Correlation of γ-rays	19
1.3.4	Resonance Methods	21
1.4	The Present Research	27
CHAPTER II	TECHNIQUES OF MEASUREMENT	28
2.1.1	Early Techniques of Nuclear Magnetic Resonance	28
2.1.2	Continuous Wave Spectrometer	29
2.1.3	Pulsed Spectrometers	30
2.1.4	Spin Echo	32
2.1.5	Nuclear Resonance in Ferromagnetic Materials	33
2.2	N.M.R. Techniques in $GdCo_2$	36
2.2.1	The Marginal Oscillator	36

Page No.

2.2.2 The Super-regenerative Detector 41
2.2.3 The Spin Echo Apparatus 44
2.3 Other Measurements in $GdCo_2$ 56
2.3.1 Crystal Structures 56
2.3.2 Bulk Magnetization 57

CHAPTER III RESULTS 58

3.1 Spin Echo Observations 58
3.1.1 $GdCo_2$ 64
3.1.2 $Gd_{1-x}Y_xCo_2$ 67
3.1.3 $Gd_{1-x}Dy_xCo_2$ 69
3.1.4 $Gd(Co_{1-x}Ni_x)_2$ 70
3.2 Line Widths 71
3.3 Relaxation Measurements 71
3.4 Magnetization Measurements 73
3.5 Lattice Parameters 74

CHAPTER IV DISCUSSION 76

4.1 The Nature of the Resonance Observations 76
4.2 $Gd_{1-x}Y_xCo_2$ Compounds 77
4.3 The $Gd(Co_{1-x}Ni_x)_2$ Series 92
4.4 The Dysprosium Substituted Compounds 96
4.5 Relaxation Rates 98

Page No.

CHAPTER V CONCLUSION 101

APPENDIX 106

A.1. The Electron-Nuclear Interaction 106

A.2. The Spin Echo Effect 111

oOo

LIST OF FIGURES AND TABLES

			Succeeding Page No.
Figure	1.1	$MgCu_2$ Structure	7
"	2.1	Marginal Oscillator Spectrometer	37
"	2.2	Resonance in the Super-regenerative Detector	44
"	2.3	The Spin Echo Spectrometer	45
"	2.4	Logic Modules	47
"	2.5	Logic Module Interconnections	47
"	2.6	The Output Amplifier	49
"	2.7	Pulse Generator Power Supplies	52
"	2.8	The R.F. Transmitter	53
"	2.9	Picture of Spectrometer	56
Table	3.1	$GdCo_2$ Spin Echo Results	61
Figure	3.1	$GdCo_2$ Resonance Line	62
"	3.2	$GdCo_2$ in External Fields	66
"	3.3	$Gd_{.81}Y_{.19}Co_2$	68
"	3.4	$Gd_{.51}Y_{.49}Co_2$	68
"	3.5	$Gd_{.4}Y_{.6}Co_2$	68
"	3.6	Variation in Resonant Frequency with Yttrium Substitution	68
"	3.7	Dysprosium Substitution Resonant Lines	70
"	3.8	$Gd(Co_{.9}Ni_{.1})_2$	71
"	3.9	$Gd(Co_{.8}Ni_{.2})_2$	71
"	3.10	Variation of Resonant Frequency with Nickel Substitution	71

LIST OF FIGURES AND TABLES Cont'd

Succeeding Page No.

Figure 3.11 Line Width Variation 72

" 3.12 Longtitudinal Relaxation in $GdCo_2$ 73

Table 3.2 Relaxation Times 73

Figure 3.13 Variation of Magnetization with Temperature $Gd(Co_{.7}Ni_{.3})_2$ H ext = 1.34 Koe 74

" 3.14 Variation of T_C with Nickel Content 74

" 3.15 Variation of Magnetic Moment with Nickel Content 74

" 3.16 Variation of Lattice-Parameter with Nickel Content 75

" 3.17 Variation of Lattice Parameter with Yttrium Content 75

" 4.1 Curie Temperatures of Rare Earth Transition Metal Compounds 87

" 4.2 Variation of Iron Moment with Curie Point in RFe_2 Compounds 87

Table 4.1 Contributions to $H_{Co.\mu}$ at various Yttrium Concentrations 90

Figure 4.3 Contribution to $H_{Co.\mu}$ from C.E. Polarization by R.F. Sublattice 90

Table 4.2 Line Widths of Yttrium Substituted Compounds 91

" 4.3 Line Widths of Nickel Substituted Compounds 91

oOo

CHAPTER I

I N T R O D U C T I O N

1.1 The Rare earths are the series of elements lying between Lanthanum and Lutetium in the periodic table and having atomic numbers from 57 to 71. Except for the elements at the ends of the series, they are characterized by an incomplete shell of 4 f electrons varying from 1 to 13. This shell is deeply embedded inside surrounding shells of electrons; the electron structure for the series being written as $4f^n5s^25p^65d^16s^2$ (ignoring shells internal to the 4f).

The chemical similarity introduced by their identical outer electron configurations prevented, until recently, the separation of the rare earths to a high degree of purity. It is only within the last decade that reasonably pure metals have been produced, and in that time investigations into this series of elements have multiplied tremendously.

Early investigations into their crystal structure

have been summarized in a review by Gschneider (1961), (ref. 1:1). All the metals of the series crystallize in modified hexagonal close packed (h.c.p.) structures, although these structures are not all the same. The heavy Rare earths from Gd-Lu have the magnesium (A3) type structure with packing sequence along the hexagonal axis ABAB, repeating after two layers. Those elements below gadolinium have a variety of packing sequences; some with ABACABAC sequences repeating after the fourth layer along the hexagonal axis and others with sequence ABCABC along the (III) direction.

The magnetic properties of the metals can be explained by assuming that they are tripositive ions surrounded by conduction electrons from the outer 5d and 6s shells. The 4f electrons are shielded by the 5s and 5p shells and act to a first approximation as free electrons. Thus the magnetic moment of the ions can be derived from Russel-Saunders coupling between the Spin and Orbital angular moments of the $4f^n$ electrons (R.J. Elliot, 1965), (ref. 1:2). The exceptions to this are europium and ytterbium which gain

an electron in the 4 f shell to complete a half shell and full shell respectively. Samarium and europium also show anomalous magnetic behaviour due to the fact that the energy difference between ground and first excited state in these two elements is very small and leads to admixture between the different states.

The magnetic structure of this series of elements is very complex. All of them show some form of magnetic ordering when the temperature is lowered, but only gadolinium is ordered at room temperature. Neutron diffraction studies have indicated that the others change their structure as the temperature is lowered. Between 228°K and 220°K, terbium changes from a helical spin structure to a ferromagnetic structure where the helical moments lie in the xy plane such that

$$\mu_n(x) = \lambda\beta JM \cos(q.R_n)$$
$$\mu_n(y) = \lambda\beta JM \sin(q.R_n)$$

where R_n is the lattice position of the plane under

consideration and q is the wave number of the helical spin structure. Other spin structures have also been reported in the literature and are summarized in the review article by Elliot, (1965).

The large unquenched orbital angular moments of the rare earth metals produce a very strong hyperfine field at the nucleus. In the transition metal elements the dominant contribution to the hyperfine field comes from the contact interaction with S electrons in the conduction band polarized by the 3d shells, (see appendix I). The orbital contribution is negligible as the 3d orbital moment is quenched by the effect of the crystalline field.

The 4f electrons however are well shielded from crystal field effects hence their orbital moment is largely unquenched. Several workers have measured the hyperfine constants of these metals (refs. 1:3 - 1:8). With the exception of Gd^{3+} and Eu^{2+} which are "S" state ions and therefore have zero angular moments, all the hyperfine fields are in excess of 1 M.oe. In fact, the large orbital field dominates all other con-

tributions and makes the hyperfine interactions at the nuclei of rare earths metals relatively insensitive to their environment.

However, Gegenwarth and co-workers (1967), (ref. 1:9) have illustrated how this comparative lack of sensitivity may be put to good use in estimating the various contributions to the hyperfine field in these metals and their compounds. By correlating the fields reported for various rare earth nuclei in the metals and in their compounds with iron, they discovered that there was a constant difference of about 800 k.oe. between the fields at the nucleus of a given element in a metallic environment and in the compound with iron.

Assuming the ionic moment remains unchanged in the two environments, then the orbital and core polarization hyperfine field contributions also remain unchanged. Hence, the field change must be due to the polarization of the outer 5d and 6s conduction electrons (common to all of the elements) by the neighbouring iron atoms.

Rare Earth Transition Metal Compounds:

1.2 Rare earth transition metal compounds have been studied for their bulk magnetic properties as well as for their hyperfine interactions. Several stoichiometries have been isolated such as A_2B_{17}, AB_5, A_2B_7, AB_3, AB_2, AB_1, and A_3B (A = rare earth, B = Fe, Co, Ni). In particular the structure and saturation moment of AB_2 compounds have been studied by several authors.

The AB_2 compounds crystallize in a cubic Laves phase $MgCu_2$ type structure (fig. 1:1), in which the A atoms lie on a simple cubic lattice while the B atoms lie on an interpenetrating tetrahedral network. These tetrahedra have a B atom at each apex by which they are joined to the neighbouring tetrahedra. (Gschneider in "Rare Earth Alloys") (1961).

The reported lattice constants for these compounds vary between 7.1°A and 7.4°A generally increasing as the atomic radius of the rare earth constituent increases (i.e. from T_m to Gd for the heavy rare earths). It must be noted, however, that the spread in reported

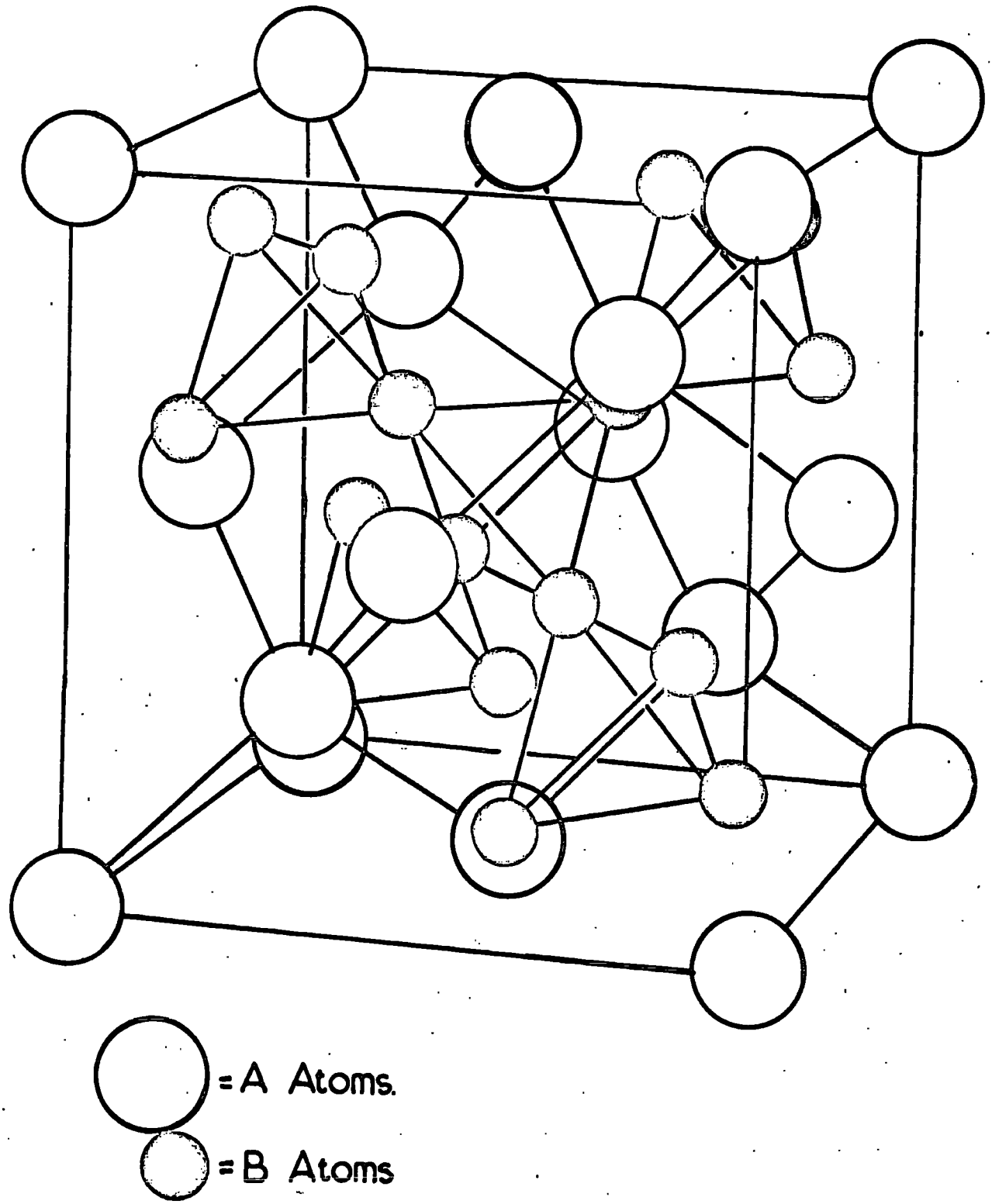

Figure 1:1 $\underline{MgCu_2}$ Structure.

values for a particular compound is very large in most cases. This is probably due to impurities present in the rare earths used for the earlier measurements and to inhomogenuous specimens.

Moon, Koehler and Farrell (ref. 1:10) have reported on the magnetic structure of some of the AB_2 compounds as determined by neutron diffraction analysis. They find that the rare earth and cobalt sublattices are aligned ferromagnetically within each sublattice but their spins are antiparallel between the sublattices. In addition the moment of the transition metal ion is less than the free ion value. Saturation moment measurements on these compounds have been explained on this basis.

As the strength of hyperfine interactions depends on the value of the local ionic moment and spin polarization at a particular atom, it is instructive to measure the interaction in the AB_2 series. The results of Wernick and Wertheim (ref. 1:11) (1962) on the hyperfine field (Hi) at the Fe nucleus in R Fe_2 compounds suggests that the moment on the iron ion remains

constant throughout the series. On the other hand, several reports (refs. 1:12 - 1:14) have stated that saturation moment measurements indicate that the rare earth ion moments in the compounds are lower than in the free tripositive ions and those on iron are variable. The determination of sublattice magnetization at varying temperatures by means of hyperfine interactions may help to clear up this problem and to assign component moments unambiguously. Bowden et al. (ref. 1:15) studied the temperature variation of the hyperfine fields at ^{57}Fe and ^{161}Dy in $DyFe_2$ using Mossbauer effect measurements. He then derived the variation in sublattice magnetization at both sites assuming that the dysprosium ion sat in an effective field generated by the iron sublattice.

Hyperfine Interactions:

1.3 Hyperfine interactions are defined as those interactions which take place between the atomic electrons and the nuclear charge and moment distributions. By their nature measurements of hyperfine interactions

are ideal for the determination of electron charge and spin distributions, magnetization and nuclear magnetic moments. They can be broadly divided into two classes: the magnetic interaction with the magnetic moment of the nucleus, and the electrostatic interaction with the electric quadropole moment of the nucleus. Appendix I gives a derivation of the magnetic hyperfine term for a single electron. Multi-electron effects are then determined by a summation of the effects from the individual electrons.

Referring to Appendix I (Equation (6), we see that the hyperfine interaction can be split into three main contributions. The last term in the equation $(\frac{8}{3}\pi\mu.S\delta(r))$ is the delta function or contact term first described by Fermi (ref. 1:16), and is non-zero for S-electrons only. The magnitude of this effect is proportional to the value of $S|\psi_s(0)|^2$ where $|\psi_s(0)|^2$ is the S-electron density at the nucleus. $|\psi_s(0)|^2$ again has three components:-

1) the density of conduction electron spin at the nucleus polarized either by an external

field or by exchange with the incomplete magnetic shell;

2) the density of core S-electrons polarized by exchange with the incomplete magnetic shell;

3) the density at the nucleus of the S-character of the incomplete shell due to admixture with the conduction electrons.

The first term in equation (A.6), $\left(\frac{2\beta\mu.L}{r^3}\right)$, is the orbital term which is zero for S-electrons. For incomplete shells which are not affected by crystal field quenching this term is large and usually dominates all other terms. For core electrons and conduction electrons there are no orbital contributions to the hyperfine field.

The second term $\left(\frac{-2\beta.\left[3(\mu.r)\ x\ (s.r) - (\mu.s)r^2\right]}{r^5}\right)$ is the spin dipolar term and is in most cases very small. According to Lounasmaa (ref. 1:17), it is about one tenth of the orbital contribution in rare earth metals.

Marshall (ref. 1:18) assigned the origin of the

field at a nucleus in a ferromagnetic material to the hyperfine interaction supplemented by the effect of an externally applied field. Measurement of the hyperfine field of a given nucleus in various environments can then give an estimate of the different contributions to the hyperfine field.

This procedure is illustrated in the similar variation of Hi in Dysprosium and Gadolinium compounds. Although the orbital moment, and hence the effective field, is vastly different in these two series the absolute value of ΔH in the two series follows almost identical curves when plotted against Re-RE separation. ΔH is the change in R.E. field in going from the salt to an Intermetallic compound. (ref. 1:9). This led to the suggestion that it was only the valence electrons which were effected by the environment as these are the same in both elements. The same authors reported a constant hyperfine field change of plus 800 koe. in going from R.E. ions to R.E. Fe_2 compounds. All of this suggests a constant core polarization field for each species being altered by the polarization of 5d

and 6s valence electrons by the neighbouring ions.

These hyperfine effects can be measured by several techniques which are discussed briefly below. They are (in order of accuracy of measurement); specific heat measurements, Mossbauer effect measurements, measurements on the angular correlation of γ rays, and resonance methods (which include nuclear magnetic resonance, electron paramagnetic resonance, molecular and atomic beam resonance).

Specific Heat:

1.3.1 Consider a nucleus with nuclear spin I and nuclear moment μ_1. If there is zero field acting on the nucleus, the 2I+1 nuclear energy levels are degenerate. However, in the presence of an applied field, the degeneracy is removed and the levels are separated by an amount depending on the strength of this field. The distribution of spin orientations amongst these energy levels is given by the Boltzmann distribution law. From a knowledge of the level separation, the mean energy at a given temperature and hence the specific heat of the nuclei considered as a

closed system can be determined.

At high temperatures other contributions to the specific heat predominate. These are:-

1) the lattice specific heat C_l which follows a T^3 law below about 4^oK but cannot be predicted at higher temperatures;

2) the electronic specific heat C_e which follows a linear T law over all temperature ranges below about 1000^oK;

3) the magnetic specific heat C_m which follows a $T^{3/2}$ law in a ferromagnet and a T^3 law in an anti-ferromagnet and is due to the exchange interactions between neighbouring spins.

In order to separate (the nuclear specific heat) C_n out from the remaining three components, the sample must be cooled down to temperatures below 1^oK. C_n can then be evaluated by extrapolating the high temperature specific heat contributions to lower temperatures and subtracting them from the total specific heat. (Lounasmaa, 1967. ref. 1:17).

This method of investigating hyperfine interactions has the advantage that it can be used on any nucleus which has a hyperfine interaction, and does not depend on the availability of radioactive nuclei as in Mossbauer effect and γray correlations. Also, the effect is instantly measurable in the sense that one does not have to search for the effect as in the resonance methods.

A great disadvantage is that the presence of even less than 0.1% impurity atoms can lead to an appreciable error in the estimation of C_n. Another disadvantage is that separation of the other components of specific heat can be analytically difficult in some cases. The requirement for very low temperatures introduces a third difficulty into this technique, although not a fundamental one.

The Mossbauer Effect:

1.3.2 The Mossbauer effect was first reported in 1958 by R.L. Mossbauer (ref. 1:19). Since then it has been applied to many branches of science including solid state physics. (see ref. 1:20 for its use in

detecting the gravitational red shift).

Consider a nucleus which decays to its ground state by the emission of a photon of energy E_γ. According to momentum conservation concepts this nucleus must then recoil with a momentum equal to the photon momentum E_γ/c. Thus the kinetic energy of the emitted photon is shared with the nucleus. Similarly the absorbing nuclei must gain a momentum equal to the photon momentum and it too gains kinetic energy.

These two processes displace the emission and absorption transitiom probabilities in opposite directions on an energy scale. Appreciable resonant absorption of γ-rays can only occur when the recoil energy is small in comparison to the natural line widths of the transition.

In cases where the nucleus recoils as a free nucleus, this condition is rarely met. However, for nuclei in a crystal, the nucleus may not be free to move. The entire crystal may recoil as a unit and although the recoil momentum is the same, the recoil energy, proportional to 1/m, is negligible. For a

solid to show this effect the individual atoms should remain bound to a fixed lattice site for a time long compared to the lifetime of the excited state. (ref. 1:21). Hence, the emission and absorption lines overlap and resonance absorption occurs. This is not strictly true as a certain fraction of the incident γ-rays excite phonons or lattice vibrations. The amount of recoil-less absorptions depends on ambient temperature, Debye temperature and recoil energy.

In Mossbauer studies, the frequency of the photon in the reference frame of either the emitting or absorbing nucleus is Doppler shifted by vibrating the source or sample holder. The resonance line shape is determined by measuring the change in the number of γ-rays transmitted through the absorber as a function of the doppler velocity (and hence the frequency shift).

If the emitter line shape has a simple structure whereas the absorber has several non-degenerate energy levels as a result of magnetic dipole or electric quadropole hyperfine interactions then the separation

between the energy levels can be determined from the velocity settings at which resonance absorption occurs. In this way the complete hyperfine spectrum of the nucleus is measured simultaneiously during the course of the experiment.

In addition to measuring the hyperfine eplitting of energy levels, the Mossbauer effect has a unique ability for measuring the property known as the isomer shift. This shift is due to the change in effective charge radius in going from excited to ground state energy levels and to a difference in the S-electron density at the nucleus in going from the emitter to the absorber. The total effect is to displace the middle of the spectrum by an amount δ from the position of zero doppler frequency shift. δ is defined by the equation:-

$$\delta = \frac{2}{3}\pi Ze^2\left[\langle r_n^2\rangle \text{ex.} - \langle r_n^2\rangle g_r\right]\left[|\psi_a(0)|^2 - |\psi_s(0)|^2\right]$$

where $\langle r_n^2\rangle$ex. and $\langle r_n^2\rangle g_r$ are the excited and ground state mean square nuclear charge radii and $|\psi_a(0)|^2$ and $|\psi_s(0)|^2$ are the total S-electron densities at

the nucleus of the absorber and source (Mossbauer and Clauser, 1967)(ref. 1:22).

The Mossbauer effect shares with specific heat measurements the ability to measure hyperfine transitions without searching for them. It also has the advantage that in many cases measurements can be made up to room temperature and in others only easily achieved cryogenic temperatures are required. It is also a simple matter to make variable temperature measurements of the hyperfine interaction and from this to deduce the temperature variation of magnetisation (Nagle etal, 1960)(ref. 1:23). However, the resolving power of the effect is limited by the lifetime of the excited state to a value much lower than that obtainable in resonance methods.

This has both advantages and disadvantages. The precision of M.E. experiments is lower than N.M.R. but inhomogenously broadened lines can easily be observed by M.E. whereas this is practically impossible in C.W. N.M.R. This is a situation often encountered in alloys.

Angular Correlation of γ-rays:

1.3.3 The technique of angular correlation of γ-rays has been used for some time by nuclear physicists to study nuclear parameters such as spin and magnetic moments. It is only recently that this technique has been used to study hyperfine interactions in nuclei. (ref. 1:24).

In general, the γ-radiation emitted by an ensemble of radioactive nuclei is isotropic. However, if this ensemble has its nuclear spins aligned by some means then the γ-radiation emitted will have an anisotropy depending on the parity of the radiation field (dipolar or quadropolar).

In the method of γ-γ correlation, a nucleus is chosen which emits two γ-rays in cascade. Spin alignment is then determined by counting only those nuclei which emit the first γ-ray in a given direction. The anisotropy of the second transition is then determined by counting those radiations emitted in coincidence with the first counter as a function of the angle between the two counters. If the magnetic moments of

the intermediate state interacts with a hyperfine field, then the nuclei will precess about the field direction and result in a rotation of the radiation patterns. A determination of the degree of rotation, $\Delta\theta = w_L \tau$ where τ is the lifetime of the intermediate state and w_L = Larmour frequency, then gives an estimate of the strength of the hyperfine interaction, $(g\mu_n H_e)$.

Another method of producing the initial nuclear alignment is that employed in the technique of angular correlation following coulomb excitation implantation. In this method the nuclei under study are propelled into a host material by high energy projectiles (oxygen nuclei O_{16} are generally used). The nuclei under investigation are placed as a thin foil on the surface of a quantity of the host material. The angular distribution of subsequent γ-rays is measured in coincidence with back-scattered oxygen nuclei. The strength of the hyperfine interaction is again determined from the change in the angular distribution pattern.

The accuracy of this method of detecting hyperfine interactions is limited, in the same way as the Mossbauer effect, by the lifetime and hence line width of the intermediate state. Mossbauer nuclei however, must be of low energy which is not the case in angular correlation. Hence a greater variety of nuclei may be studied. In other respects the two methods are very similar.

Resonance Methods:

1.3.4 Resonance methods of detecting hyperfine interactions are the oldest methods in use today. The first experiment of this type was performed by Rabi et al. (ref. 1:25) in 1939 on atomic beams in which the space quantization of the beam by an inhomogeneous magnetic field is destroyed by feeding in radiofrequency energy.

In the following decade the method of nuclear resonance in bulk material was introduced as is discussed in section 2.1 where an extensive examination of the techniques of N.M.R. is given. Consider

a nucleus with spin I and magnetic moment μ. The application of a magnetic field to a group of such nuclei results in the splitting of its energy level into 2I + 1 energy levels with energy

$$E_m = M\mu.H_n/I$$

where $-I \leq M \leq I$ and M are the 2I + 1 quantized eigenvalues of I with respect to a Z direction defined by H_n.

Transitions take place between eigenstates with energy differences $E = \mu H_n/I$. These transitions are induced by the application of a radiofrequency field of frequency ν such that the quantum energy $h\nu$ is equal to the energy separation ΔE between adjacent eigenstates. The absorption of energy by the nuclei is detected by its effect on the circuit producing the r-f energy in conventional N.M.R. spectrometry or by detecting the subsequent nuclear precession in pulse methods.

The resonance technique is the most precise

method of detecting hyperfine interaction. Its precision when used with externally applied magnetic fields is limited only by accurate knowledge of the field strength and the homogeneity of the field over the sample volume.

The high precision of this method is counteracted by its disadvantages; one of these is that resonsnces are not immediately observable, but must be searched for. This can be time consuming but its effect may be reduced by using N.M.R. in conjunction with other methods such as Specific heat or Mossbauer effect measurements. The approximate value of the hyperfine constant is determined by the less accurate measurement and then precisely defined by searching for the resonance in the frequency range indicated.

The tendency of conducting solids to exclude radiofrequency energy from the interior of the solid also presents a problem for the detection of N.M.R. in solids. This is partly overcome by using metal powders usually dispersed in a non-conducting medium such as paraffin. None of the other methods suffer

from this defect.

Resonance detection of hyperfine interactions is also affected by interactions between the various spin states of the nuclei under investigation and by interactions between the ensemble of nuclear spins and the crystal lattice. F. Bloch (ref. 1:26) derived the original phenomenological equations describing these interactions. His results indicated that during resonance, the nuclear magnetism should be exponentially damped and he defined a longitudinal or spin-lattice relaxation time (T_1) which represented the damping of the Z component of nuclear magnetism and a transverse or spin-spin relaxation time (T_2) which represented the damping of nuclear magnetism normal to the Z direction. The Z direction above is defined by the direction of the externally applied field.

Subsequent authors (Abragam, 1961)(ref. 1:27) have described several ways in which spin-lattice relaxation may take place. In metals the dominant mechanism is the coupling of the nuclear spin to the

conduction electron spins by means of the contact hyperfine term (Appendix I). This coupling can induce a simultaneous flip of the electron and nuclear spins in opposite directions, the energy given off in the transition being used to increase the electronic kinetic energy. The process continues until it produces an equilibrium distribution between nuclear spins and conduction electron spins determined by the lattice temperature T_L.

Spin-spin relaxation is caused by a dipolar coupling between the spins of various nuclei which results in an exchange of energy between them. This exchange produces an equilibrium distribution of nuclear spins characterized by a spin temperature T_s which is not necessarily equal to T_L above. (Abragam, 1961). In fact, if the difference between T_1 and T_2 is sufficiently large the spin states during relaxation may sometimes be characterized by a spin temperature T_s^1 which gradually "cools" to the lattice temperature T_L.

A small value of T_1 facilitates the observations of nuclear magnetic resonance, especially when using

continuous wave excitation. If a given nucleus did not re-emit the energy it absorbed when it was excited to a higher energy level, then the populations of the energy levels would soon be equalized and no further absorption could take place (saturation). Consequently, rapid re-emission, i.e. shorter T_1, allows the use of a greater excitation power and results in greater ease of detection.

The spin-spin relaxation processes in ferromagnetic metals are strongly influenced by the hyperfine interactions and there is no direct relationship between the width of the resonance line and the relaxation time. However, in ordinary nuclear magnetic resonance a large value of relaxation time generally indicates a narrow, highly peaked resonance line. In such a case T_2 is related to the spread ΔH in the resonance field seen by the nucleus and is of order, $1/\gamma\Delta H$, where ΔH is the field variation due to spin-spin interactions between nuclei and not to a non-uniform external field.

The Present Research:

1.4 In the work reported below an attempt was made to measure the hyperfine field at both the gadolinium (Gd) and cobalt (Co) nuclear sites in $GdCo_2$ and related pseudobinary compounds formed by the continuous substitution of yttrium for gadolinium or of nickel for cobalt. Resonance measurements were also made on compounds formed by the substitution of dysprosium for gadolinium.

Bulk magnetization measurements were made on the nickel substituted compounds as no previous measurements have been made on this series. The saturation moment per formula unit and the Curie temperature was determined for each sample in the series.

The measured hyperfine field was compared with fields reported in similar compounds in order to obtain an estimate of the different contributions to the hyperfine field.

oOo

CHAPTER II

TECHNIQUES OF MEASUREMENT

Early Techniques Of Nuclear Magnetic Resonance:

2.1.1 Nuclear magnetic resonance measures the properties of the nucleus of a given species directly, and can distinguish between nuclei at different magnetic sites in the crystal. This technique was first reported in 1946 by two independent groups, that of Purcell, Torrey and Pound (ref. 2:1) and that of Bloch, Hansen and Packard (ref. 2:2). Purcell et al. measured the unbalance produced in one arm of a balanced r.f. bridge when there was a resonant absorption of energy in that arm. Bloch et al. observed the voltage induced in a receiving coil which was orthogonal to both the applied field and the transmitting coil. Both of these experiments were used to determine the magnetic moment of the proton nucleus from a knowledge of the applied field and the measured resonant frequency.

These initial experimenters were followed by others who used modified versions of the original methods. These modifications usually involved the addition of more sophisticated electronics to the detection part of the apparatus in order to improve the signal to noise ratio for samples with weak signals.

Continuous Wave Spectrometer:

2.1.2 The above methods were useful in experiments conducted at a fixed frequency but were found to be cumbersome to adjust if the frequency were changed. Therefore a new arrangement was required if the frequency was to be varied continuously. This problem was solved by the introduction of the marginal oscillator. In this circuit the sample is placed in a coil which forms part of the resonant circuit of an oscillator. The frequency is swept by slowly varying a capacitor. When resonant absorption occurs the energy loss in the coil increases and hence causes a decrease in the level of oscillation of the oscillator. This circuit can also be used in conjunction with a "lock-

in" amplifier set at the modulation frequency. A wide frequency range can thus be covered merely by changing the coils of oscillator. Two early spectrometers of this type are those of Pound and Knight (ref. 2:3) and Proctor (ref. 2:4).

Pulsed Spectrometers:

2.1.3 The three methods mentioned above all act by continuous excitation of the sample under study. There are, however, two techniques which make use of discontinuous excitation of the nuclei. These are the super-regenerative detection of N.M.R. and "Spin-Echo".

In a super-regenerative detector only one coil is used and the oscillator is used as both transmitter and detector. The oscillator valve is turned "on" and "off" alternately by the application of a sinusoidal quench voltage to its control grid. During the "on" period, the oscillation amplitude builds up in two ways:-

a) from thermal noise present at the frequency of the tuned circuit;

b) from any signal induced by precessing nuclear moments present as a result of the previous excitation period.

Since the signal in b), if present, is likely to be larger than that in a), the oscillations start to build up from a higher level and the integrated intensity of the "on" pulse will be greater. This change is detected as the oscillator frequency passes through resonance.

It is obvious from the above that the inverse of the quench frequency must be shorter than the transverse relaxation time (T_2) so that the precessing nuclear moments have not decayed to zero amplitude during the "off" interval. A circuit for the above method of detection was first reported by Roberts (ref. 2:5) and modified versions have been used since then. Recent report has been made of its use by Narath, O'Sullivan, Robinson, and Simmons (ref. 2:6) who used it for the detection of the nuclear quadropole resonance of Cl^{35} in $CuCl_2.2H_2O$ at $76^{o}K$.

Spin Echo:

2.1.4 The phenomenon of "Spin-Echoes" was first reported by Hahn in 1950 (ref. 2:7). It was discovered during a study of the related phenomenon of free induction decay (F.I.D.). In F.I.D. the decay of precessing nuclear moments is observed immediately after the application of a short intense pulse of radio-frequency energy. In the echo effect two pulses of r.f. separated by a time interval τ are applied to the sample under study. At a time 2τ after the application of the first pulse a third pulse is observed in the receiver coil. The F.I.D. of the previous two pulses is caused by spin-spin interactions and by decoherence between nuclei precessing at slightly different resonant frequencies (i.e. in slightly different effective fields). The third pulse results from a recoherence of these spins due to the application of the second pulse (Appendix II). This pulse, the "echo" pulse, has an amplitude depending on the ratio of τ to T_2 and T_1, the transverse and longitudinal relaxation times.

Since the original experiment several reports have been made of equipment designed to observe the effect and the technique has been used both in nuclear and electron resonance detection. A comprehensive spectrometer has been reported by W.G. Clark (1964) while other spectrometers have been reported by W.B. Mims (1965), Streever and Uriano (1965) and J. Schwarz (1957). The theory of the effect has been derived by E.L. Hahn (1950), Das and Saha (1954), Jaynes and Bloom (1955) and by A. Abragam (1961).

Of the references mentioned, Jaynes and Bloom give an elegant matrix treatment of the "Spin-Echo" effect. Das and Saha, and Abragam have derived these equations in the presence of diffusion effects and have shown that the two pulse "echo" has a non-exponential decay with diffusion damping term of form $(\exp.(-1/3kt^3))$; k being a function of field gradient and diffusion coefficient. (Appendix II).

Nuclear Resonance In Ferromagnetic Materials:

2.1.5 All of these methods observe the resonance in an externally applied field. However, in 1959,

Portis and Gossard (ref. 2:15) observed resonant absorption of r.f. energy in ferromagnetic cobalt in zero applied field. In the original experiment, a marginal oscillator was used as the spectrometer. Since that time, ferromagnetics have been examined using most of the methods described above excepting the bridge technique which is unsuitable for use at variable frequencies. The remaining three methods (Marginal oscillator, Super-regenerative and Spin-Echo) can all be used for variable frequency measurements but they vary in both complexity and sensitivity.

The marginal oscillator is simplest to use as there is only one parameter to vary in addition to the frequency of oscillation. This variable is the modulation frequency. The modulation depth is not critical as long as it is small. This method is of little use for detecting a resonance line whose width is more than a few percent of the central resonance frequency, as it would be difficult to separate the resonant peak from variations in the base line

due to the changing frequency.

The super-regenerative detector is more complex as it requires a variation in quench frequency in addition to variations in modulation frequency and modulation depth. This complexity is compensated by the improved ability to measure wider lines (Narath et al. 1964) by using more incoherent frequency pulses (i.e. pulses containing a greater range of frequencies). This detector can also measure weaker resonances than the marginal oscillator since a higher radiofrequency (r.f.) amplitude can be used.

Spin-Echo detection is complicated by the necessity to vary pulse width, pulse separation and radio-frequency intensity as well as frequency. However, as it can measure a line shape point by point (ref. 2:16), it is the most accurate for determining the distribution of the effective field and is least affected by spurious effects, such as oscillator noise and microphonics. The absence of oscillator noise when the echo pulse is being received helps to increase the sensitivity of this technique; further

improvement in sensitivity results from the use of a high r.f. amplitude.

N.M.R. Techniques In $GdCo_2$:

2.2 As mentioned in section 1:4, these measurements were performed in an attempt to measure the hyperfine constants of the various nuclei present in $GdCo_2$ and related intermetallic compounds. From a knowledge of the magnetic moment and nuclear spin of the resonant nucleus, the internal field at that nucleus, can then be determined.

During the course of the work reported here, all of the nuclear magnetic resonance (n.m.r.) methods mentioned in section 2:1 subsections 2,3, and 4 of this chapter were used.

The Marginal Oscillator:

2.2.1 Initial attempts were made to observe the $GdCo_2$ resonance using a marginal oscillator which was a modified version of one reported by R.C. LaForce in 1961 (ref. 2:17). For a block diagram and circuits see figure 2:1. The oscillator used was a Hartley

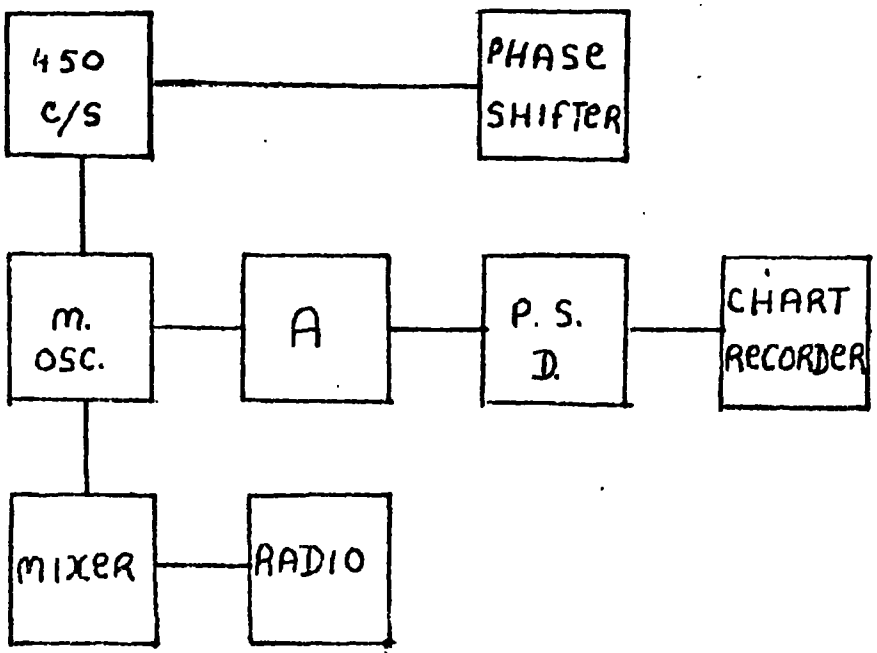

Block Diagram of Spectrometer

Marginal Oscillator

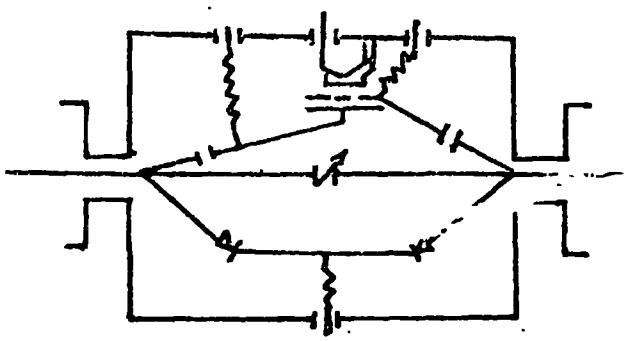

Cobalt Resonance

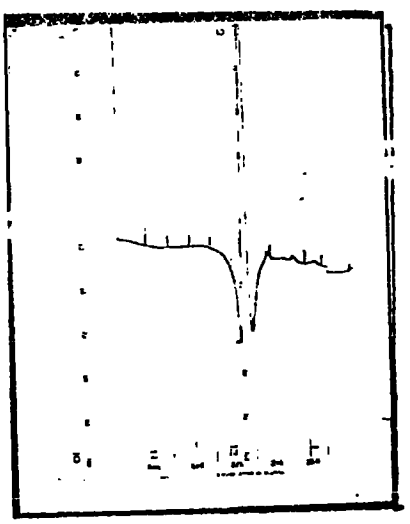

Figure 2:1

oscillator, the grid and plate inductors being formed by shorted lengths of coaxial tubing. The sample was enclosed in a plastic bag, and placed at the shorted end of the grid inductor while the plate inductor had an adjustable shorting contact so that it could be varied to obtain the best signal.

These two inductors were connected to the main body of the oscillator by U.H.F. connectors. The oscillator itself was built around a 955 acorn triode and was constructed inside a rectangular metal box. This triode is tuned by means of a butterfly capacitor, the stators of which were connected to the inner conductors of the two coaxial tubes. The rotor of the condenser was rotated by means of an insulated shaft connected to a slow motor drive thus varying the oscillator frequency.

The oscillator was frequency modulated as it was used for zero field measurements. This frequency modulation was produced by two variable capacity diodes D_1, D_2 placed back to back across the stators of the butterfly. The diodes, were biased as far as possible

in the back direction in order to increase their sensitivity. The modulation voltage was then superimposed on the bias voltage in order to vary their capacity and hence the frequency of oscillation. The circuit for producing this bias is shown in the paper reported by LaForce.

As the frequency of oscillation varied, the power level of the oscillations also varied because of the variations in capacity. This would produce a spurious frequency dependent variation in output amplitude if not corrected. Consequently, a circuit was incorporated for maintaining the grid bias, and hence oscillation level, constant as the frequency was varied (LaForce, 1961).

The amplitude modulation produced at the plate of the marginal oscillator was passed into an amplifier tuned to the modulation frequency. The amplifier was of conventional design with twin-T feedback tuning and will not be described further here.

The amplifier voltage was then fed into a phase sensitive detector which had a reference voltage de-

rived from the modulation oscillation. The phase shifter was used to make the relative phase between the reference and signal voltages either 0^{o} or 180^{o}. The D.C. voltage thus produced was fed onto a strip chart recorder.

As the oscillator passed through the resonant frequency, the added losses in the sample appeared as an increased resistance in the grid inductance and hence changed the level of oscillation of the oscillator. This caused a change in the amplitude modulation at the anode and was amplified and recorded on the strip chart recorder.

The frequency of oscillation was measured by weakly coupling a single loop of wire into the oscillator box. The r.f. signal picked up was then passed on to a mixer and local oscillator. The output from the mixer was fed into a fixed frequency radio receiver. Frequency markers were superimposed on the chart recorder by means of a manual push button.

This apparatus was initially used to observe the nuclear resonance signal of finely powdered face-

centred-cubic cobalt at room temperature, as a means of checking its operation and obtaining some indication of its sensitivity. The signal obtained was well resolved with high signal to noise ratio. (fig. 2:1).

Once this was completed, an extensive search was made for a resonance in $GdCo_2$. The sample was again in the form of a powder, sealed in a polythene bag and situated in the grid inductance of the spectrometer. The spectrometer frequency was then varied from its maximum value of 250 MHz to a minimum of 30 MHz. This was achieved in several stages as no single tuned circuit was sufficient to cover the entire frequency range.

At room temperature, measurements were made from 250 MHz to 140 MHz using two sets of coaxial tubes as the resonant circuits. At liquid nitrogen temperatures it was essential to replace these coaxial lines by coils made from copper strip above 100 MHz and from 18 s.w.g. copper wire for frequencies from 100 MHz to 30 MHz. These coils had a diameter of approximately one inch, and the grid coil was placed around

the tail of a narrow tailed dewar which contained the sample.

Unfortunately, no resonance was observed in the material for any frequency at either temperature.

It was then considered essential to move to a system with higher sensitivity, and to this end a super-regenerative technique was chosen as this could be rapidly assembled and based on some of the component parts of the marginal oscillator.

The Super-regenerative Detector:

2.2.2 The basic theory and circuits of super-regenerative receivers are described in a book by J.R. Whitehead (ref. 2:18). The advantage of super-regenerative detectors over marginal oscillators is that they can detect resonances with a much broader line width. It has the disadvantage that it cannot measure line shape directly due to the numerous sidebands, spaced at intervals $\Delta\nu$ (equal to the quench frequency fq). The central frequency can be determined, however, by varying the quench frequency and thus spreading the sidebands.

The value of the quench frequency is limited by the values of T_1 and T_2. It cannot be greater than $1/T_1$, or else the sample under study becomes saturated by the high power levels present in a super-regenerative detector. Again it cannot be less than $1/T_2$ since then the signal due to the precessing nuclei will have decayed to zero before the initiation of the next pulse; see section 2.1.3 above. Maximum sensitivity is obtained when the width of the individual sidebands ($\sim$fq) are equal to the resonance line width (Narath et al., 1964).

The oscillator used in this case was the same as described in section 2.2.1 above, except that it had been modified to allow a quenching voltage to be applied to it. Instead of having a grounded cathode, a potential divider was placed between the cathode and ground, and the quenching voltage was applied to the centre of this divider. The level control circuit was used to set the grid current to a value approximately 10 times greater than that used in the marginal oscillator mode. This was in order to pro-

vide for the much greater power level used in the super-regenerative mode.

This spectrometer was also tested on cobalt at room temperature for high frequency sensitivity. In addition, powdered iron was used at liquid nitrogen temperatures to test for low frequency sensitivity.

When first used, the super-regenerative detector picked up the cobalt resonance very easily. The graph shown in figure 2.2 is with reduced amplifier sensitivity. In order to obtain the best absorption curve, both quench frequency and quench amplitude had to be varied. The quench amplitude controls the degree of coherence (Narath, 1964) between the various sidebands given out by the oscillator and this in turn influences the sensitivity of the spectrometer.

In order to observe the iron resonance it was necessary to increase the depth of frequency modulation to a value well in excess of the iron resonance line-width. (fig. 2:2).

It will be noticed that the signal to noise ratio is greater in the cobalt resonance than in the iron

IRON

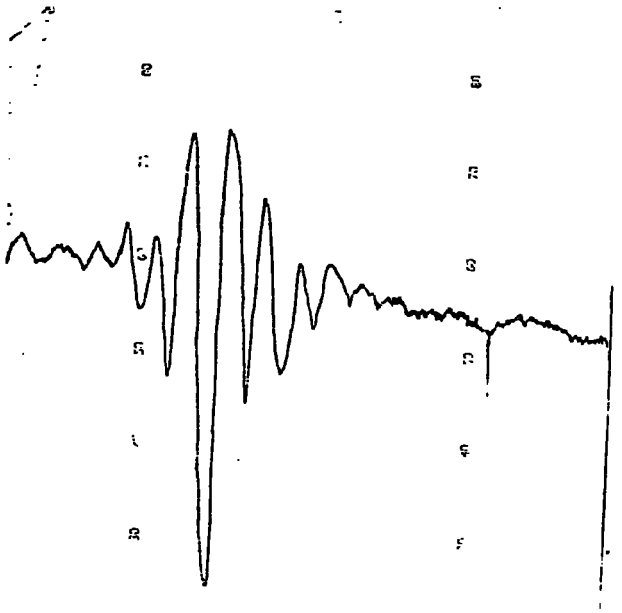

Figure 2.2

Resonance in the Super-regenerative detector

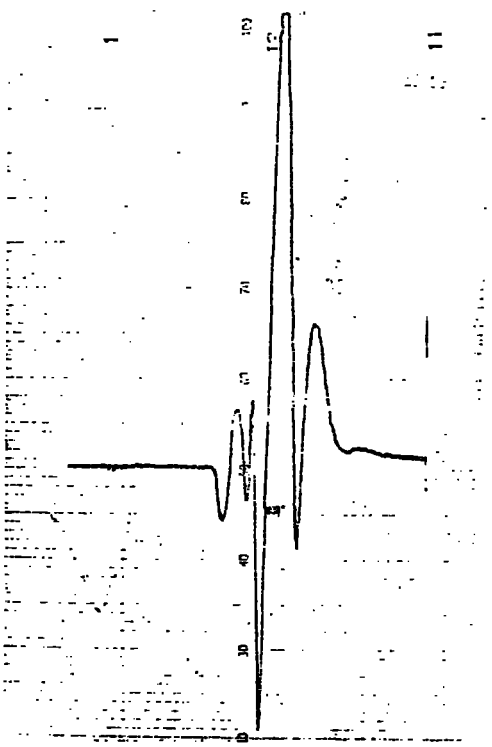

COBALT

resonance. This gives some indication of the difference in resonance signal intensity between the two elements and why it was necessary to use a more sensitive spectrometer in order to observe the iron resonance.

A search was again made to detect a resonance in $GdCo_2$ at liquid nitrogen temperatures. Unfortunately, however, this was unsuccessful over the entire frequency range from 35 to 250 megacycles. The search was repeated with various combinations of quenching frequency, quenching voltage and modulation depth, but at no time was a resonance observed.

The Spin Echo Apparatus:

2.2.3 Because of the lack of success in detecting a resonance in $GdCo_2$ by the above methods, it was decided to attempt to detect the effect using the experimentally more complex but more sensitive "Spin-Echo" technique.

(a) A block diagram of the "Spin-Echo" apparatus is shown in fig. 2:3. The pulsed oscillator was con-

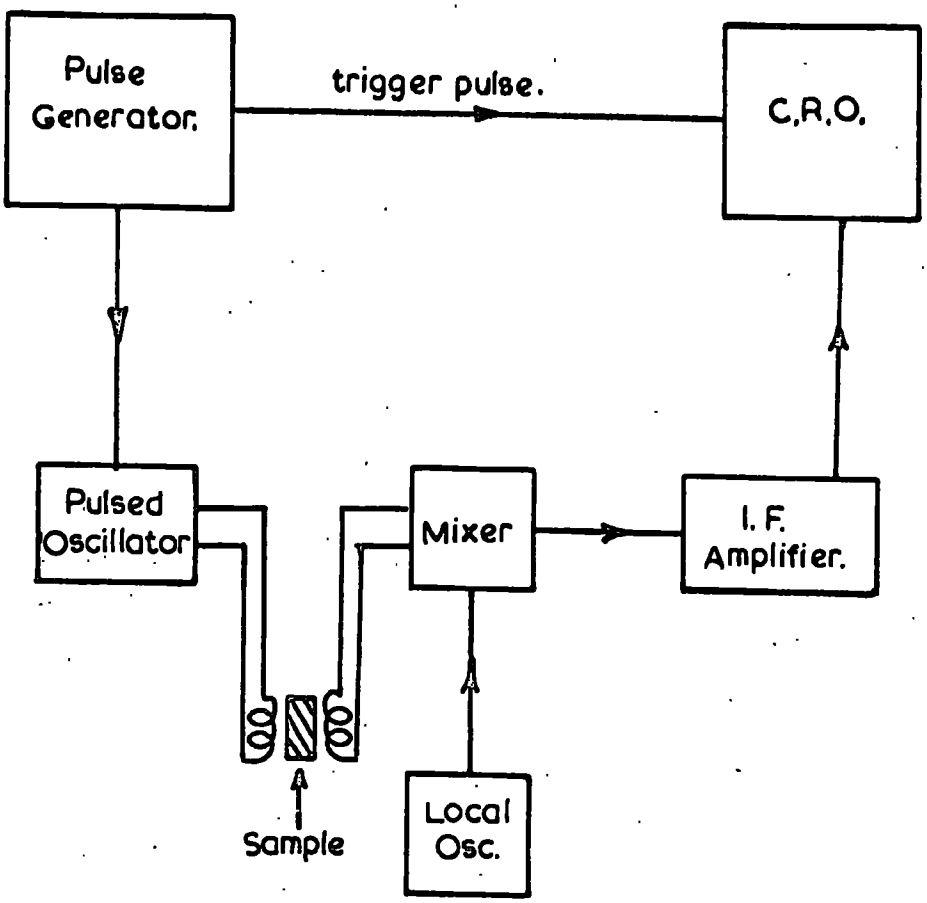

Figure 2.3

The Spin Echo Spectrometer

nected by means of 300 ohm cable to a coil surrounding the sample and a concentric receiving coil was used to detect any echoes produced by the sample. This detected signal was heterodyned with a c.w. signal from the local oscillator (a Marconi TF.01/B.) in the mixer circuit. The frequency was then shifted to approximately 34 MHz. and passed into an I.F. amplifier strip, tuned to that frequency, where it was amplified and rectified. The output of the I.F. strip was connected to the input of an oscilloscope which was synchronised by a pulse from the pulse generator. The echo then showed up as a pulse of short duration on the oscilloscope.

The pulse generator was able to provide three pulses which were either positive or negative going with the negative level held at ground potential. The widths of these pulses could be varied independently from a minimum value of about $\frac{1}{2}\mu$ sec. to a maximum value of 25 μ sec. Depending on whether a two or three pulse echo sequence was being used, the separation between the pulses could have a common

control or be independent.

The basic pulse sequence was produced by a series of six Ferranti logic modules. The sequence was initiated by a pulse from a free running multivibrator (L.C.E. 507) (see fig. 2:4), the frequency of which was determined by six stepped capacitors. These capacitors were added in parallel to each other by means of a shorting switch thus allowing the repetition rate to be varied from 20 - 1000 p.p.s.

The output from the L.C.E. 507 then goes to the input of three univibrator modules (L.C.E. 506). These modules have diode-capacitor inputs which are connected so that they were triggered only on the negative going edge of the input pulse.

The first two modules produce the delay pulse width. These widths could be varied in a similar manner to the repetition rate except that three switches were now used to vary the first delay width from 5 μ sec. to a maximum of $\sim$500 μ sec. in 125 steps. The capacitors for the second delay width were ganged to those for the first, but the voltage levels in the

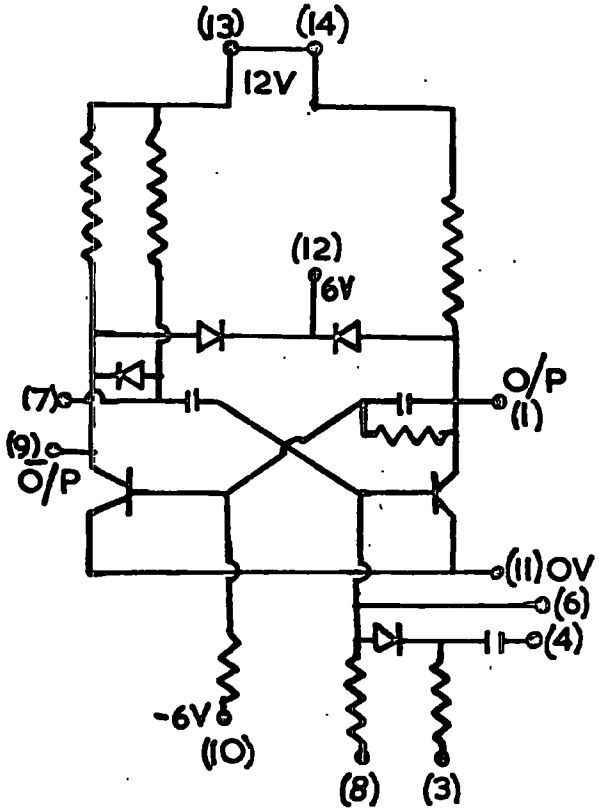

LCE 506

Figure 2.4

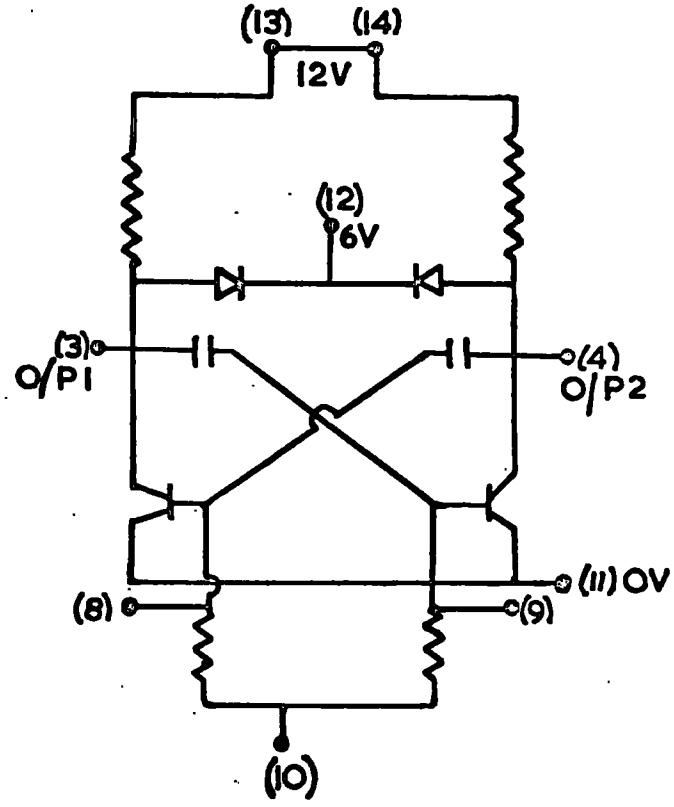

LCE 507

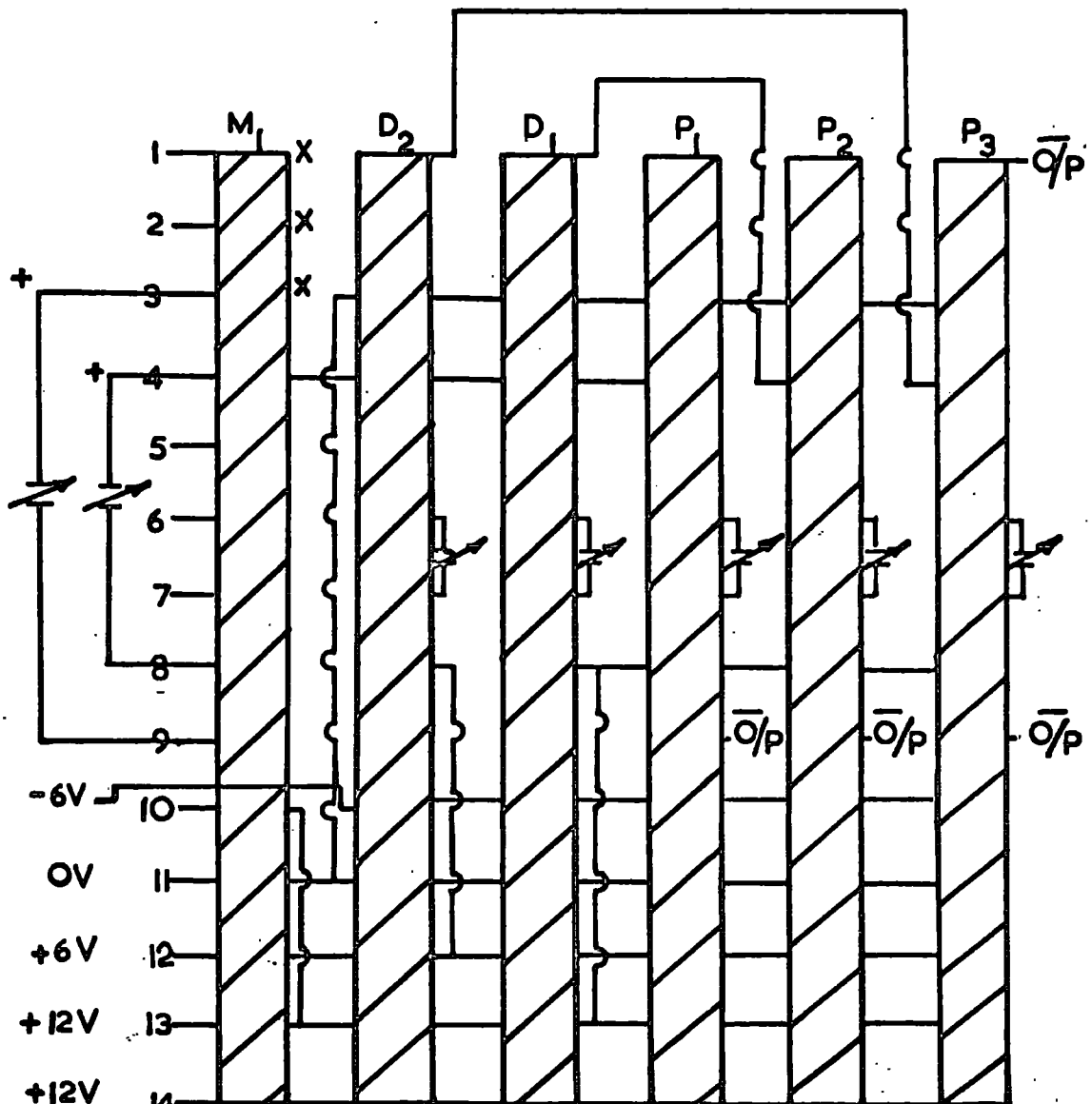

Figure 2.5

Logic Module Interconnections

second module were so arranged that the delay widths were approximately twice those of the first. Two variable capacitors provide the fine control of the delay widths. When used in the three pulse echo mode an additional switch was provided so that the first delay width could be held constant while the second was varied.

The third univibrator provided the first pulse for the output amplifiers. The second and third output pulses were provided by the remaining two univibrators which were triggered by the second and first univibrators respectively. Each of the output pulse widths were switched from .5 μ sec. to 25 μ sec. in 25 steps.

These output modules could provide either positive or negative going pulses switched between the plus six and zero voltage levels. These were then fed into the output amplifiers.

The two output amplifiers are identical except that one has a three terminal "or-gate" input, whereas the other has only a single input. These ampli-

fiers were used to change the output pulse power from 6 volts at 6 m.a. maximum, to a value of 40 volts at 500 m.a. maximum. It was desirable that this great increase in power should produce very little degeneration in pulse rise and fall times. For this reason all transistors employed were of the high current fast switching type and were used in complementary configurations in order to increase switching speeds. For a schematic diagram of the circuit employed, see figure 2:6.

The input transistor was a PNP transistor with the emitter at plus 6v and collector load at 0v. With the input voltage level at plus 6v the transistor was switched off and no current was drawn by the collector. There was then no voltage drop across the collector load and its voltage was zero. If the input voltage level dropped to zero volts, the current drawn through the base saturated the transistor and forced its collector voltage up to just less than 6 volts.

The remainder of the circuit had a ground pot-

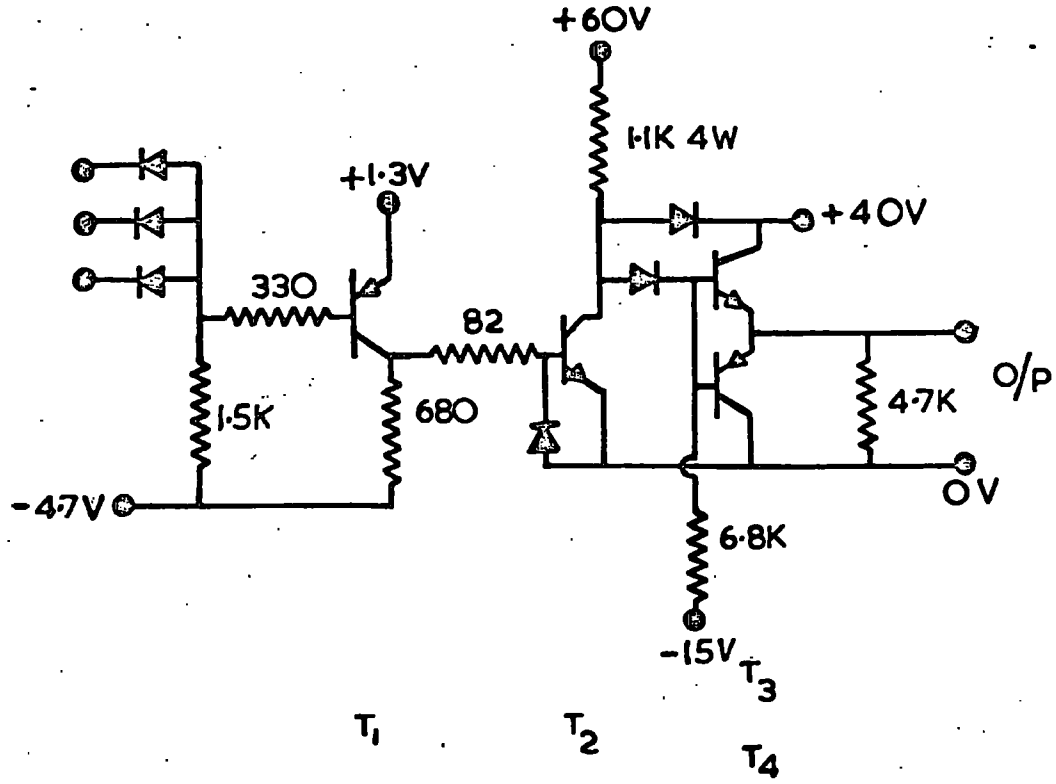

T_1 . 2N2894
T_2 . 2N2369
T_3 . 2N2218
T_4 . 2N2904

Figure 2.6 The Output Amplifier

ential which was 4.7v positive with respect to the previous voltages. There was thus only a 1.3v drop between the positive output voltage level of this transistor, and the emitter voltage of the following transistor. This helped to decrease the rise and fall times during switching. T_2 was an NPN transistor which was complementary to T_1. The collector of T_2 was connected through a resistor to 60v. It was shorted by means of a diode to the 40v line so that the maximum collector voltage did not rise above this value. The extra 20 volt drop across the resistor provided sufficient current so that, under load conditions, the output pulse height did not drop below 40 volts. The emitter of T_2 was at zero potential.

With the collector of T_1 4.7v negative with respect to the emitter of T_2, T_2 was cut off. There was then no collector current through T_2 and the collector voltage rose to its maximum of 40v. As the collector of T_1 rose through zero volts to a positive value of 1.3 volts, T_2 was switched on and its collector was pulled down to zero volts. Thus an input

pulse at the base of T_1 was reproduced at the collector of T_2 with the same polarity but increased voltage. The fall time of the pulse output at T_2 was small because it occurred when the transistors T_1 and T_2 were switched on and this process is very fast for transistors operated in the saturated mode. The rise time was shortened because, during both stages of amplification, the amplifier was using only the linear part of an exponential curve.

A further stage of amplification was required in order to increase the maximum current in the output pulse; i.e. to lower the output impedance. In order that the rise and fall times of the final output pulses might remain as short as possible, it was desirable that both these edges were caused by switching a transistor on. For this reason, a pair of complementary emitter followers were used, consisting of the transistors T_3 and T_4. T_3 was an NPN transistor with its collector connected directly to the 40 volt line; T_4 was a PNP with its collector connected to ground. The bases were connected together for the input, and

the output was taken from the emitters which were again common.

As the collector of T_2 rose towards 40 volts, T_3 was switched on. This caused the emitter of T_3 to rise towards the collector voltage which was held at 40 volts. The load current was then drawn through T_3 while T_4 was cut off. As the collector of T_2 dropped towards zero volts, T_3 was switched off and T_4 switched on. T_4 then drew a large current which must, in this case, be supplied by the voltage across the load. The collector of T_4 was held at zero volts therefore the output voltage was forced down to this value.

The collector junctions of T_3 and T_2 tended to break down if the collector of T_2 was connected directly to the base of T_3. This probably took place during the moment of switching when large currents were being drawn and there was no resistor present to limit the current through these junctions. A diode was introduced in order to correct this defect and as a result, a negative voltage had to be applied through the resistor shown to provide the current for switch-

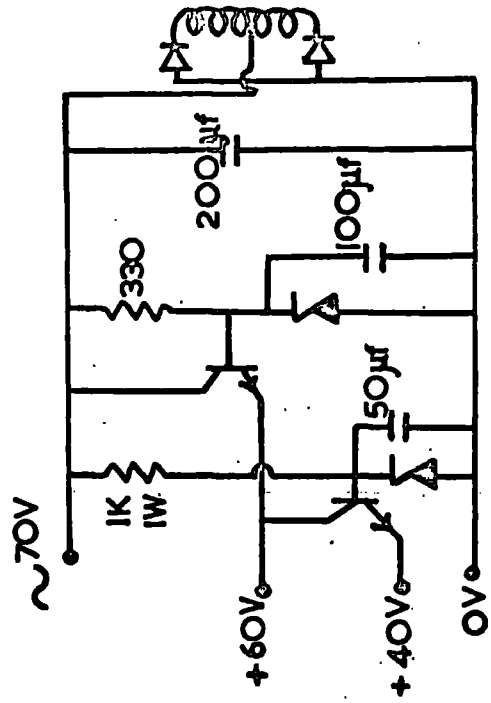

Figure 2.7

Pulse Generator Power Supplies

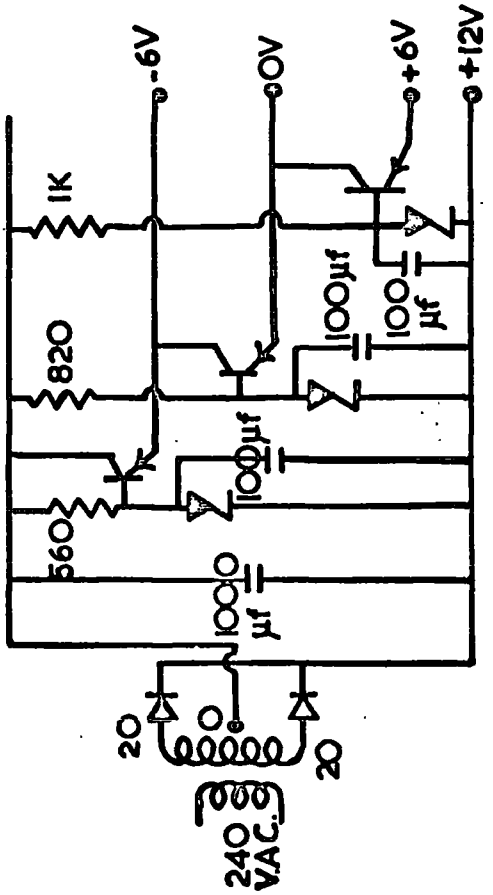

ing on T_4. The final output provided a 40 volt pulse with rise and fall times of about 50 nanoseconds.

The logic modules required 4 voltage levels of +12v, +6v, 0v and -6v with low impedance at the switching rates employed, while the output amplifiers required voltage levels of +60v, +40v and 0v. The Offset voltage between the two systems was provided by a Zener diode fed from the +6v line.

The circuit used was adapted from one described by D. Grollet (1962, ref. 2:19) in Mullard Technical Communications. It consisted of a series of emitter followers with a zener stabilised voltage applied at the base. They provided a high current 12v source for the modules while the remaining voltages lines were mainly used as reference voltages. The 60v and 40v lines both drew high currents.

(b) The r.f. energy was supplied by a plate tuned push-pull oscillator using a QQV03-10 double tetrode, the circuit of which is shown in fig. 2:8. The valve was switched on by a 40 volt negative-going pulse applied at the cathode. It was normally biased be-

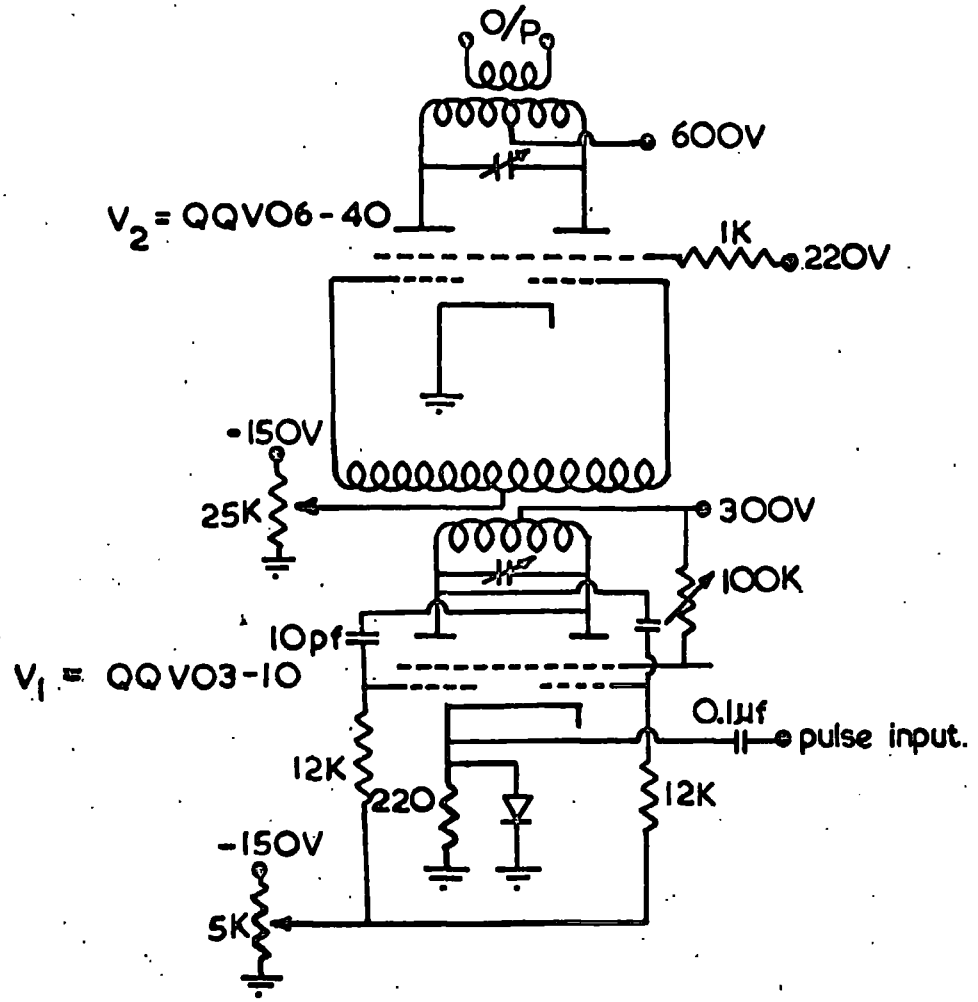

Figure 2.8

The R.F. Transmitter

yond cutoff by a negative voltage of about 40 volts applied to the grid but during the pulse interval, the cathode voltage fell below grid voltage and oscillations were allowed to build up at the frequency of the tuned section. A diode was used to hold the cathode at ground potential to prevent ringing following the trailing edge of the switching pulse.

The output of the pulsed oscillator was inductively coupled into the grid section of a QQV06-40 double tetrode used as a push-pull tuned amplifier. From there, the short length of 300 ohm twin lead cable passed down to the sample transmitting coil.

(c) The twin lead was secured by adhesive tape against the outside of an 8 mm.i.d. stainless steel tube. A 6 mm.o.d. glass test-tube containing the sample was held at the bottom of this tube. About 20 turns of 26 s.w.g. enamelled copper wire close wound on the test-tube served as the transmitting coil. The reactance formed by the combination of transmitting coil and twin lead was matched to the oscillator by a butterfly capacitor placed at the upper end of the steel

tube.

The receiving coil consisted of about 10 close wound turns of 18 s.w.g. enamelled copper wire and was co-axial with the transmitting coil. One end was grounded against the wall of the steel tube while the other was connected to the inner conductor removed from a 70 ohm coaxial cable. This led down the centre of the tube and was connected at the other end to a coaxial cable leading to the mixer.

(d) The signal from the receiving coil was transformer coupled to the input to the mixer. The transformer secondary was tuned to the echo frequency by a capacitor and was connected to the grid of a 6CW4 Nuvistor, low noise triode. The signal was then heterodyned with a signal from a Marconi variable frequency oscillator, to produce a constant intermediate frequency of about 34 megacycles. The anode was tuned to this frequency by a fixed capacitor and slug tuned inductor and was then coupled to the input of the r.f. strip.

(e) The r.f. strip which had been removed from an air borne radar system, consisted of six, stagger tuned transformer coupled amplifiers. The input was modified by the removal of one of the matching inductors and by changing the turns ratio on the other to improve matching to the output from the mixer. The signal was amplified in this way by about 100db and was finally rectified by one half of a double diode valve. It was then fed into the input of a Cossor base oscilloscope. The oscilloscope was synchronised to the pulse sequence by a trigger pulse taken from the second output of the multivibrator.

(f) The power supplies used in the circuits described above were all of conventional design and will not be described in detail. They provided 300v for the r.f. oscillator; 220v for the r.f. amplifier screen bias; +150v for the I.F. strip and mixer H.T.; -150v for the bias voltage for the r.f. unit; -6.3v for the valve heaters in the r.f. strip and mixer; and 600v for the r.f. amplifier. The 600 volt supply is un-stabilised while all the others are stabilised.

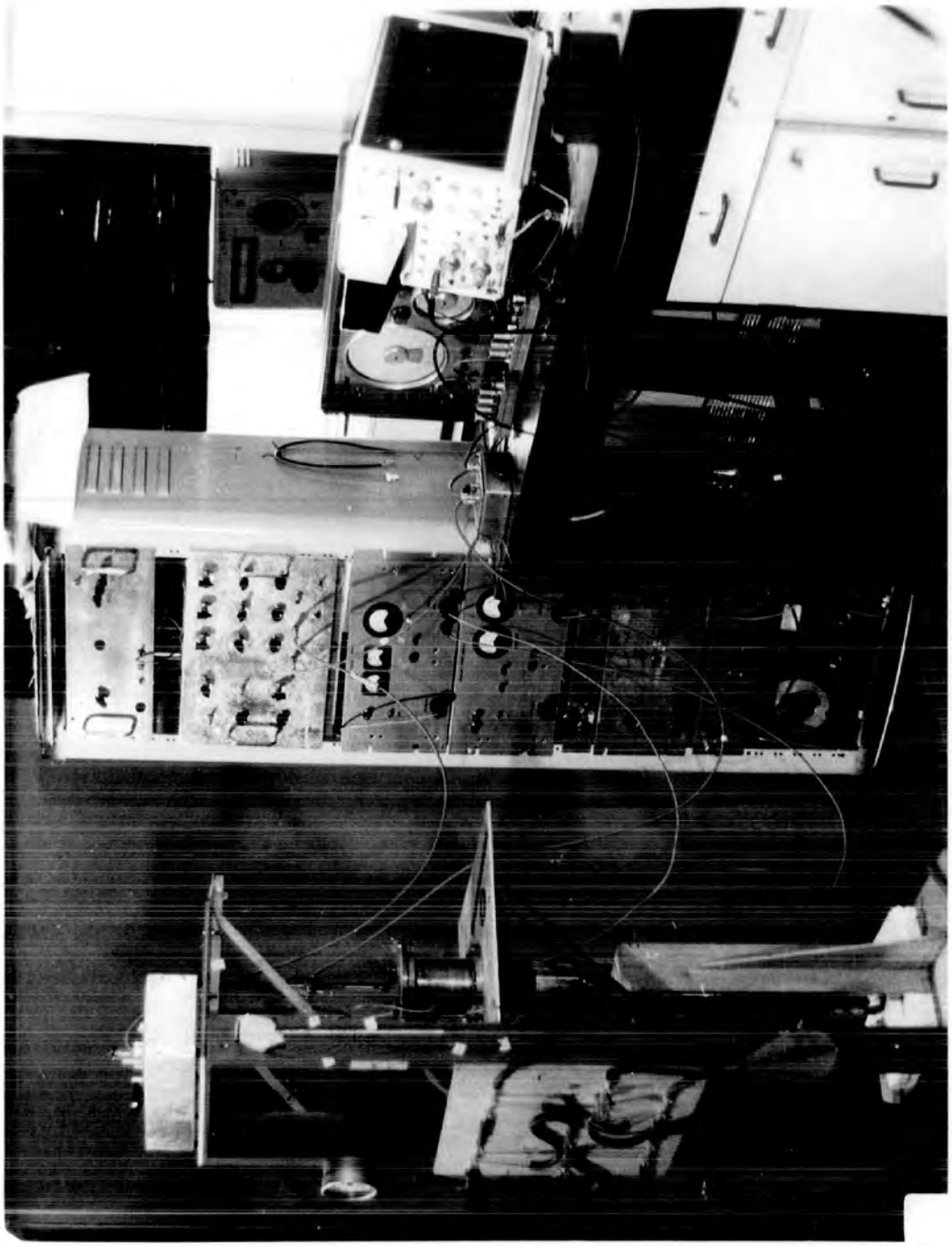

Figure 2.9

(g) The samples were cooled to helium temperatures in a glass cryostat of conventional design which will not be described in detail here.

Other Measurements in $GdCo_2$:

2.3 All metals used in the following investigations were provided by Koch-Light laboratories. The gadolinium, dysprosium and yttrium contained 0.1% impurities, whereas the iron, cobalt and nickel contained about .001% impurities.

Crystal Structure:

2.3.1 The specimens were prepared by melting together stoichiometric quantities of the metals concerned in an argon arc furnace. The resulting pellet was turned over and reheated about three times to ensure homogeneity. After crushing $GdCo_2$, it was vacuum annealed in a quartz tube at $1000^{o}C$ for 24 hours. As the quartz tubing was severly attacked by the gadolinium, no other member of the series used was annealed.

In order to check for specimen purity and homogeneity, the crystal structures of the compounds were

determined by x-ray powder photographs in an 11.46 cm. diameter Debye-Scherrer camera. The camera was used with the cobalt $K\alpha$ doublet, having wavelengths $K\alpha_1 = 1.790^{\circ}A$, $K\alpha_2 = 1.7889^{\circ}A$, and weighted mean value $K\alpha = 1.790^{\circ}A$. The correct value of the lattice constant was then obtained by extrapolation of the measured values using the Nelson Riley extrapolation function. (ref. 2:22).

Bulk Magnetisation:

2.3.2 The magnetisation measurements were made using a vibrating sample magnetometer in which the sample was placed at the centre of a pair of coils wound in series-opposition. The magnetic field was provided by a water cooled solenoid. A full description of the apparatus is given in the theses of H.D. Ellis (ref. 2:20) and A.R. Piercy (ref. 2:21).

oOo

CHAPTER III

R E S U L T S

Spin Echo Observations:

3.1 Spin echo resonance measurements were made on the binary series of compounds $Gd_{1-x}Y_xCo_2$, $Gd(Co_{1-x}Ni_x)_2$ and $Gd_{1-x}Dy_xCo_2$ at 4.2^oK. In the first two series x varied from 0 to 1 in steps, whereas in the last series measurements were only possible for $0 \leqslant x \leqslant 0.2$.

For line shape measurements, a two pulse sequence was used. The pulses were of equal width, $\sim$ 1.6μsec., for most of the series but rising to $\sim$ 3μsec. for some of the dysprosium measurements. The separation between the pulses was kept constant at about 20μsec., ensuring that there was a negligible loss of echo amplitude due to relaxation effects. The sample, contained in a 6 mm. I.D. glass phial, was cooled to helium temperatures in the cryostat and the frequency

of the pulsed r.f. signal varied in discrete steps over the range of interest. When an echo was observed on the oscilloscope the widths were varied to obtain the maximum echo amplitude. These pulse conditions were then kept constant across the width of the resonance.

The echo height was obtained by measuring the pulse height as shown on the oscilloscope and the line shape was given by the variation in echo height with frequency. From the known nuclear gyromagnetic ratio (nuclear moment and nuclear spin) the distribution in magnetic field strength at the nuclear sites was readily evaluated.

In many of the materials investigated it was noticed that the transmission frequency and the echo frequency were not the same at all points. This was originally observed with the compound $Gd_{0.9}Y_{0.1}Co_2$, the effect being much smaller in the terminal compound $GdCo_2$. It was found that as the input pulse frequency was varied over a wide range, the frequency of the tuned receiver for maximum signal amplitude varied

over a much smaller range. The observed results for $GdCo_2$ are given in table 3.1, in which this discrepancy can be easily seen.

This effect was originally thought to be due to the receiver bandwidth obscuring frequency variations. However the discrepancy in frequency was observed to be so large that this proposal had to be abandoned.

The possibility was then considered that it might be similar to the effects observed by M.B. Stearns (ref. 3:1), however this was abandoned too as in these $(GdY)Co_2$ compounds there was none of the marked oscillatory behaviour which that author described. In addition the lines considered in that case were narrow compared with the r.f. field intensity, which is certainly not the case for the observations described in this work.

It was noticed that the 'transmission' line width decreased if the power level was decreased, but as no means of continually varying the r.f. amplitude was available, the effect of a continual decrease in power level could not be investigated. A similar

TABLE 3.1

$GdCo_2$

F_T MHz	F_E MHz	E(volts)	F_T MHz	F_E MHz	E(volts)
61.6	61.3	10	60.9	61.0	9.4
62.1	61.9	8.6	60.6	60.8	7.2
62.4	62.2	6.8	60.3	61.1	5.6
62.7	62.6	4.8	59.8	60.8	3.4
63.4	63.0	2.4	59.2	61.1	2.6
64.5	61.8	2.0	58.4	61.6	3.0
61.5	61.2	11			

effect has been observed by Budnick and Skalski (ref. 3:2), who reported that the r.f. amplitude could be decreased to such an extent that transmission frequency and echo frequency were everywhere the same. They showed that the echo and transmission frequencies approached one another for any given observation as the pulse duration was increased and the r.f. amplitude simultaneously decreased in order to keep the turn angle constant. In these measurements, as far as possible, the echo frequency has been taken as the correct resonant frequency.

In attempting to follow the behaviour of the echo and transmission frequencies through a resonance line, and hence gain some insight into how best to interpret the observations a variety of graphs were plotted detailing the features of the measurements for $GdCo_2$. These were as follows:

a) echo amplitude v transmission frequency (f_T) (fig. 3:1a)

b) echo amplitude v echo frequency (f_E) (fig. 3:1b)

Figure 3.1 $GdCo_2$

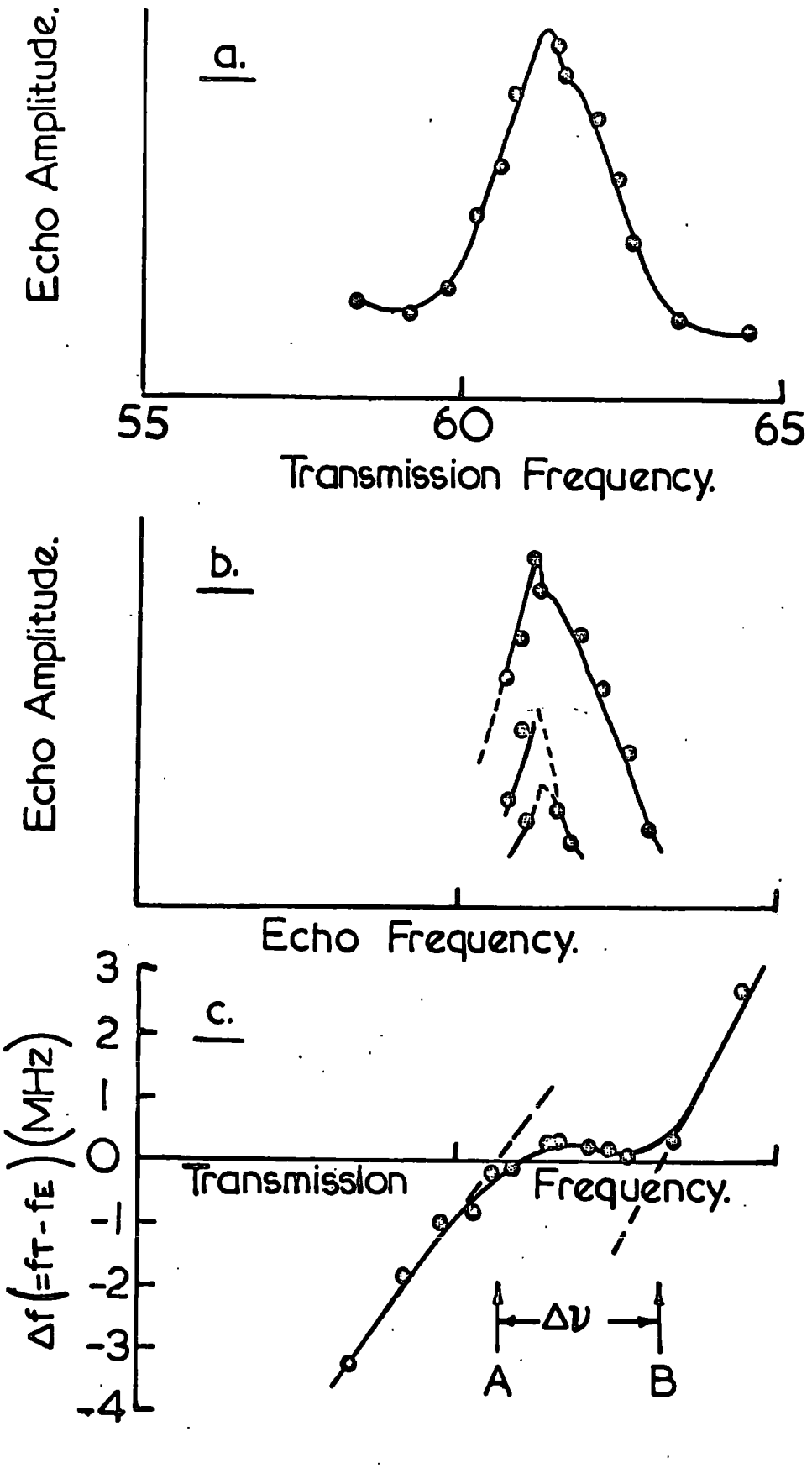

c) $(f_T - f_E)$ v f_T (i.e. the correction frequency) (fig. 3:1c)

From these it was possible to make the following generalisations.

a) Under the conditions at which these echoes are obtained it is possible to obtain signals at transmission frequencies well away from the resonant frequency, which are not characteristic of the shape of the wings of the true resonance line. Rather they appear to be related to the shape of the centre of the line, but correspond to a decreased amplitude. Consequently not all echo amplitude-echo frequency observations can be expected to fit on a single curve, but in fact may be representative of a family of curves of decreasing power.

b) the difference frequency between the transmission and echo pulses varies in the way shown in fig. 3:1c, at least for a fairly simple resonance of the type considered here. This variation consists of a reasonably constant Δf region (for which $\Delta f \simeq 0$)

in the vicinity of the resonance line, lying between two rapidly increasing regions in which the correction frequency increases with the distance the transmission frequency is from the centre frequency of the resonance, the correction frequency always being towards the centre frequency.

c) The full line width, at half amplitude, is different for the transmission and echo frequency cases.

d) A line width may also be defined from the Δf observations, as being the length of the constant Δf region. This may be defined as (A.W B) MHz. (see fig. 3:1c).

e) The echo frequencies appear to give a sharper line than the transmission frequencies, and consequently provide a more accurate value of the reaonance frequency. This method of obtaining the resonance frequency is further supported by the observations to be described in the following, in which extensive differences in line shape exist between transmission and echo frequency observations.

$GdCo_2$

3.1.1 On the basis of the foregoing discussion of the results obtained for $GdCo_2$ and shown in fig. 3:1, this compound from which all later materials are derived, was found to have a central resonant frequency of 61.4 MHz, with frequency spread, at the echo frequency, of 2 MHz.

In order to determine whether this resonance was associated with either of the gadolinium ions (Gd^{155} or Gd^{157}) or with the Co^{59} nucleus, a search for other echoes was made at frequencies in the region of 46 MHz and 82 MHz. These were chosen, since the gyromagnetic ratios of the two gadolinium nuclei are in the ratio 3:4, consequently for an observed frequency of ν res. for one, the other resonance should occur at either 1:33 ν res. or 0.75 ν res., depending on which of the isotopes was responsible for ν res.

No resonances were observed in the vicinity of these frequencies and consequently for this resonance and for the following, the results were taken to be those associated with the cobalt ion. Intuitively,

this conclusion is also supported by the usual ease of observation of the cobalt resonance compared with either of the gadolinium resonances.

The cobalt hyperfine field in $GdCo_2$, derived from these observations is then 60.8 Koe, with a line width of 1.98 Koe. This compares with the large field of 230 Koe, observed by Gegenwarth et al, (ref. 3:3), at the iron nucleus in isostructural $GdFe_2$ at $78^{\circ}K$, and with the field of 217 Koe observed by many workers in cobalt metal. (ref. 3:4).

In an attempt to determine the sign of the hyperfine field at the cobalt nucleus, the spin echo observation was repeated with an external field applied to the sample. These results, some of which are given in fig. 3:2, show

i) a decrease in echo amplitude at resonance with increasing field,

ii) a possible decrease in the resonant frequency. This is comparable to the resolving power of the system and consequently it can only be said that any frequency shift which occurs

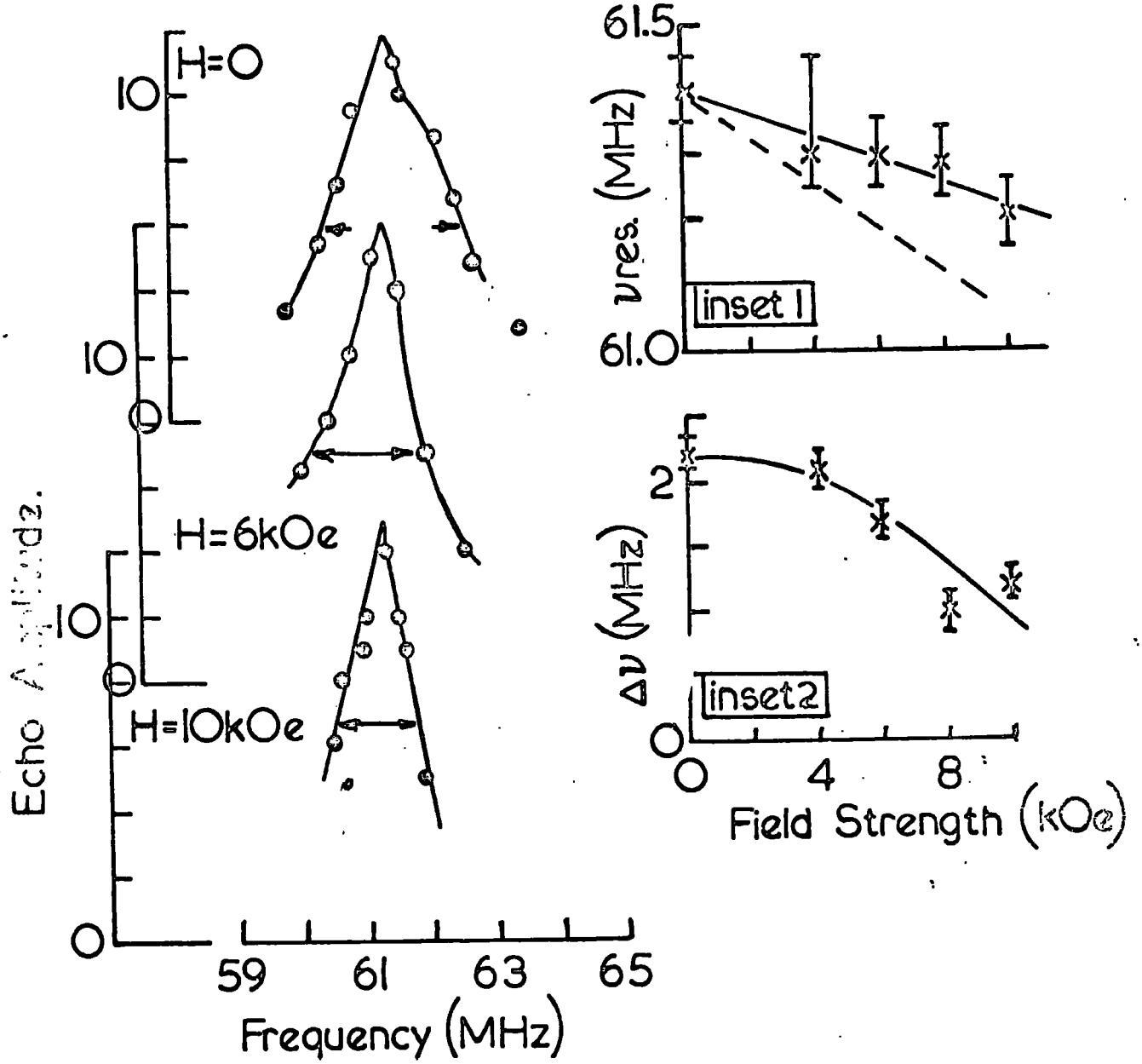

Figure 3.2

$GdCo_2$ in External Fields

is not a positive one.

iii) a continuous decrease in the line width with increasing applied field.

The decrease in amplitude and negligible frequency shifts observed are to be expected if the specimen consists of multidomain particles and the resonance arises from nuclei in the domain walls of these particles. Indeed the observation of these two details is often used to confirm this fact.

Inset 1 of fig. 3:2 shows the variation of resonance frequency with applied field, after the results have been modified to allow for a demagnetizing field (assuming a spherical particle shape). As may be seen, the most optimistic variation is still appreciably smaller than that given by $d\omega/_{dH} = -\gamma$. The negative gradient, however, indicates reasonably conclusively that the hyperfine field at the cobalt nucleus is negative; this is in agreement with the results of Wertheim et al. (ref. 3:5) for the field at the iron nucleus in the related AFe_2 compounds.

Measurements were also made on $GdCo_2$ as a function

of temperature. As the temperature was lowered to $2.4^{\circ}K$ (using a pumped helium bath) the discrepancy between transmission and echo frequencies increased. However, on raising the temperature above $4.2^{\circ}K$ (using the vapour above the helium bath), the echo amplitude decreased rapidly, disappearing completely at $20^{\circ}K$. No variation in echo frequency was observed in any of the variable temperature measurements.

$Gd_{1-x}Y_xCo_2$

3.1.2 The continuous substitution of yttrium for gadolinium in the series $Gd_{1-x}Y_xCo_2$ results in the appearance of additional peaks in the variation of echo height with transmission frequency. The variation with echo frequency however showed little evidence for this extra line structure. These results are shown in fig. 3:3 to fig. 3:5, along with the variation of Δf with transmission frequency for $(1-X) = 0.81$, 0.57 and 0.4.

It is evident from these results, and those of fig. 3:1, that with yttrium substitution the frequency of the Co^{59} resonance decreases with increasing yttrium

Figure 3.3

$Gd_{.81}Y_{.19}Co_2$

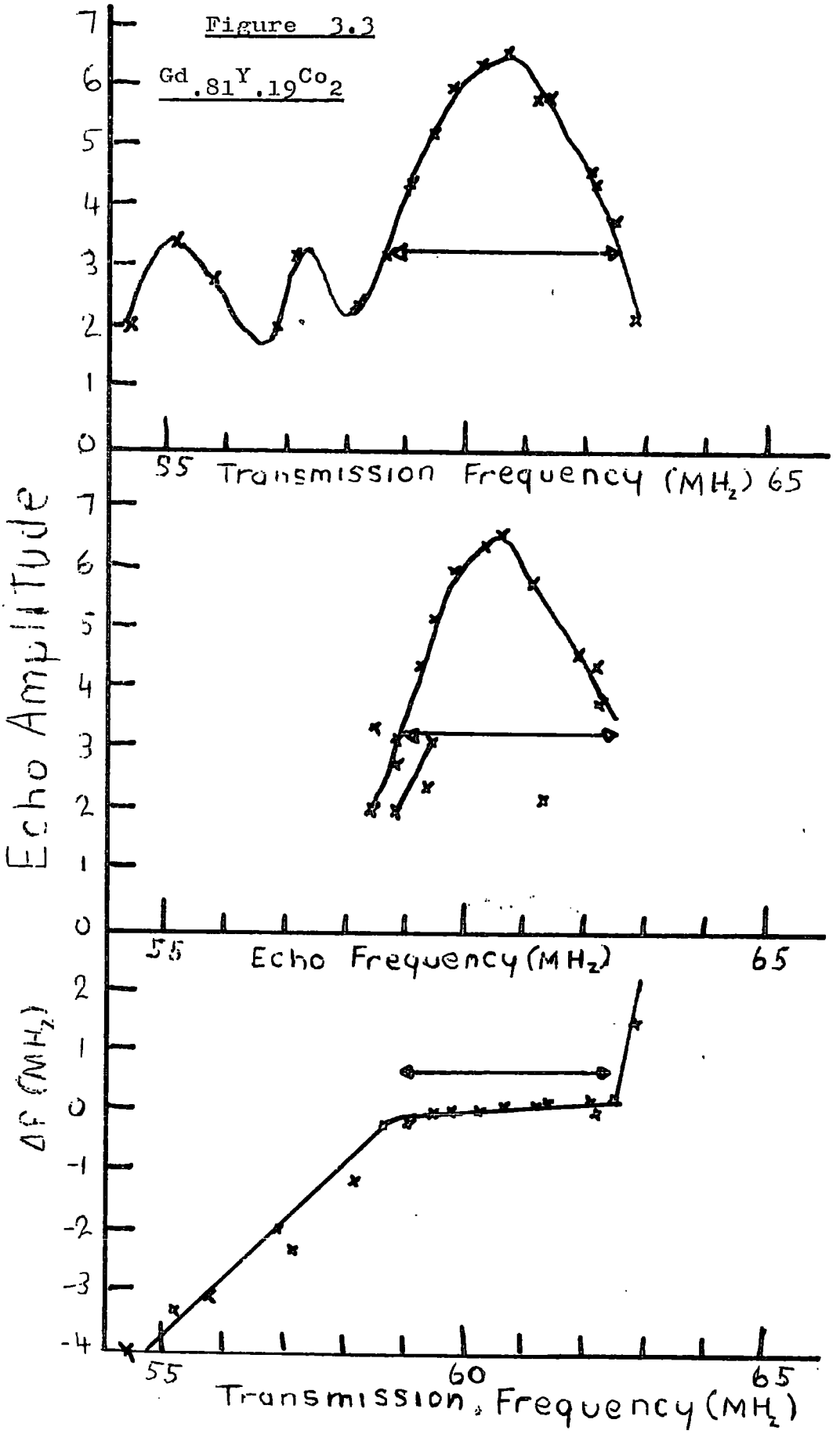

Figure 3.4

$Gd_{.51}Y_{.49}Co_2$

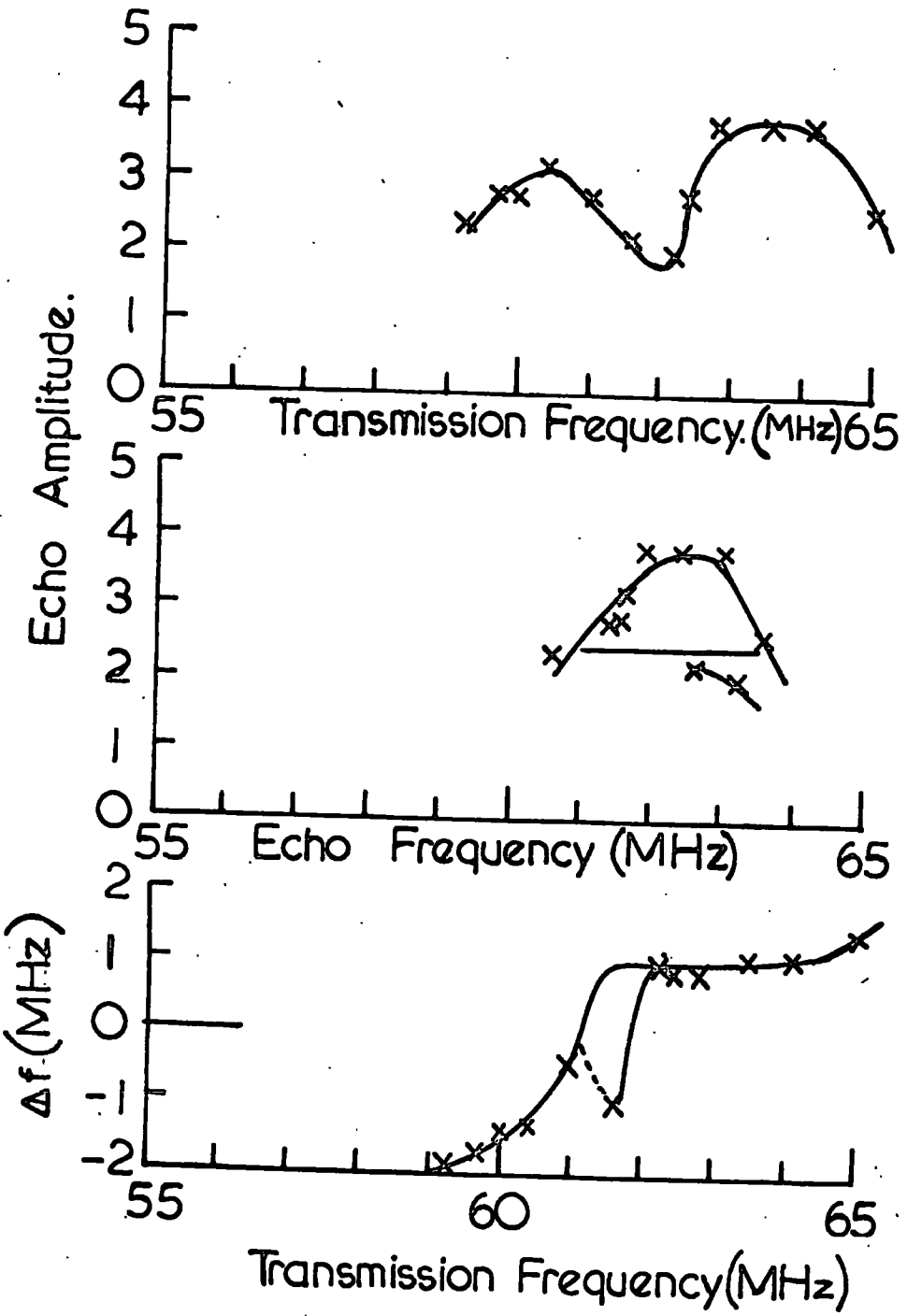

Figure 3.5

$Gd_{.4}Y_{.6}Co_2$

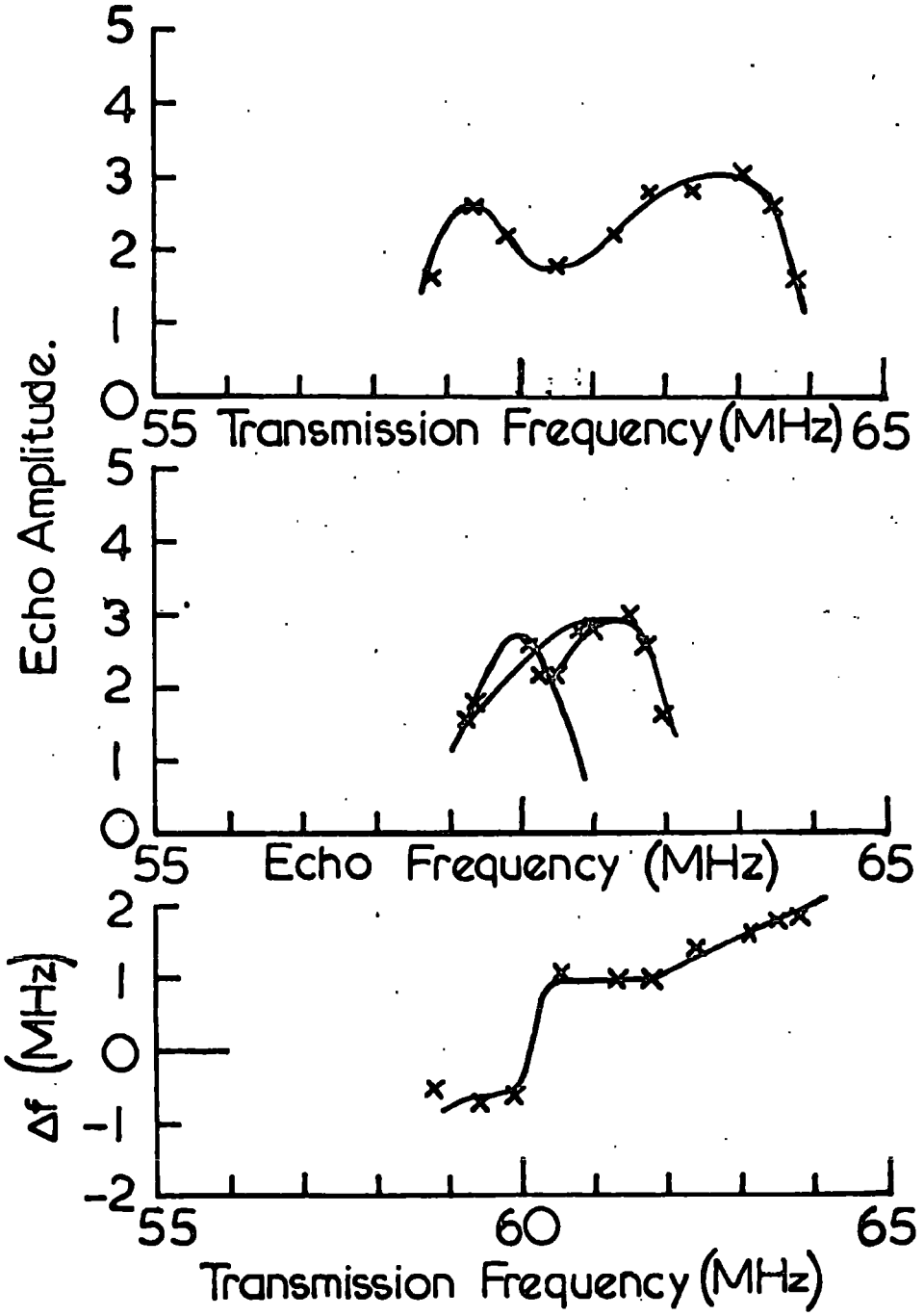

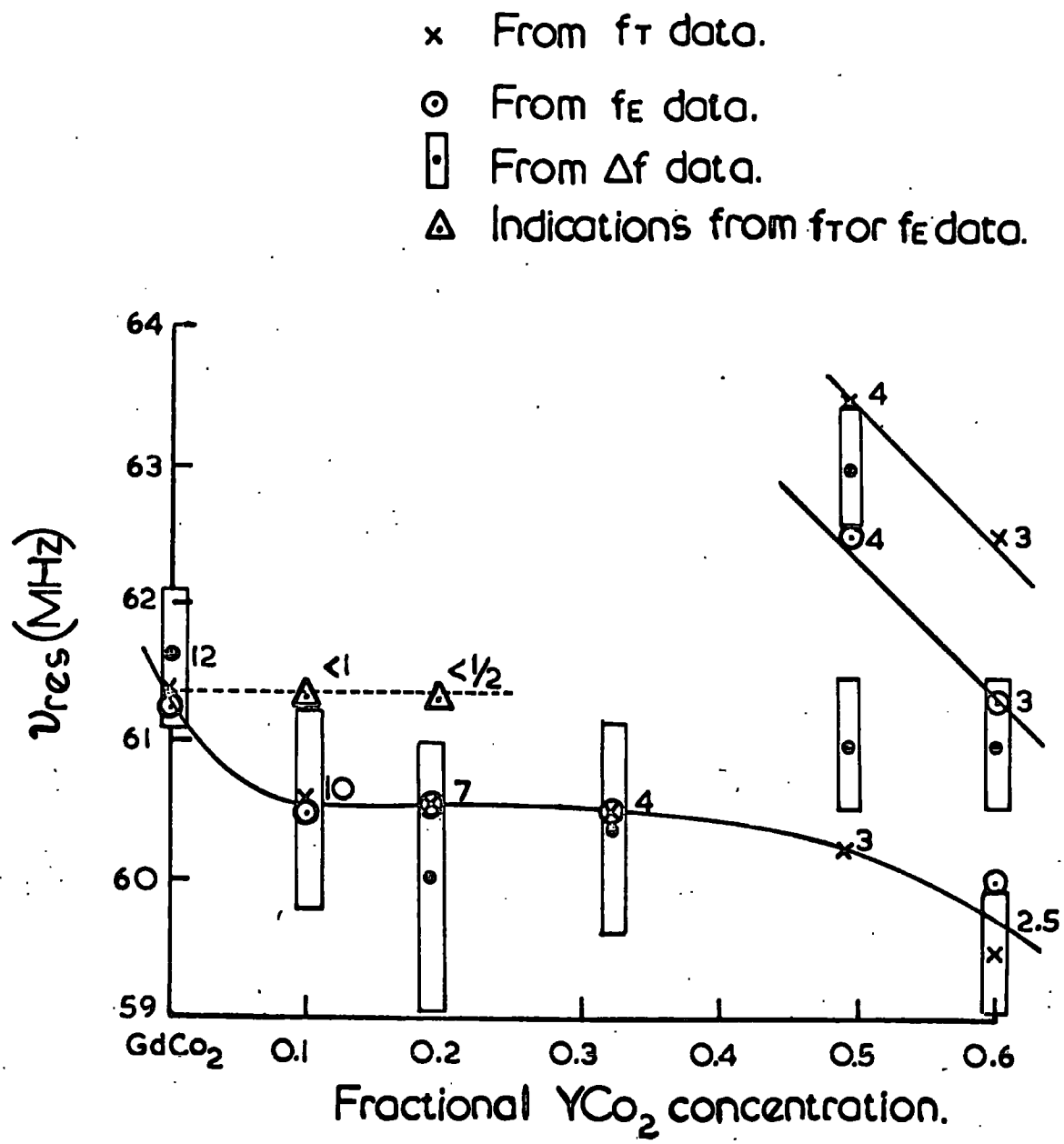
× From fT data.
⊙ From fE data.
From Δf data.
Δ Indications from fT or fE data.
64
63
62
61
60
59
νres (MHz)
12
<1
<½
10
7
4
3
4
4
×3
3
2.5
GdCo2
0.1
0.2
0.3
0.4
0.5
0.6
Fractional YCo2 concentration.

Figure 3.6

content. The detailed form of this variation is difficult to obtain, since resonance frequency values can be obtained in a variety of ways, namely, from Amplitude versus f_T, Amplitude versus f_E or Δf versus f_T graphs. An attempt has been made in fig. 3:6 to summarize all of these results. From this graph, it may be seen that an overall, non linear, decrease in ν res. occurs as X increases. In addition for $X \geqslant 0.5$ other lines appear with ν res. greater than that in $GdCo_2$. The Δf results in this presentation must be treated with extreme caution and at best used as an indication of where lines may be expected to appear. Consequently the solid curve has been drawn using the f_T or f_E results. Apart from the general decrease in ν res. the following points are worthy of note.

a) the existence of the $GdCo_2$ resonance at 61.3 MHz to $X = 0.2$, but with decreasing amplitude.

b) the additional high frequency resonance for $X > 0.5$, whose frequency decreases with X increase in a manner comparable to that of

the main resonance.

c) the continuous decrease in resonance amplitude across the series as the YCo_2 concentration increases. (these amplitudes are indicated by numbers on the graph adjacent to each point and may be used as a general guide to the behaviour of the resonance).

$\underline{Gd_{1-x}Dy_xCo_2}$

3.1.3 With small substitutions of dysprosium to the basic $GdCo_2$ compound the echo amplitude was observed to decrease very rapidly and become unobservable for more than 5% $DyCo_2$ concentration. The resonance lines are shown in fig. 3:7, from which may be seen a slight shift in the resonance frequency as indicated in the inset.

The large deviations between transmission and echo frequency results was not observed in this case, and indeed the resonance line is narrowed for these compounds compared with the terminal compound $GdCo_2$. The curves also show some sign of fine structure but it has not been possible to resolve this.

Attempts were also made to observe the resonance

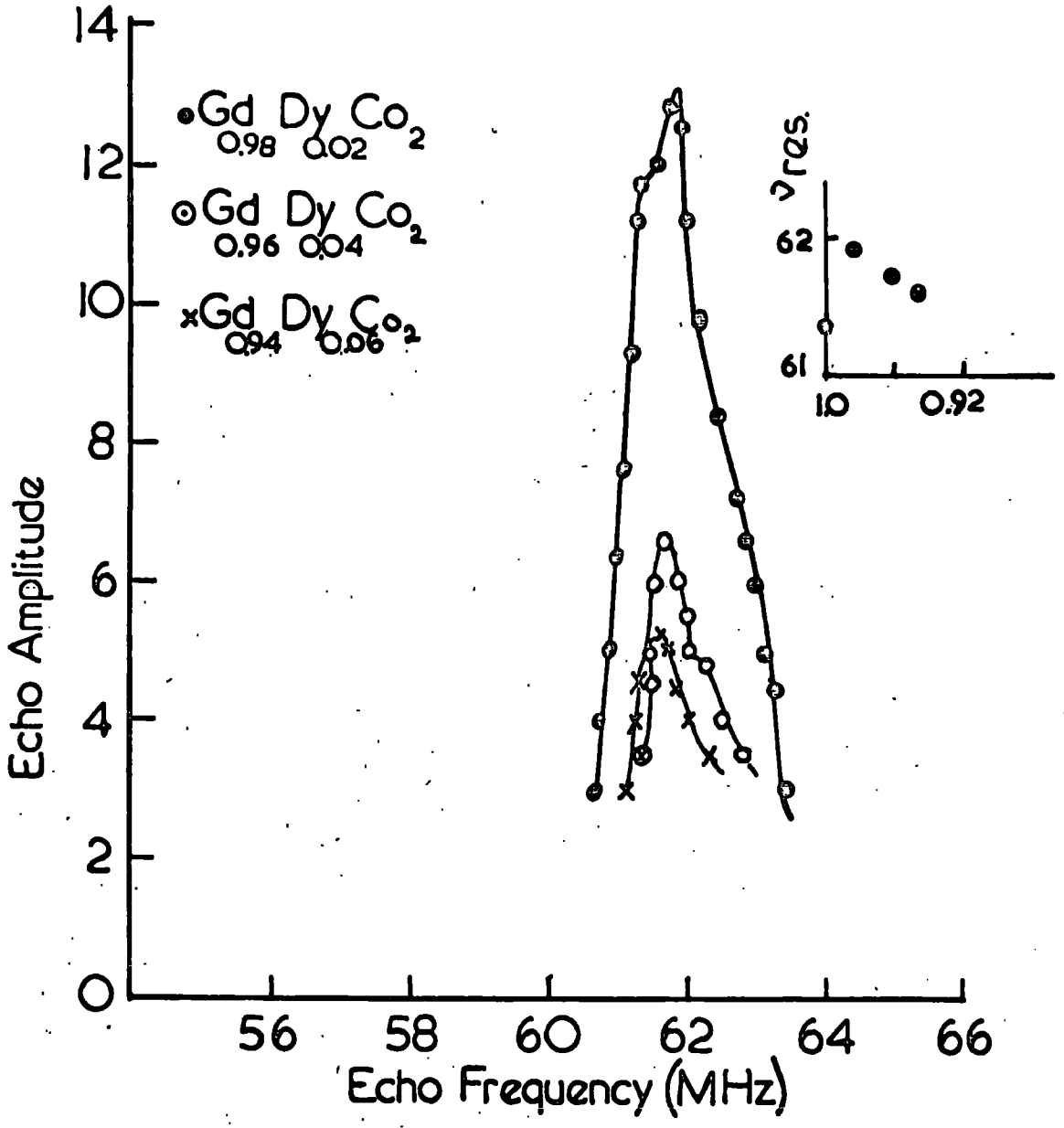
14
12
10
8
6
4
2
0
Echo Amplitude
•Gd 0.98 Dy 0.02 Co2
⊙Gd 0.96 Dy 0.04 Co2
×Gd 0.94 Dy 0.06 Co2
56
58
60
62
64
66
Echo Frequency (MHz)
νres.
62
61
1.0
0.92

Figure 3.7

in pure $DyCo_2$ but without success.

$Gd(Co_{1-x}Ni_x)_2$

3.1.4 As may be seen from figs. 3.8 and 3.9, the addition of nickel into the cobalt sites in $GdCo_2$ results in the appearance of extremely complex resonance lines. While the detail is readily analysed in the transmission frequency plot (3.8a and 3.9a) the more meaningful 'echo frequency' and 'difference frequency' graphs are much more difficult to interpret. As may be seen, the points on the echo frequency graph which arise from the wings of the transmission frequency line often given a series of echo amplitudes for one echo frequency, thus making the nature of the line shape obscure. It is interesting that the centre of gravity of the line is moved to lower frequencies when the echo frequency results are derived from the transmission results.

In spite of these difficulties it has been possible to identify some line structures in these resonances, the line positions being indicated by an arrow. The variation of the frequency of these lines with

Figure 3.8

$Gd(Co_{.9}Ni_{.1})_2$

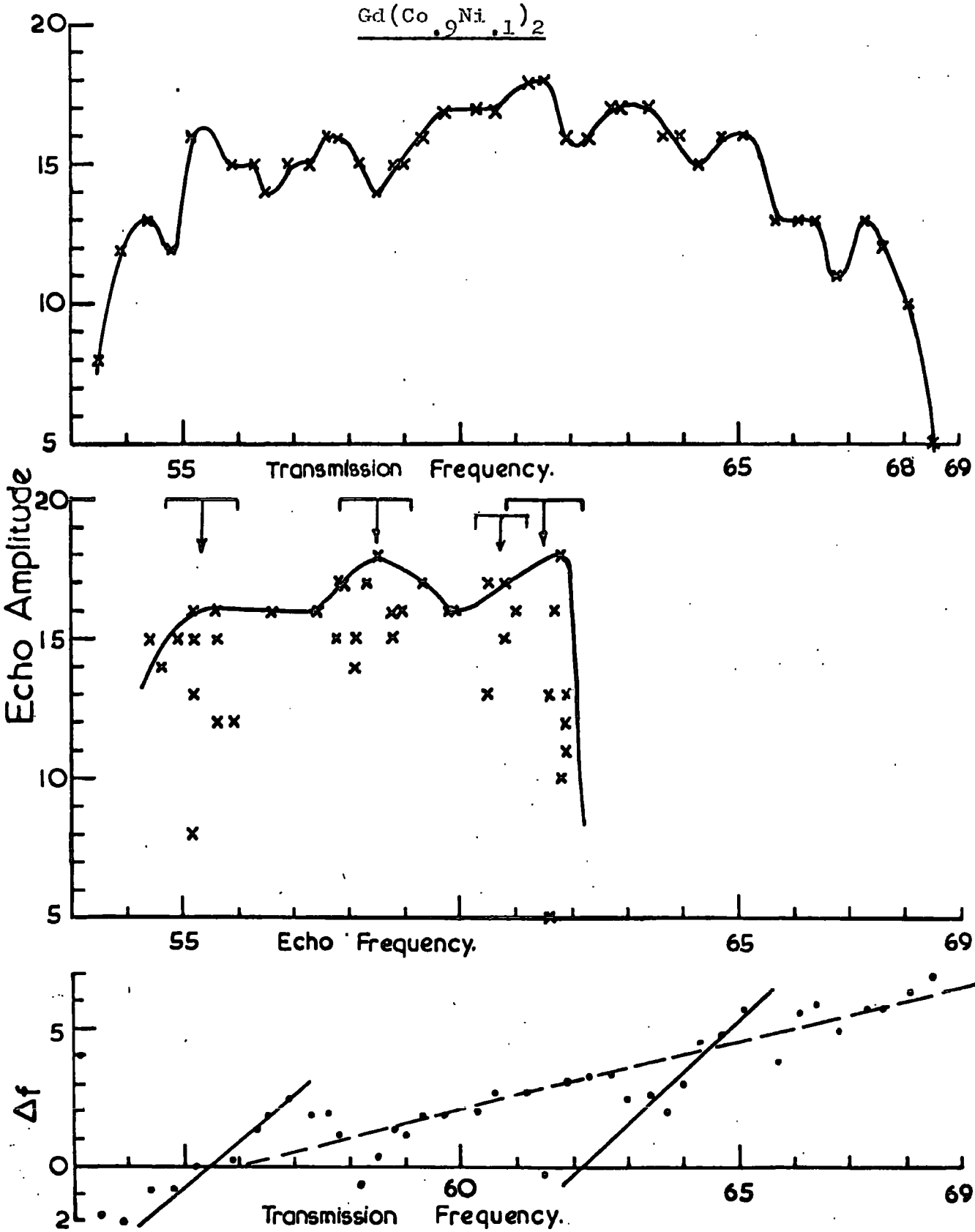

Figure 3.9

$Gd(Co_{.8}Ni_{.2})_2$

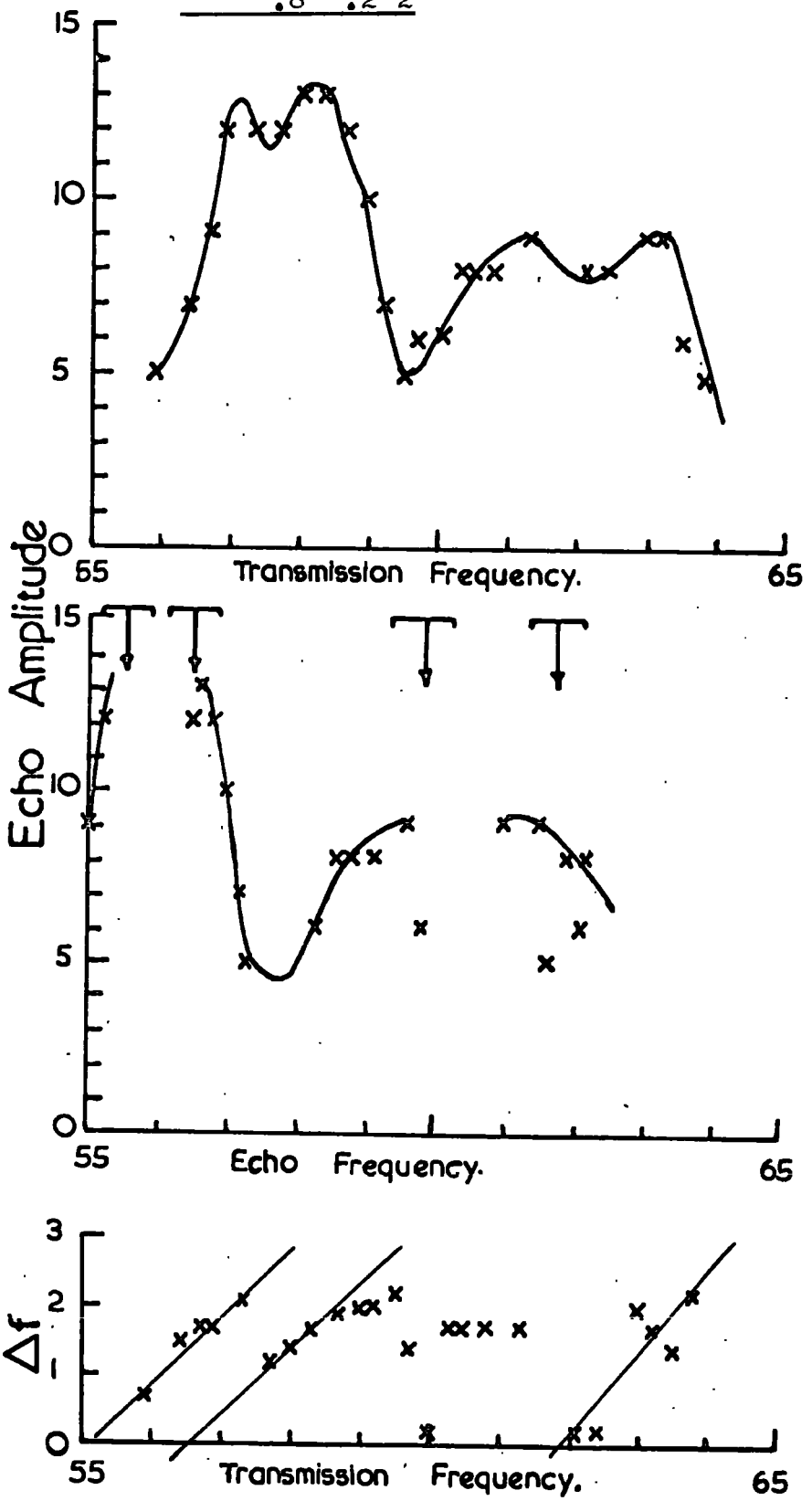

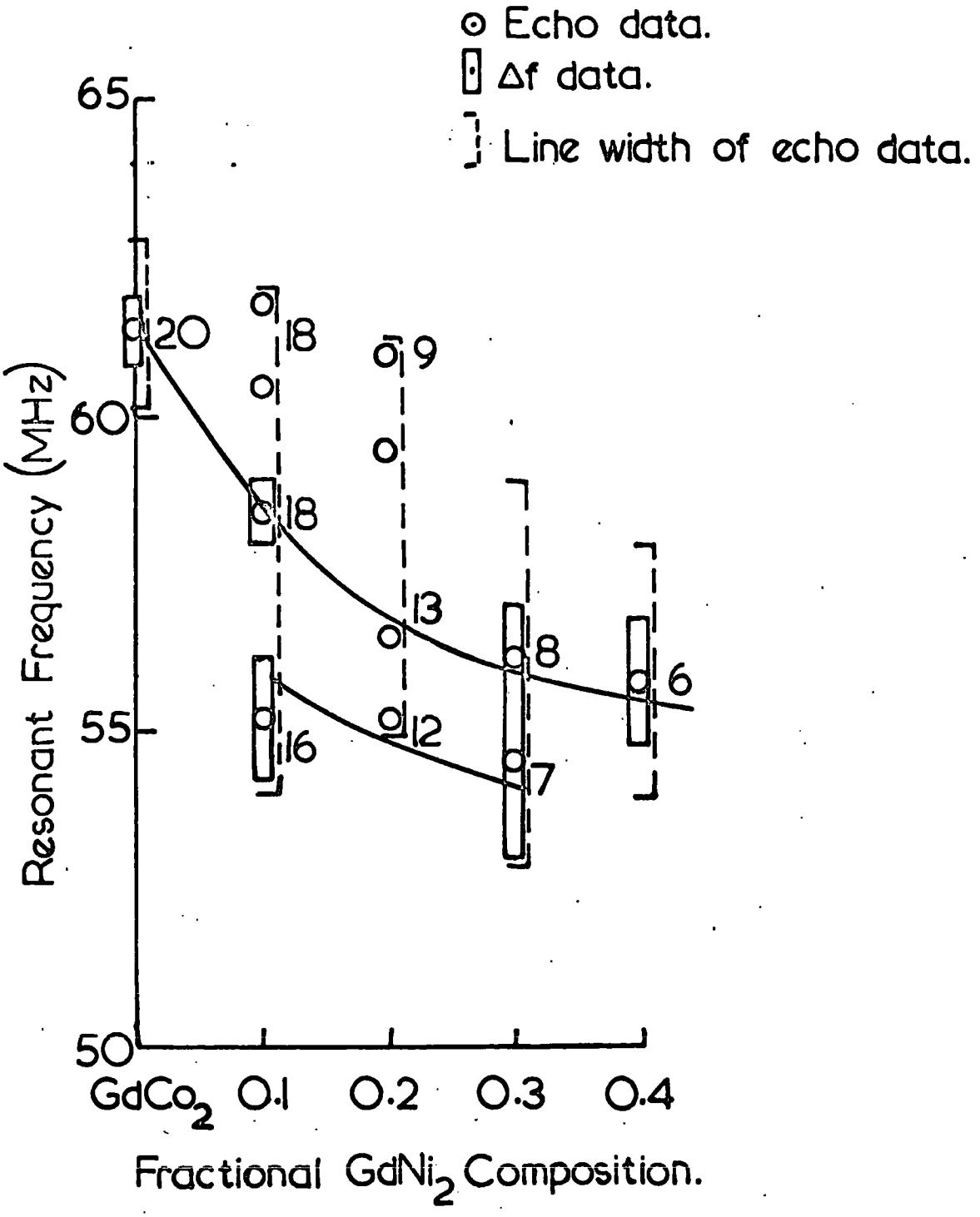
Echo data.
Δf data.
Line width of echo data.
65
60
55
50
Resonant Frequency (MHz)
20
18
18
9
13
8
6
16
12
7
GdCo2
0.1
0.2
0.3
0.4
Fractional GdNi2 Composition.

Figure 3.10

composition is given in fig. 3:10. Again there is multiple evidence for line position and the results given in this figure are based primarily on the echo frequency results. It is very evident from these measurements that the $GdCo_2$ resonance at 61.4 MHz decreases in both frequency and intensity and several new lines appear, the relative intensities of which change with nickel concentration.

Line Widths:

3.2 The variation in line width of both the transmission and echo resonance are shown for the three series examined in fig. 3:11. Here the width is defined at the half power point for the total line, since in general it was not possible to resolve the components of a given resonance.

Relaxation Measurements:

3.3 Using both two and three pulse sequences to obtain the spin echoes. It was possible to make relaxation measurements on some of the materials. The compounds on which this was achieved were the following: $GdCo_2$, $Gd_{.9}Y_{.1}Co_2$, $Gd_{.982}Dy_{.018}Co_2$ and $Gd(Co_{.9}Ni_{.1})_2$.

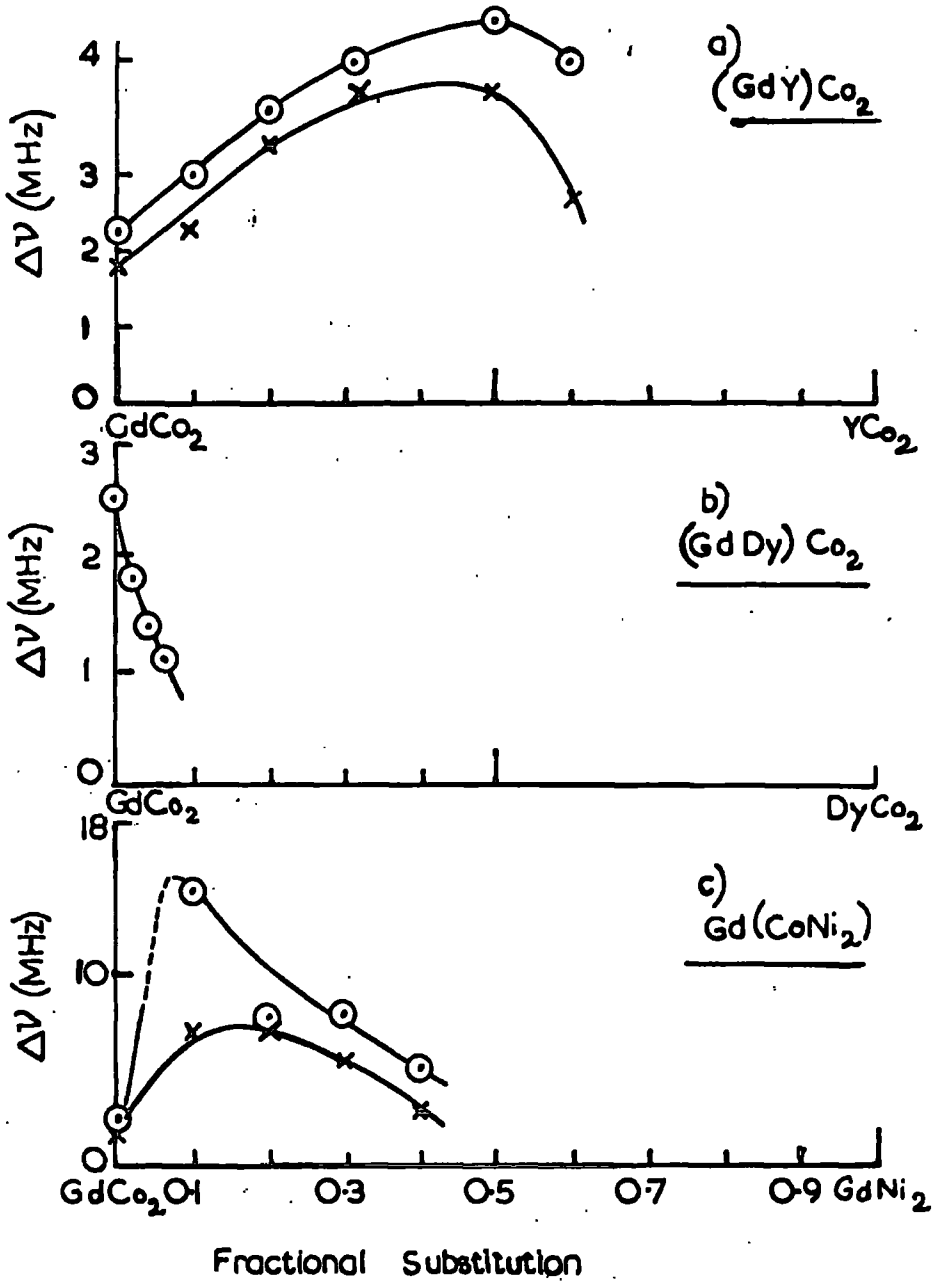

Figure 3.11

Line Width Variation

In the three pulse technique, the separation between the first and second pulses was kept constant at 25 μsec., while the delay of the third pulse was varied. All the echo amplitudes obtained in this way could be fitted to an exponential relation of the form

$$\text{Echo Amplitude} = Ae^{-t/T_1}$$

where t is the delay of the third pulse and T_1 is the longitudinal (Spin-lattice) relaxation time. The results for $GdCo_2$ at both $2.4^{\circ}K$ and $4.2^{\circ}K$ are shown in fig. 3:12, the values of T_1 being listed in Table 3:2 along with those of T_1 T(μsec. $^{\circ}K$).

The two pulse measurements were obtained by varying the separation between the two pulses and observing the echo amplitude as a function of the delay time. These observations were fitted to a function of the delay given by

$$\text{Echo Amplitude} = Be^{-t^3/\alpha}$$

where t is the delay between the pulses and $1/\alpha$ is a constant depending on the field gradient and the coefficient of spin diffusion is the sample. (App. II)

Figure 3.12

Longtitudinal Relaxation in $GdCo_2$

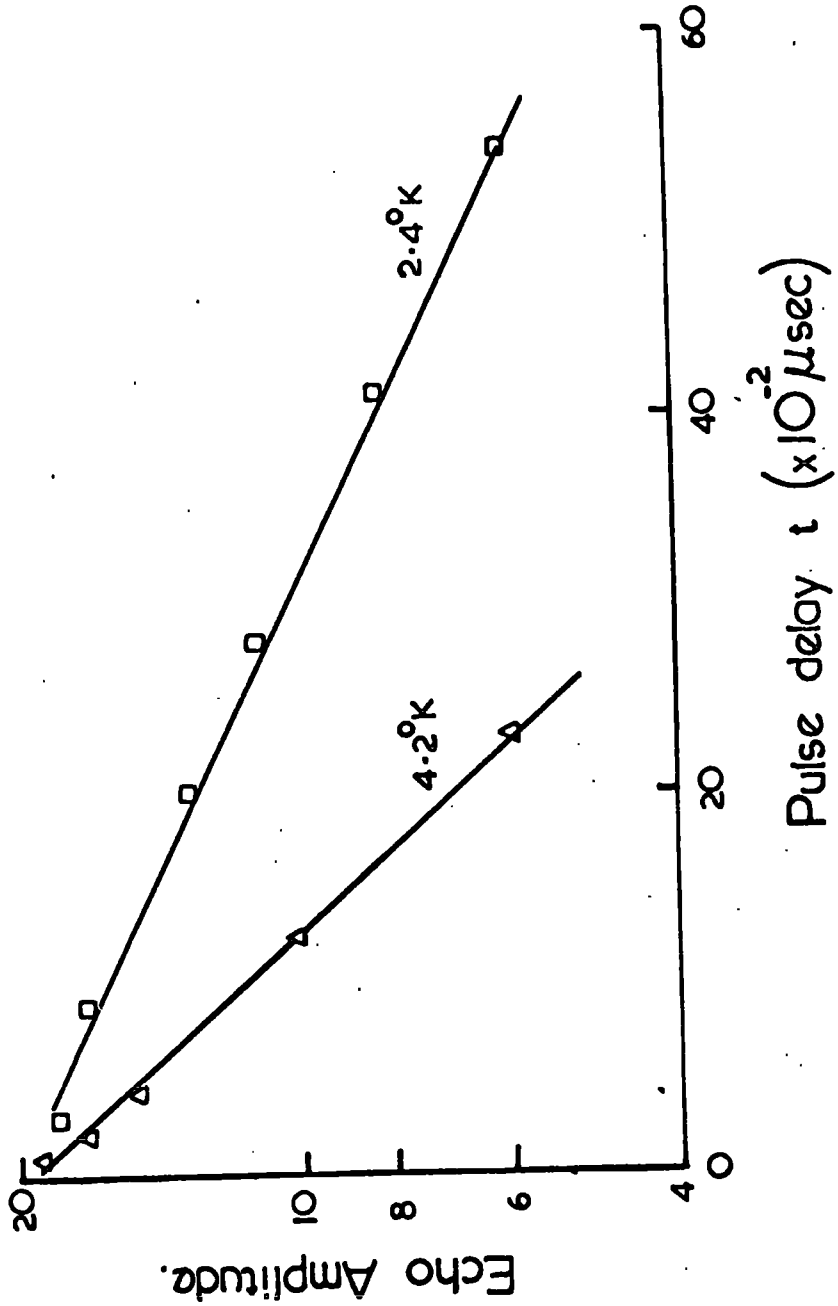

TABLE 3.2

Temperature	4.2°K			2.4°K	
Compound	α μsec^3	T_1 μsec	T_1T $\mu sec\,^oK$	T_1 μsec	T_1T $\mu sec\,^oK$
$GdCo_2$	114	1960	8250	4400	10550
$Gd_{.9}Y_{.1}Co_2$	291	2120	8900		
$Gd_{.982}Dy_{.018}Co_2$	94.5	765	3210		
$Gd(Co_{.9}Ni_{.1})_2$	252	4660	19650		

From table 3:2 it may be seen that both T_1 and α decrease when dysprosium is substituted into $GdCo_2$; whereas they both increase when yttrium or nickel is substituted.

Magnetization Measurements:

3.4 The Curie temperatures (T_C) and the saturation moments (μ_s) of the $Gd_{1-x}Y_xCo_2$ specimens have previously been reported by Taylor et al. in 1965 (ref. 3:6) and Lemaire (ref. 3:7). In the present work the Curie temperatures and magnetizations (I) were determined for the $Gd(Co_{1-x}Ni_x)_2$ series.

The values of T_C were determined in an applied field strength of 1.34 Koe by extrapolating the I^2 versus temperature curve to $I^2 = 0$. Fig. 3:13 shows the results for $Gd(Co_{.7}Ni_{.3})_2$, and is a typical example of these magnetization curves. The saturation moments were obtained by plotting the magnetization at 4.2^oK against the inverse of the field strength (for $0<H<10$ Koe) and extrapolating to $1/H = 0$.

The results obtained in this way are shown in fig. 3:14 and fig. 3:15 from which it may be seen that:

a) The Curie temperatures lie on a smooth curve

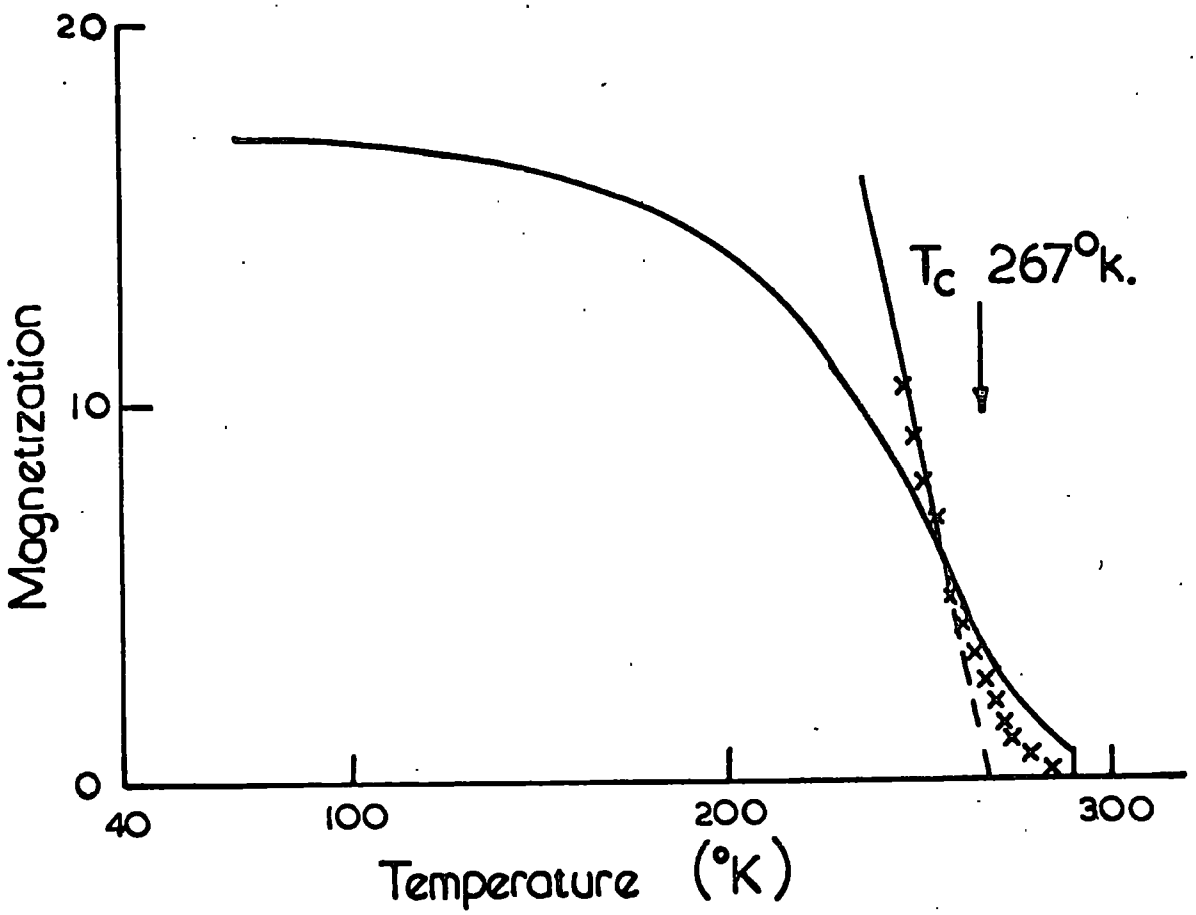

Figure 3.13

$Gd(Co_{.7}Ni_{.3})_2$ Hext. = 1.34 Koe

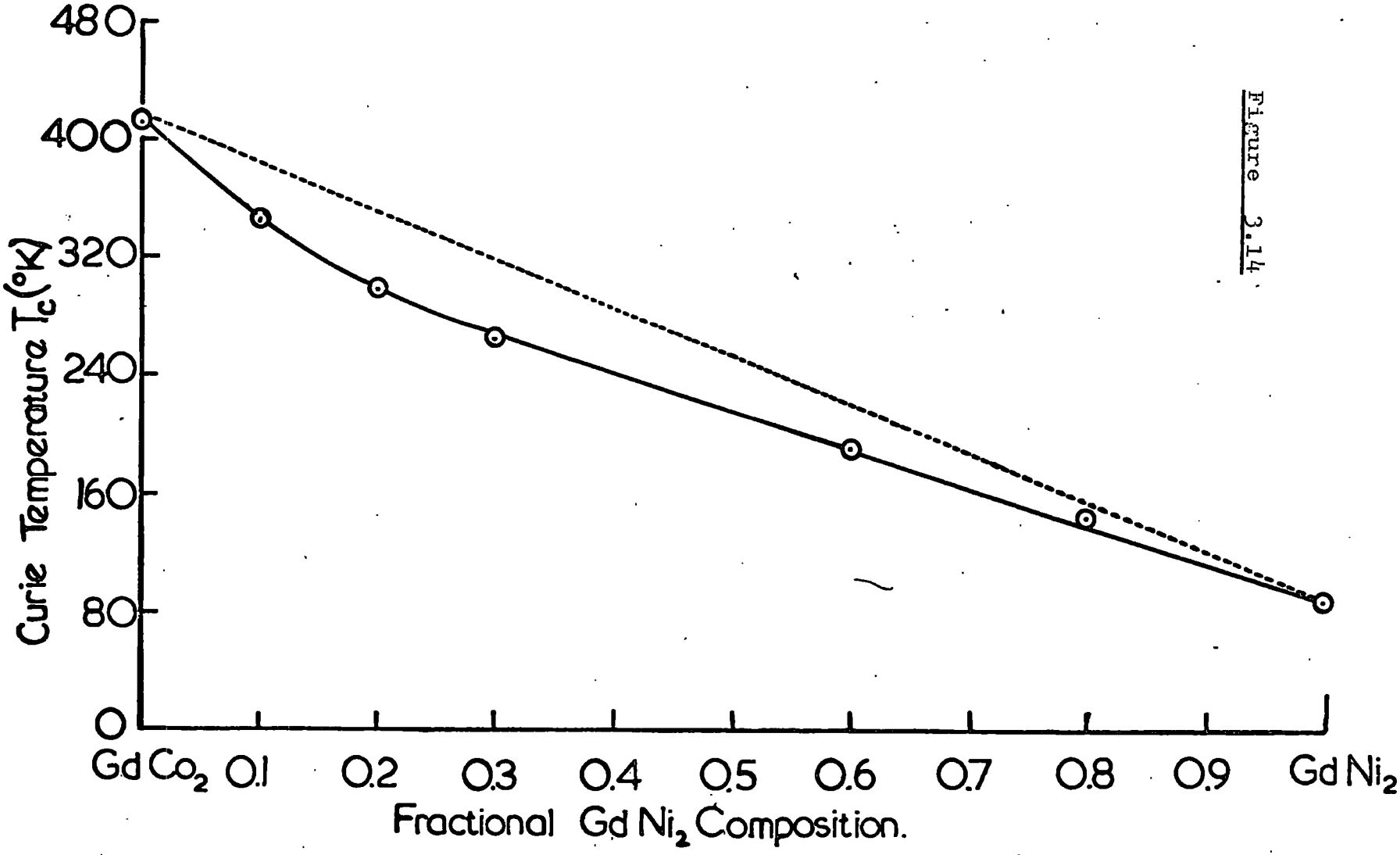
480
400
320
240
160
80
0
Curie Temperature T_c(°K)
Gd Co_2
0.1
0.2
0.3
0.4
0.5
0.6
0.7
0.8
0.9
Gd Ni_2
Fractional Gd Ni_2 Composition.

Figure 3.14

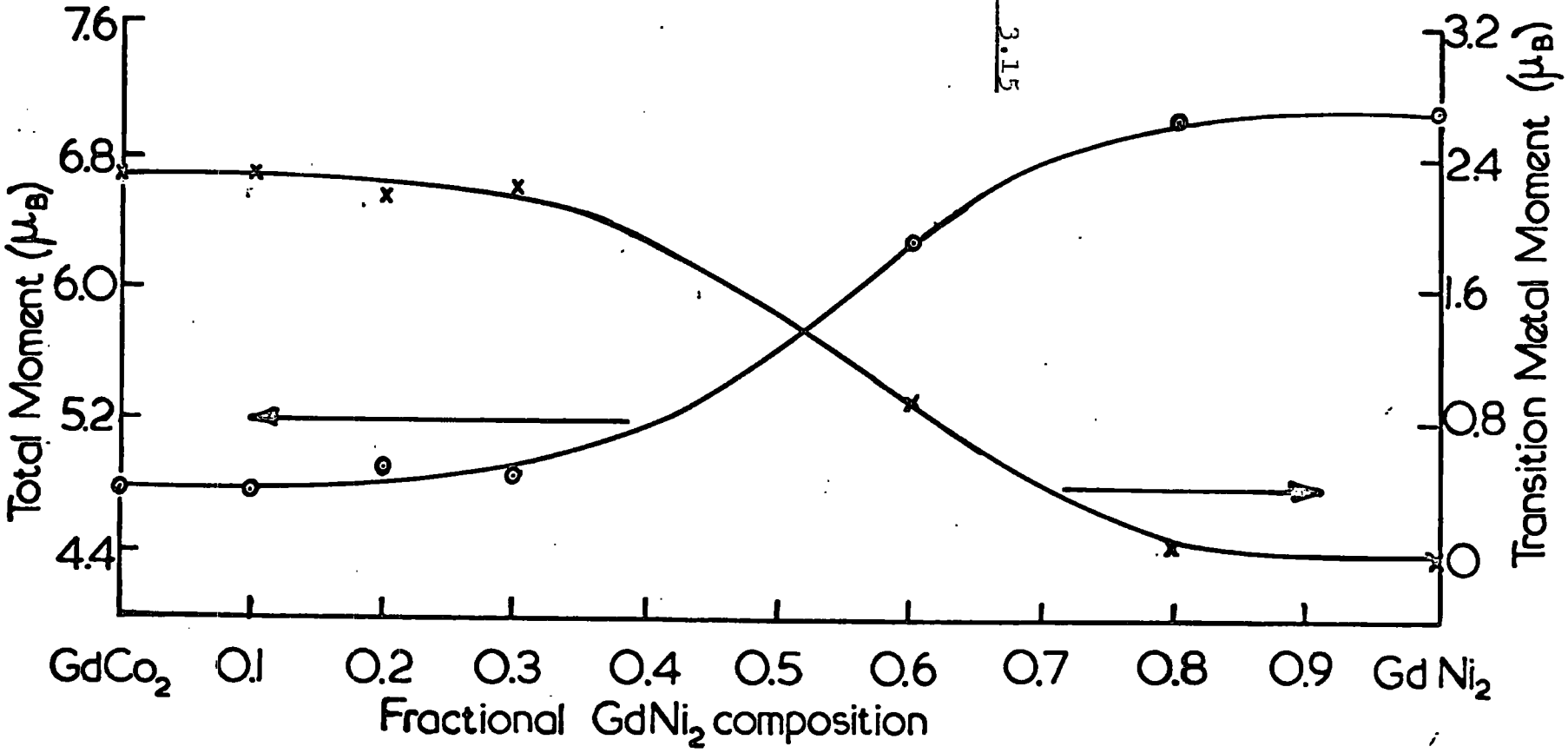
7.6
6.8
6.0
5.2
4.4
Total Moment (μ_B)
3.2
2.4
1.6
0.8
0
Transition Metal Moment (μ_B)
$GdCo_2$
0.1
0.2
0.3
0.4
0.5
0.6
0.7
0.8
0.9
$GdNi_2$
Fractional $GdNi_2$ composition

Figure 3.15

which falls below the linear interpolation between the extreme values at all compositions.

b) The moment per formula unit in the $Gd(Co_{1-x}Ni_x)_2$ series shows little change for $0 < x < 0.4$, increases rapidly between $x = 0.4$ and $x = 0.7$ and then for $x > 0.7$ remains at a constant magnitude approximately equal to that of $GdNi_2$ in which the nickel ion is believed to carry no moment.

Lattice Parameters:

3.5 All samples investigated exhibited the same diffraction lines, i.e. those of the cubic Laves phase, $MgCu_2$, structure, to which all of these compounds were expected to belong. In addition, in all photographs, there was an extra line which could not be identified. This line has been observed in other alloy series and does not appear to be characteristic of these specimens. Consequently, this line was ignored in all the measurements.

As mentioned in section 2.3.2, the lattice constants were determined from the X-ray powder photographs using

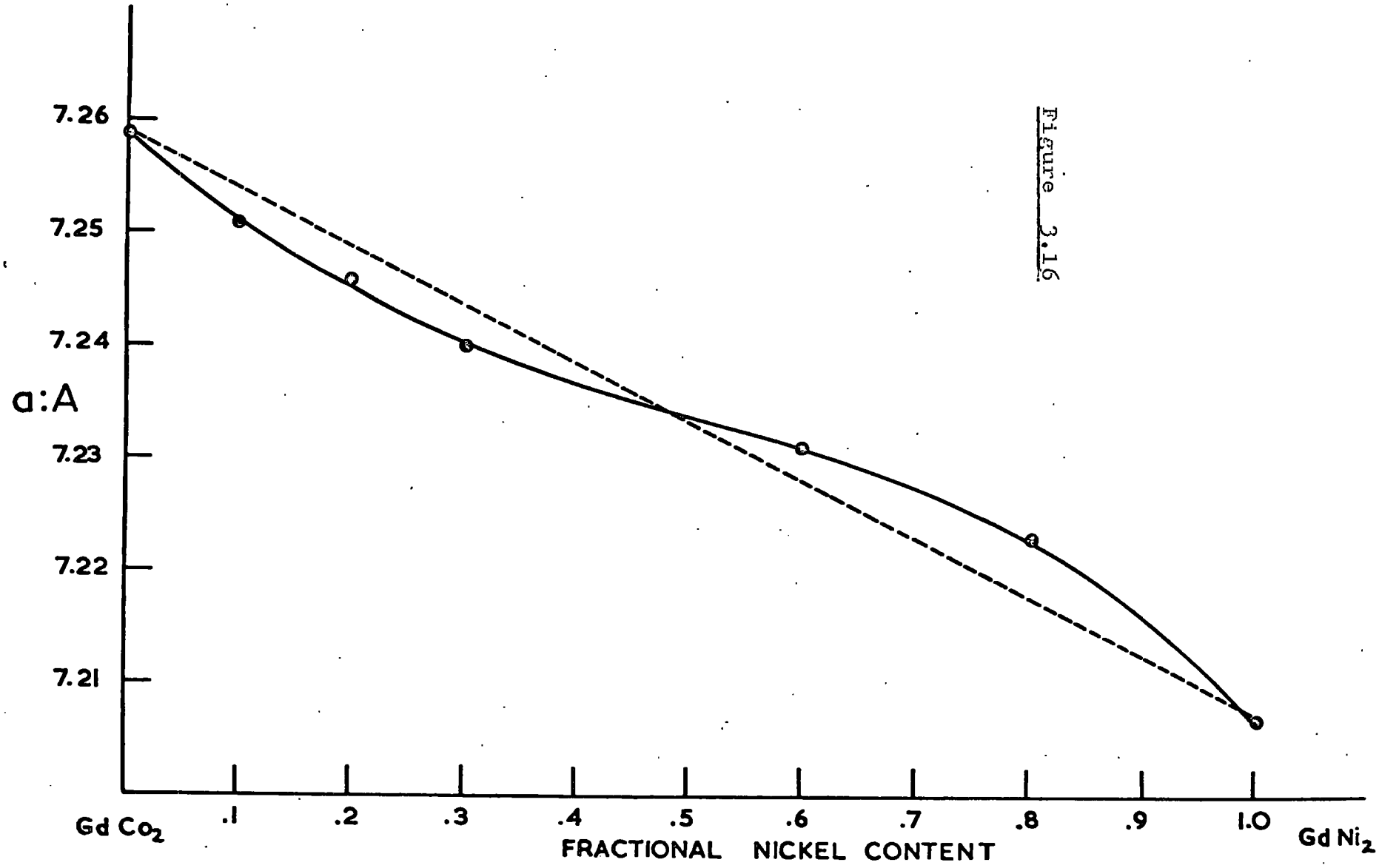
7.26
7.25
7.24
a:A
7.23
7.22
7.21
Gd Co2
.1
.2
.3
.4
.5
.6
.7
.8
.9
1.0
Gd Ni2
FRACTIONAL NICKEL CONTENT

Figure 3.16

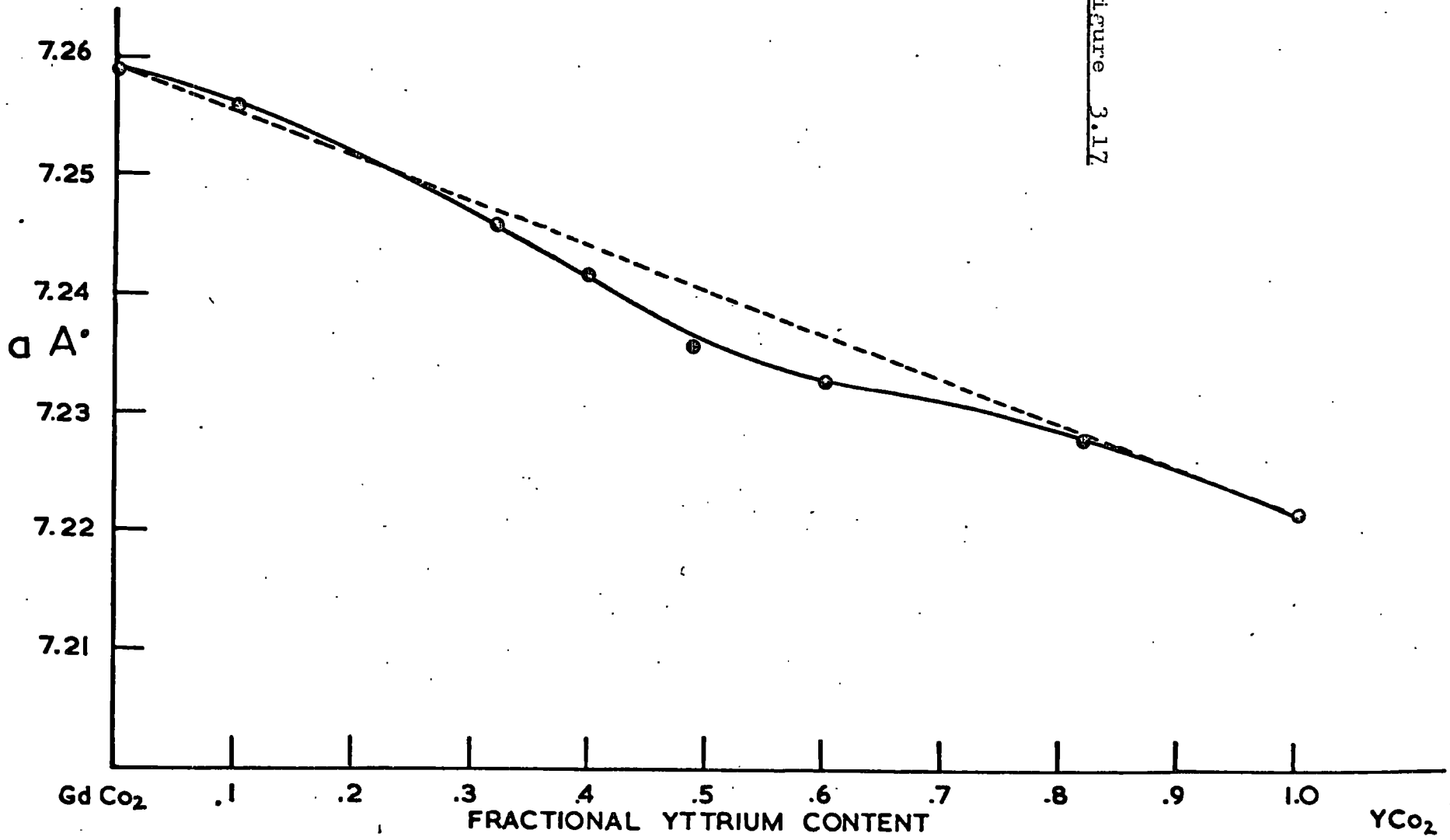
7.26
7.25
7.24
a A°
7.23
7.22
7.21
Gd Co2
.1
.2
.3
.4
.5
.6
.7
.8
.9
1.0
YCo2
FRACTIONAL YTTRIUM CONTENT

Figure 3.17

the Nelson-Riley extrapolation function. The results for the $Gd(Co_{1-x}Ni_x)_2$ series are shown in fig. 3:16, from which it may be seen that the spacings of compounds with high cobalt concentration lie slightly below the line giving Vegards Law and those with low cobalt concentration lie above this line. The $Gd_{1-x}Y_xCo_2$ series (fig. 3:17) also shows a deviation from Vegards Law, the deviation being negative for all compositions except $x>0.8$. No lattice parameters were determined for the $Gd_{1-x}Dy_xCo_2$ series.

oOo

CHAPTER IV

D I S C U S S I O N

The Nature Of The Resonance Observations:

4.1 In section 3.1, it was reported that the echo frequency and transmission frequency are not equal at all points across the resonance line. Reports of similar effects have been made by M.B. Stearns (ref. 4:1) and Budnick and Skalski (ref. 4:2). Meanwhile Mims (ref. 4:3) has examined the shape of the echo wave forms in an electron echo apparatus for which the r.f. field intensity is less than the linewidth. In this work he shows that the echo signal obtained is the resultant of several spin packets spaced at different frequency intervals from the centre of the resonance line. The major echo contributions are then obtained from spin packets in the range $-w_1 < \Delta w < w_1$ where Δw is the frequency difference between the spin packet and the input (or transmission)

frequency and $w_1/\gamma = H_1$, the r.f. field intensity.

In ferromagnetic specimens, the r.f. field intensity is enhanced by several orders of magnitude as a result of the well established domain wall enhancement effect. Consequently, a given transmission frequency can excite spin packets over a wider range, so that forced resonance may occur when the transmission frequency is completely outside the true resonance line. When the driving pulse is switched off, the nuclei precess at their natural frequency and hence a discrepancy may be observed between the transmission and echo frequencies. It is the opinion of the author that such an effect is responsible for the nature of the observations reported in section 3.1.

$Gd_{1-x}Y_xCo_2$ Compounds:

4.2 Several authors have reported on the hyperfine fields found in ferromagnetic elements and compounds. In particular Gossard and Portis (ref. 4:4) reported a resonance frequency in cobalt at absolute zero of 217.2 MHz indicating a hyperfine field of 216.5 Koe. This field was originally assumed to be

positive, i.e. parallel to the ionic magnetization, however subsequent work by Hanna et al. (ref. 4:5) on the sign of the field at the Fe^{57} nucleus in iron showed that in this case it was negative and these authors suggested that this might be the same in cobalt. In 1965 Gossard et al. (ref. 4:6) confirmed that this was true.

Previous to Hanna's work it had been assumed that the hyperfine fields were always positive since the major negative term then known, the core 's' electron polarization, was considered too small to dominate the positive contributions from the other terms. Anderson and Clogston (ref. 4:7) suggested as a possibility the existence of a negative contribution from the conduction electrons arising from the covalent interband mixing between the s and d bands.

An experimental determination of the various contributions to the cobalt hyperfine field has not been reported, however an attempt has been made in the case of gadolinium to distinguish between the factors affecting the field at the gadolinium nucleus. From

an examination of the hyperfine field at the europium nucleus in an Eu-Yb alloy system, Hüfner (ref. 4:8) deduced that there were two approximately equal but opposite contributions to the gadolinium field over and above the core polarization term. These were;

a) the contributions from the conduction electrons (C.E.) polarized by the 4f electrons of the ion concerned

and b) overlap contributions from the neighbouring ions plus the contribution from the conduction electrons polarized by these neighbours. The 'neighbour' contribution due to b) was negative while the 'own' contribution a) was positive.

In the present work with $GdCo_2$ only one resonance frequency was observed and as explained in 3.1.1 this was taken to the Co^{59} resonance corresponding to a hyperfine field of 60.8 Koe.

If the 3d electrons at the cobalt ion site are localized then this field can be ascribed to three general sources, namely:

aa) the 'own' field which includes core polarization and C.E. polarization by its own ionic moment.

bb) the field due to overlap and C.E. polarization by neighbouring cobalt ions.

cc) the field due to overlap and C.E. polarization by neighbouring gadolinium ions.

If however, the cobalt moment is an itinerant electron moment, as seems likely from the observations of Piercy and Taylor (ref. 4.9) then the contributions from a) and b) are indistinguishable.

By substituting non-magnetic yttrium ions for gadolinium in $GdCo_2$, it had been hoped to determine the contribution of c) to the cobalt hyperfine field. However, Lemaire (ref. 4:10) has shown that in the compounds $Gd_{1-x}Y_xCo_2$ the cobalt moment varies across the series from about 1.1 μ_B to less than 0.1 μ_B with increasing yttrium content. If this is the case then the variation in the gadolinium contribution c) due to alloying may be masked by the corresponding change in the hyperfine field caused by the varying cobalt

moment. The results of fig. 3:10, indicates that in this series of compounds only a very slight change occurs in the hyperfine field at the cobalt nucleus as the rare earth sublattice is diluted with up to 60% yttrium. This is somewhat surprising since associated with the change in the rare earth environment of any cobalt ion there is a corresponding change in the moment of the six nearest neighbour cobalt ions and of the moment of the ion itself. This change in cobalt moment was shown by Lemaire to be a 30% decrease at 60% yttrium content.

In view of these large changes in the factors which one might expect to affect the nuclear field, we are forced to consider two possibilities in attempting to understand the behaviour of this field. These are as follows:-

(i) There is little or no change in either of the contributions aa) plus bb), cc) to the hyperfine cobalt field

(ii) The changes in the cc) contribution is approximately balanced by corresponding changes

in the aa) and bb) terms in the nuclear field.

The first of these alternatives requires that the gadolinium ionic moment makes no contribution to the cobalt hyperfine field and that either the cobalt moment does in fact remain constant across the series in contradiction of Lemaire or that the various effects due to changes in this moment (C.E. polarization, core electron polarization and the d shell contribution) are exactly balanced at all compositions.

The behaviour of the cobalt ionic moment across the series was obtained by Lemaire, from observations of a decreasing saturation magnetization of the mixed compounds in going from $GdCo_2$ to YCo_2. Since yttrium has no moment, the almost zero moment of YCo_2 can be understood either from an antiferromagnetic ordering of the cobalt sublattices or from a lowered ionic moment. Neutron diffraction studies on related RCo_2 compounds (ref. 4:11) indicate that the intra-cobalt sublattice coupling is ferromagnetic and it seems reasonable to extend this result to the case of YCo_2. In addition, the Curie temperatures of the (GdY) Co_2

series were found to be proportional to the cobalt moment under the assumption of a ferromagnetic coupling. If we take this temperature to give an indication of the sum of the exchange energies (Gd-Gd, Gd-Co, Co-Co) present in the compounds and assume that the Gd-Gd exchange energy can be represented by the Curie temperature of 78°K observed for $GdNi_2$ (Nickel is known to carry zero moment in this compound), then the negligible Curie temperature reported by Lemaire for YCo_2 must be due to a small Co-Co interaction which in turn may arise from a small cobalt moment. Consequently, it would appear that the cobalt moment does indeed vary from $GdCo_2$ to YCo_2.

If this is so, we are left to examine whether the various contributions due to this moment can vary so as to leave their total effect constant. Clearly this can not be true for zero cobalt moment, however, as direct observations were only made to $Gd_{0.4}Y_{0.6}Co_2$, for which the cobalt moment is still $0.73\mu_B$, we are not concerned with this limiting case. In order to see if this balancing could occur, let us examine the

results obtained for the Fe^{57} hyperfine field in the RFe_2 compounds.

In these iron compounds, the field at the iron ion nucleus has been shown by Wertheim and Wernick (ref. 4:12) to remain constant at approximately 230 Koe independent of the rare earth with which it is associated in the compound. These authors used this constant field value to argue that the iron atomic configuration (and therefore moment) and the conduction electron polarization, were also independent of the rare earth involved in the compound. However as Piercy and Taylor (ref. 4:13) have shown the iron moment is not the same in all of these compounds but varies in a range from 1.5 μ_B to 2.2 μ_B. Consequently, it would appear that in these compounds too, the various contributions to the hyperfine fine adjust as the rare earth sublattice is changed, so as to leave the magnitude of the field almost constant.

This can occur either by the contributions from the iron ions moment just cancelling or alternatively the change in the rare earth contribution is compensated

for by the change in the iron ion contribution. If this second alternative is to be applicable, then the iron ion moment must be dependent on the value of the spin of the rare earth element, since it is the spin of the rare earth ions which will determine their contribution to the iron hyperfine field. As the result of a series of measurements on substituted RFe_2 compounds Piercy and Taylor (ref. 4:9) indicated that the iron ion moment is an iterant electron moment and consequently, its value will depend on the difference in the occupation of the spin-up and spin-down sub-bands of the iron 3d band.

At absolute zero these sub-bands are fully occupied up to the Fermi energy (E_f) and empty above that energy. Exchange interactions cause the sub-bands to be displaced along the energy axis with respect to each other, resulting generally in a difference in the occupation of the two bands and hence in a macroscopic moment. To a first approximation the Curie temperature may be taken as an indication of the strength of the exchange interaction and consequently

of the energy spearation between the two bands.

The Curie temperatures of the RFe_2, RCo_2 and RNi_2 compounds are shown in Figure 4:1 versus the rare earth element R. In general these temperatures vary in a regular way with the spin of the element, gadolinium always having the largest value. Following the argument given above it may then be expected that the iron moment should also depend to some extent on the spin of the rare earth metal. That this is indeed the case is obvious from Figure 4:2 in which the iron moment is plotted as a function of the Curie point for each of the heavy rare earth elements (ref. 4:13).

With both the iron moment and the rare earth contribution to the hyperfine field depending on the rare-earth spin, it remains to show that these two are in opposition. That this is so, is evidenced by the decrease of the iron nuclear filed in RFe_2 compounds to approximately 230 Koe, as compared to the field of 340 Koe in metallic iron.

From the above, it seems likely that the iron

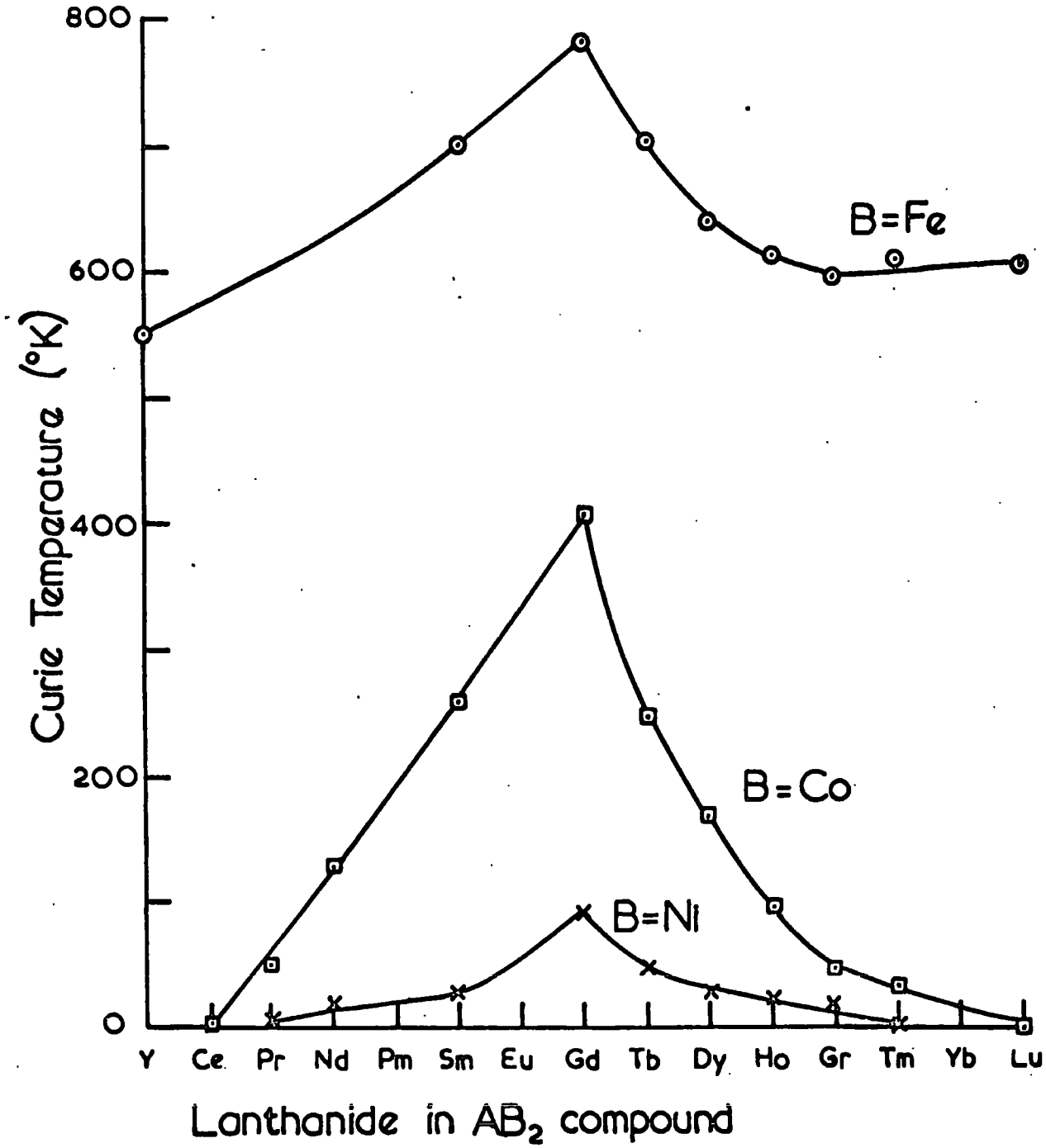
800
600
400
200
0
Curie Temperature (°K)
B=Fe
B=Co
B=Ni
Y
Ce
Pr
Nd
Pm
Sm
Eu
Gd
Tb
Dy
Ho
Gr
Tm
Yb
Lu
Lanthanide in AB_2 compound

Figure 4.1

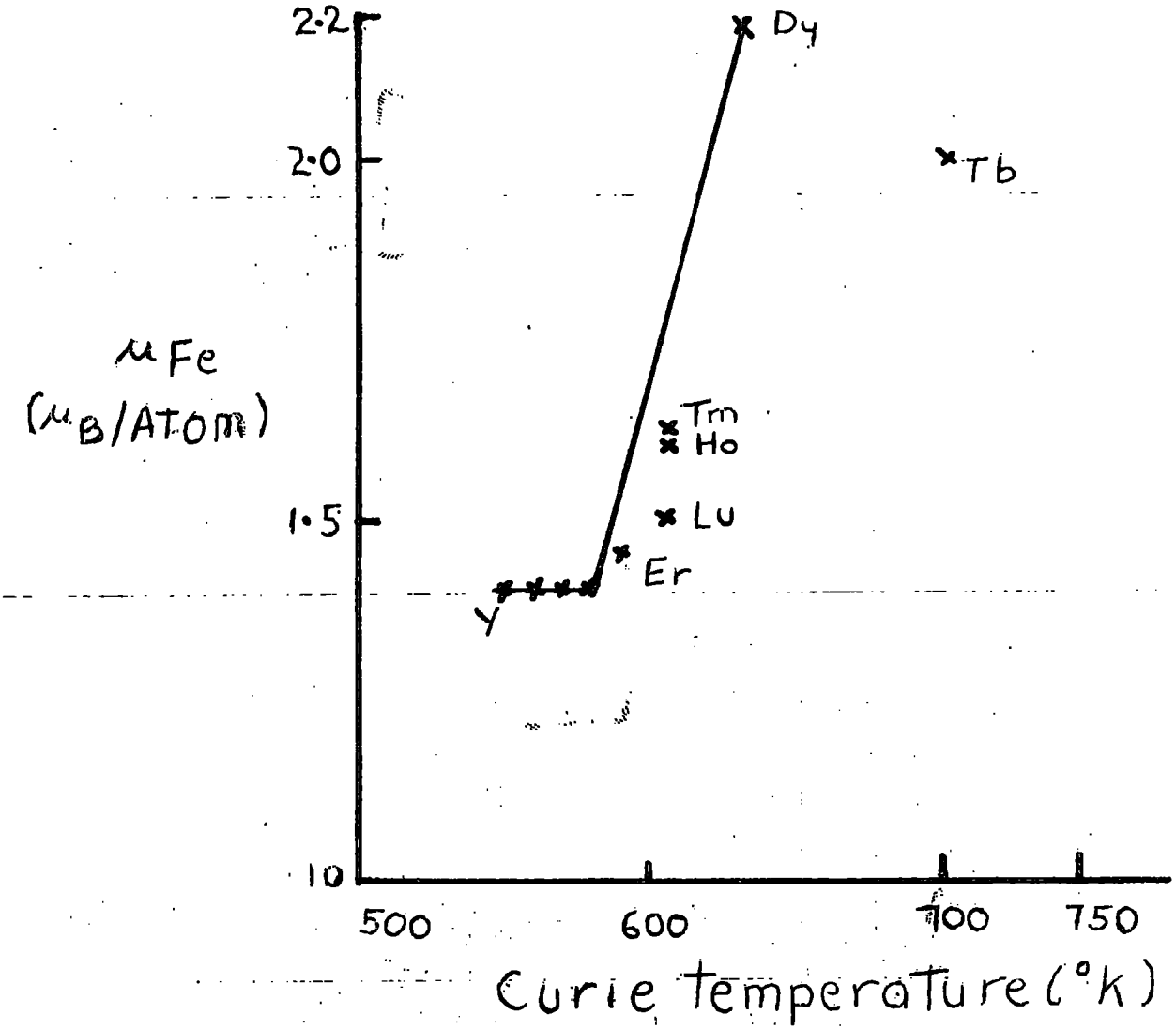

Figure 4.2

Variation of μ_{Fe} with T_C in RFe_2 Compounds

hyperfine field remains constant in these compounds as a result of cancellation of the changes due to the variation in the iron ion moment and the rare earth spin moment.

Returning to the $Gd_{(1-x)}Y_xCo_2$ observations, it appears that the near constnat cobalt hyperfine field may be explained on a similar basis to the above. The cobalt moment is directly proportional to the exchange energy as measured by the Curie temperature (Lemaire, ref. 4:10). This temperature is, in turn, proportional to the fraction (1-x) of gadolinium ions present per formula unit of the compound (up to 1-x = 0.6); hence it is proportional to the mean spin magnetic moment of the gadolinium - yttrium sublattice. This, therefore, gives a direct relationship between the effective rare earth spin and cobalt ionic moment.

As the spin dipole contribution to the cobalt hyperfine field is fairly small, the decrease in the magnitude of the cobalt moment and the consequent alteration in this contribution will not have too large an effect on the resonant frequency. On the

other hand, the contact hyperfine terms due to both core polarization and C.E. polarization are the main contributors to the hyperfine field, and both may tend to decrease in magnitude with a decrease in the cobalt moment. However, some C.E. polarization arises from the rare earth spin, but it can be shown that this polarization is in opposition to the previous two.

The orbital moment of cobalt ions is normally quenched by the crystal field and may be ignored in calculation of the hyperfine field. Therefore all the contributions of the cobalt ions to their own field are proportional to the cobalt spin ionic moment. The decrease of this moment from 1.7 μ_B in pure cobalt to 1.05 μ_B in $GdCo_2$, should then result in a decrease in the hyperfine field from 213 Koe to about 130 Koe. The observed field of 60 Koe must therefore result from a gadolinium contribution to the C.E. polarization which opposes the remainder of the hyperfine field. A smaller value of the gadolinium spin would therefore tend to increase the hyperfine field but this is slightly more than compensated for by the

proportional decrease in the cobalt moment.

On the basis of this analysis it should be possible to represent the hyperfine field at the cobalt nucleus as the sum of two contributions. The first of these is proportional to the cobalt moment and may be given as

$$H_{Co.\mu} = 213.\frac{\mu_{Co}}{1.7}$$

That is, we are scaling down from the cobalt metal case. The second term results from the polarization of the conduction electrons by the rare earth (gadolinium) ions, and as we have shown this is in opposition to the cobalt contribution. By subtracting the observed hyperfine field values from those given by $H_{Co.\mu}$ for all the compounds across the series the magnitude of the contribution to the field from the rare earth sublattice may be obtained. Table 4.1 and Figure 4:3 shows the breakdown of these component values as a function of (1-x). From these results it is evident that over most of the range the contribution due to the rare earth sublattice is indeed

TABLE 4.1

1-x	1	0.9	0.8	0.7	0.6	0.5	0.4	0.3
$\mu_{obs.}$ Lemaire μ_B	1.05	1.02	1.0	.93	0.86	.81	0.73	0.65
$-H_{Co.\mu}$ Koe	131.5	128	125.1	116.3	107.5	101.2	91.5	81.5
$H_{obs.}$ Koe	60.7	59.9	59.7	59.6	59.5	59.5	59	(57.5)
$H = H_{CE}$ (due to RE) Koe	70.8	68.1	65.3	56.6	47.9	41.7	32.5	(24)

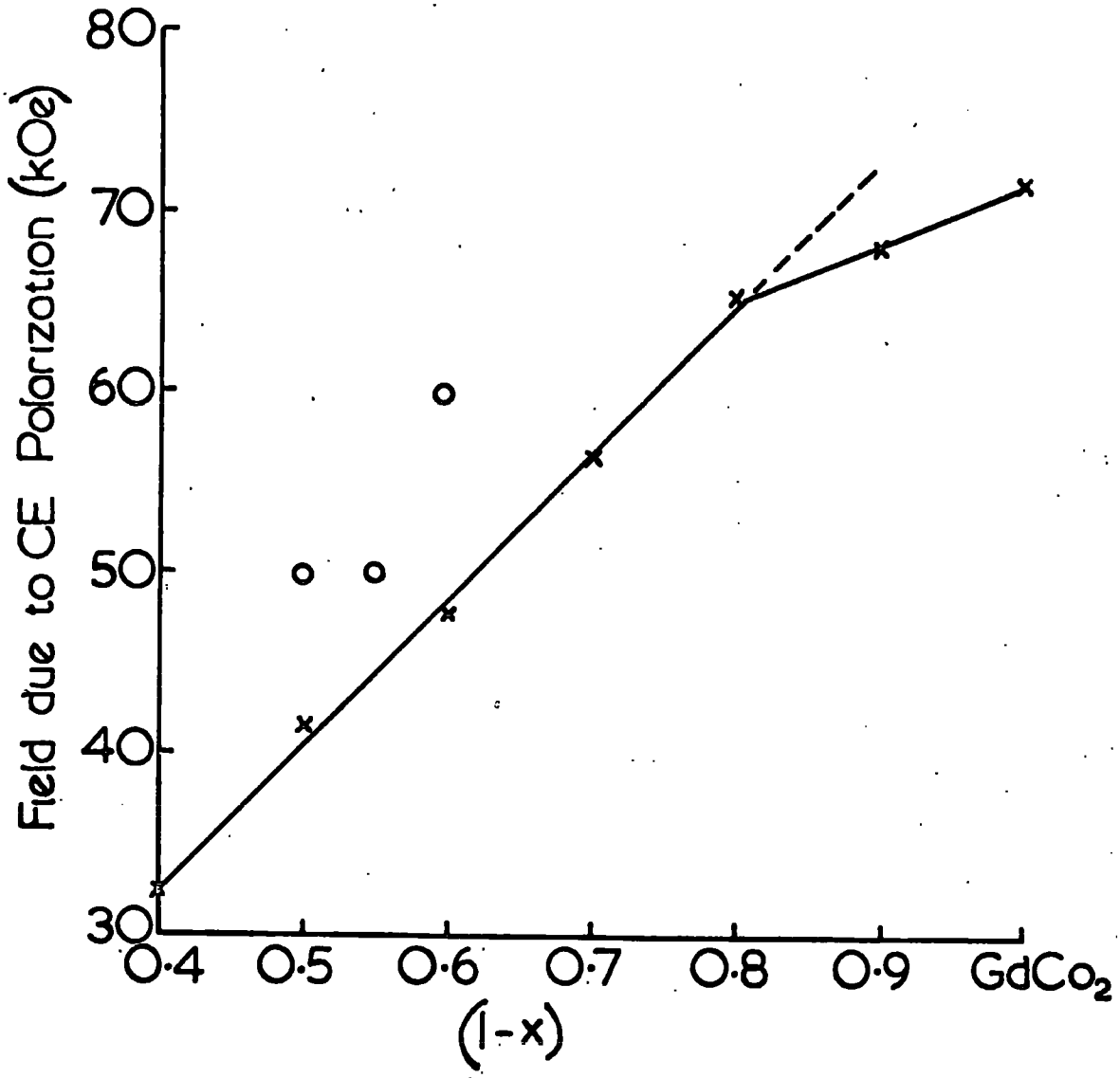
80
70
60
50
40
30
Field due to CE Polarization (kOe)
0·4
0·5
0·6
0·7
0·8
0·9
GdCo2
(1-x)

Figure 4.3

directly proportional to the average moment of the ions in the sublattice. At high gadolinium concentration however, it deviates appreciably from this linear variation. It must be remembered however, that this variation has been obtained using an assumption that $H_{Co.\mu}$ is directly proportional to the cobalt moment. It seems likely that the conditions will not be as ideal as this and in practice one should probably allow some slight nonlinearity in the variation of both the cobalt and rare earth contributions to the hyperfine field.

Any such nonlinearity however, would appear to occur near the $GdCo_2$ composition, as the results in fig. 4:3, for $(1-x) < 0.8$, pass through the origin, indicating direct proportionality for all but the highest gadolinium concentration.

The variation in the linewidth of these compounds, shown in fig. 3:11a, may be examined in terms of the statistical distribution of the yttrium and gadolinium ions about the cobalt ions. If we consider that the nearest neighbour gadolinium interaction is predominant,

TABLE 4.2

YCo_2 Composition	0	.17	.33	.5	.67	.83	1.0
$\Delta\nu$ predicted (MHz)	2	4	8	10	8	4	2
$\Delta\nu$ observed (MHz)	2	3	4	4	1	?	?

TABLE 4.3

$GdNi_2$ Composition	0	0.1	0.2	0.3	0.4	.5
*$\Delta\nu$ predicted (MHz)	2	4	8	8	4	2
$\Delta\nu$ observed (MHz)	2	7	7	6	4	?

*based on $\Delta\nu$= 0 for composition 0.6

then the width of the line across the series may be obtained from the different distributions of the yttrium and gadolinium atoms among the nearest neighbour sites. If the basic linewidth of any resonance is comparable to that in the terminal compound, then the predicted linewidth is as given in Table 4.2. The experimental values are also given for comparison.

Two things are immediately apparent, namely:-

i. The observed linewidths are very much less than those predicted on nearest neighbour terms only; consequently it would seem that the rare earth-cobalt interaction is a long range interaction which would tend to give a narrower line.

ii. The form of the experimental variation at high $GdCo_2$ compositions is similar to the predicted variation, but for more than 50% YCo_2 composition, the experimental linewidth falls off rapidly. In this region, of course, the cobalt moment is itself decreasing, and in turn depends to some extent on the

gadolinium-yttrium environment. Analysis of this case is then rather complicated, particularly since the rare earth cobalt coupling is a long range interaction.

The $Gd(Co_{1-x}Ni_x)_2$ Series:

4.3 As has been stated earlier, the nickel ion in all the RNi_2 compounds appears to carry zero moment. If its 3d electrons are localized, then the substitution of nickel for cobalt in $GdCo_2$ should enable an estimate to be made of the effect of varying numbers of neighbouring cobalt ions on the hyperfine field at the cobalt nucleus. If however, the nickel 3d electrons enter a 3d band which is formed from both cobalt and nickel states, then the substitution of nickel for cobalt must be considered as the addition of one electron per nickel ion to this band. This will lead to a change in moment of the transition metal ions and consequently result in a change in the hyperfine field.

Referring to Section 3.4, we find that the moment of the transition metal sublattice remains almost constant in the series $Gd(Co_{1-x}Ni_x)_2$ for $x < 0.4$, but beyond

this collapses rapidly to zero and remains zero to $x = 1$.

In terms of a localized transition metal moment one would expect a linear variation of the moment between the terminal values. The fact that this is not observed must be taken as evidence for the existence of an itinerant electron behaviour associated with the nickel ions. As we have seen this is also the case for both the iron and cobalt ions in the RFe_2 and RCo_2 compounds respectively.

Referring to the earlier Section 4.2, we see that the decrease in exchange energy of $Gd_{1-x}Y_xCo_2$ leads to a decrease in the separation of the cobalt spin-up and spin-down sub-bands and consequently to a decrease in the observed cobalt moment. In the present case, the Curie temperature measurements (fig. 3:14) again indicate a decreased exchange energy but not an associated decrease in transition metal moment. Unlike the case of yttrium substitution in which no electrons are added to the cobalt 3d band, the extra electron donated by the nickel ions must enter one of the 3d

sub-bands.

The low Curie temperatures make it possible that the band separation is sufficiently small for the Fermi level to intersect both sub-bands. In such a case, Mott (ref. 4:14) has suggested that as electrons are added to the band the Fermi level in the spin-down sub-band may be trapped at a minimum in the density of states curve until the spin-up band is full. This will tend to increase the moment in opposition to the decrease in moment due to the fall in band separation as the exchange interaction decreases. In the event, these two varying moments just cancel, leaving the moment constant to about 30% nickel substitution. Once the spin-up sub-band is full the moment decreases rapidly as the other sub-band is filled.

The hyperfine field in these nickel substituted compounds shows a slight shift to lower values in the composition range for which the transition metal moment is nearly constant. This shift increases with increasing nickel content, but shows some sign of flattening off for $x = 0.4$ i.e. when the transition metal moment is beginning to collapse. In addition to this constant

transition metal moment there is no change in the gadolinium sublattice, consequently the change in the resonant frequency must arise from a change in the hyperfine field due to the C.E. polarization. This can only occur in these materials through a change in the conduction electron concentration.

Now as we have seen earlier, the $(GdY)Co_2$ observations can best be understood in terms of negative C.E. polarization. This of course is also true of the pure metals iron and cobalt (ref. 4:15). Consequently, any increase in the conduction electron concentration should result in an increase in the absolute value of the hyperfine field.

The observed decrease in the magnitude of the field in the $Gd(CoNi)_2$ compounds must result then, from a decrease in the conduction electron density as nickel is substituted for cobalt into the $GdCo_2$ lattice. Since the hyperfine field for a single unpaired conduction electron is of the order of 10^3Koe, even a small change in electron concentration can have a marked effect on the total field. Such a change is also

observed in the pure metals, as the conduction electron concentration changes from 0.7 per ion (cobalt) to 0.6 per ion (nickel).

The variation in linewidth can again be understood in terms of a statistical distribution of the cobalt and nickel ions among the six nearest transition metal ion neighbours to a cobalt ion. The predicted and observed linewidth values for the resonance are given in Table 4.3 from which it is obvious that the two sets of values are of the same order. This would seem to imply that it is adequate to think of the transition metal - transition metal interactions as a short range interaction.

The Dysprosium Substituted Compounds $(GdDy)Co_2$:

4.4 The substitution of dysprosium for gadolinium results in the rapid disappearance of the cobalt resonance line, the resonance being only observable to approximately 10% dysprosium substitution. The minute variation of the centre of the resonance line precludes the possibility of a change in hyperfine field causing the line disappearance.

It is thought that the very short relaxation times, observed in Section 3 compared to the pulse separation during the echo measurements may have led to the spins relaxing before pulse recoherence could occur. Under these conditions, of course, no echo would be observed.

If, as the previous results suggest, the contribution to the hyperfine field due to the conduction electron polarization by the rare earth sublattice is proportional to the average spin of that sublattice, then the dysprosium addition should cause a change in the observed nuclear field. A 10% substitution of dysprosium into the gadolinium sites will then cause the average spin to change from 3.5 to 3.4. This in turn will lead to a net increase in the total hyperfine field at the rate of approximately 20 Koe dysprosium ion. This is in fact about the rate observed during these measurements for extremely small dysprosium content (see inset fig. 3:7), the subsequent decrease of the field strength perhaps arising from slight changes in the cobalt moment with dysprosium addition. The change necessary would need only to be

of order 3% in the transition metal moment. Such a change would not be observed reliably in magnetostatic measurements, but could indeed take place due to the change in the exchange interaction caused by dysprosium substitution.

Relaxation Rates:

4.5 The longtitudinal relaxation time, T_1, for pure $GdCo_2$ was measured at both 4.2^oK and 2.4^oK. From the product T_1T at the two temperatures it can be seen that T_1 at 2.4^oK is slightly larger than would be expected from a relationship $T_1 \alpha 1/T$. Now this law of inverse proportionality is derived by assuming that the only relaxation mechanism for the longtitudinal nuclear moment is the hyperfine coupling between the nuclear and conduction electron spin systems. It is apparent that in the present case a second relaxation mechanism must also be present. This could possibly be spin diffusion as a result of the strong interactions between spins in a ferromagnetic metal.

Relaxation times were measured by both two and

three pulse methods for the substituted compounds at $4.2^{\circ}K$. If the values for T_1 and α for the substituted compounds are compared to the corresponding values for $GdCo_2$ at $4.2^{\circ}K$ it can be seen that yttrium and nickel substitution lead to an increase in T_1 and α while dysprosium leads to a decrease. The increase in α for nickel substitution can be understood by the fact that there is a decrease in the concentration of the resonant nuclei. As transverse relaxation involves spin-spin interactions between these nuclei this will obviously lead to a decrease in the strength of interaction and hence to an increase in "relaxation time" α.

The effect of yttrium and dysprosium on α are opposite although neither of them have any effect on cobalt concentration. They also have opposite effects on the linewidth of the resonance. As $1/\alpha$ depends on the field gradient, the change in resonant field width must lead to the difference in the value of α.

The increase in T_1 is very much greater for nickel substitution than for yttrium substitution. If C.E.

concentration has decreased with nickel substitution as suggested in Section 4:3, then this would lead to an increase in T_1. C.E. concentration does not change with yttrium substitution however. The relatively small change in T_1 in this case is probably due to changes in spin diffusion effects with the decrease of the effective rare earth ionic spin. The decrease in T_1 with dysprosium substitution cannot be easily understood on the above basis however. No change is expected in C.E. and the effective R.E. spin is only slightly lowered. More work must be done on dysprosium substituted compounds to understand why such small concentrations of dysprosium effect the resonance as they do.

oOo

CHAPTER V

C O N C L U S I O N

In Section 3.1.1 we have shown that cobalt has a resonant frequency (ν res.) in $GdCo_2$ of 61.4 MHz, indicating a hyperfine field of 60.8 Koe. A slight decrease in ν res. occurs upon the application of an external field. This frequency decrease is very much less than that given by $dw/dH = -\gamma_{Co}$, as is to be expected for multi-domain particles. The ν res. decrease indicates that the cobalt hyperfine field is negative, i.e. in opposition to the macroscopic magnetization. A negative hyperfine field has also been reported by Wertheim et al. (ref. 3:5 1964) in related RFe_2 compounds.

This cobalt hyperfine field is composed of two main contributions

i) from Core polarization and conduction electron

(C.E.) polarization by the cobalt sublattice along with a much smaller orbital and dipole contribution from this lattice

and ii) from C.E. polarization by the gadolinium sublattice.

The main contributions from cobalt vary directly with the cobalt moment, hence as a good approximation we may say that $H_{Co.\mu} \propto \mu_{Co}$. Therefore, from a knowledge of the cobalt moments in pure cobalt and in $GdCo_2$, and from the fact that the hyperfine field has the same sign in both cases, it can be seen that the cobalt contribution is approximately -135 Koe while the gadolinium contribution is +70.8 Koe.

When yttrium is substituted for gadolinium in $GdCo_2$ there is a decrease in the effective spin of the rare earth sublattice. This leads to a fall in the hyperfine contribution from this sublattice as the C.E. polarization depends on the R.E. spin. From fig. 4:3 it may be seen that the rate of fall is approximately 10 Koe. per unpaired 4f electron, allowing for the

further decrease in $H_{Co.\mu}$ as a result of the drop in the value of the cobalt moment.

The substitution of nickel for cobalt also leads to a decrease in the hyperfine field at cobalt. This decrease takes place when the moments of both the rare earth sublattice and the transition metal sublattice are constant. The constant T.M. moments indicate that nickel-cobalt lattice has an itinerant electron configuration rather than one consisting of localized ionic moments. The decreased hyperfine field must then result from a gradual decrease in conduction electron concentration as nickel substitution increases. A similar change has been noticed in C.E. concentration in going from cobalt to nickel in the pure metals.

The substitution of dysprosium for gadolinium leads to a decrease in R.E. spin once more. This should cause a decrease in the R.E. contribution to the cobalt hyperfine field, but at a slower rate than with yttrium substitution as dysprosium ions do have a spin of their own. The observed changes in $H_{Co.\mu}$ are small and show an initial increase followed

by a decrease in the absolute value on substituting dysprosium.

The dysprosium substituted did not cover a sufficient range to check whether the latter trend would continue. The initial increase is as expected if the R.E. contribution falls while the subsequent decrease may be due to a change in μ_{Co} with Dy substitution.

The linewidths of the resonances were measured on substituting yttrium for gadolinium and were compared with the theoretical expectation for a nearest neighbour only R.E. - T.M. interaction. As these widths were consistently smaller than predicted, we are led to conclude that the interactions have a range of at least a few atomic diameters. If the R.E. atoms interact by means of indirect exchange through the conduction electrons, i.e. by the R.K.K.Y. mechanism, then the range of this interaction is not unexpected.

Linewidth variation was also measured when nickel was substituted for cobalt. The experimental linewidths were compared to theoretical values for a nearest

neighbour T.M. - T.M. interaction and were found to be of the same order. It is therefore concluded that the transition metal - transition metal interaction is of short range.

oOo

APPENDIX I

A1 The Electron-Nuclear Interaction:

In order to determine the interaction between the nucleus and the surrounding electrons, let us consider the effect on an orbiting electron of the magnetic field created by the nucleus.

A dipole of moment μ, situated at the origin, has associated with it a vector potential A at a position r such that

$$A = \nabla \times \mu/r = \frac{\mu \times r}{r^3} \qquad \text{A.1.1}$$

The Hamiltonian for an electron in this vector potential is

$$H_{fs} = \frac{1}{2m}\left(p-\frac{e}{c}A\right) - \frac{e}{mc} S.H \qquad \text{A.1.2}$$

where m = the mass of an electron

e = the charge on an electron

p = the mechanical momentum of the electron under consideration

s = the spin momentum of the electron

and $H = \nabla \times A$, the magnetic field associated with the vector potential A.

Expanding A.1.2, we have

$$H_{fs} = \frac{1}{2m}\left(p^2+\frac{e^2A^2}{c^2} - \frac{e}{c}(p.A+A.p)\right)-\frac{e}{mc} S.H. \quad A.1.2'$$

If we calculate the interaction only to first order in A then we have

$$H_{fs} = -\frac{e}{2mc}(p.A+A.p) - \frac{e}{mc} S.H \quad A.1.3$$

Now the operator $p = -i\nabla$

and it can be shown that $-i(\nabla A+A\nabla)\psi$

$$= -2iA.\nabla\psi - i\nabla.A\psi$$

but $\nabla.A = \nabla.\nabla \times \mu/r = 0$

therefore equation A.1.3 reduces to

$$H_{fs} = -\frac{e}{mc} A.p - \frac{e}{mc} S.H \quad A.1.3'$$

We know that $L = r \times p$, where L = the orbital angular

momentum of the electron, therefore we have from equation A.1.1 above

$$H_{fs} = - \frac{e}{mc} \frac{\mu . L}{r^3} - \frac{e}{mc} S.H \qquad A.1.4$$

Now considering the second term in equation A.1.4

$$H = \nabla x A = \nabla x (\nabla x \mu / r)$$

therefore

$$- \frac{e}{mc} S.H = - \frac{e}{mc} S. \nabla x (\nabla x \mu / r)$$

$$= - \frac{e}{mc} \left[(S. \nabla)(\mu . \nabla) - S.\mu \nabla^2 \right] \left(\frac{1}{r} \right) \qquad A.1.5$$

A.1.5 has a singularity at the origin; considering two cases, $r = 0$ and $r \neq 0$ Messiah (ref. A.1) shows that A.1.5 reduces to

$$- \frac{e}{mc} \frac{3(\mu . r)(S . r) - (\mu . S) r^2}{r^5} \qquad \text{for} \quad r \neq 0$$

and

$$- \frac{e}{mc} \frac{8\pi}{3} S \, \delta (r) \qquad \text{for} \quad r = 0$$

Summing all terms together we have

$$H_{fs} = -2\beta \left[\frac{\mu.L}{r^3} + \frac{3(\mu.r)(S.r) - (\mu.S)r^2}{r^5} + 8\pi/3\ \mu.S\ \delta(r) \right] \qquad A.1.6$$

where $\beta = \frac{e}{2mc}$

for a nucleus of spin I and moment $\mu = \mu_I$

where $\mu_I = g_I\ \mu_n I$ A.1.6 may be rewritten

$$H_{fs} = -g g_I\ \beta\mu_n \left[\frac{8\pi}{3}\ \delta(r) S.I + \frac{(L-S).I}{r^3} + \frac{3(I.r)(S.r)}{r^5} \right] \qquad A.1.6'$$

The first term in A.1.6' is known as the Fermi contact term and is non-zero for S-electrons only, while the last two terms are dipole-dipole interactions. The hyperfine field H_{hf} produced by the electron at the nucleus is then defined by

$$H_{fs} = \mu_I\ H_{hf} \qquad A.1.7$$

If several electrons surround the nucleus, the interaction Hamiltonian is the sum of the contributions of the individual electrons.

It was originally assumed that the inner closed shells of an atom could not contribute to the hyperfine interaction because of the pairing of its electrons. However it was later realized (ref. A.2) that because of the exchange interactions with the open shell electrons, the positive and negative S-electron spin densities at the nucleus were not equal. This "core polarization" led to a contribution to the hyperfine field via the contact interaction.

The orbital (L.I) term is unimportant in the iron series elements as orbital angular momentum is made practically zero by crystal field "quenching". The rare earths, on the other hand, have large orbital contributions as their 4f electrons are shielded by the outer 5s, and 5p electrons from most environmental effects, and are therefore unquenched.

oOo

APPENDIX II

A2 The Spin Echo Effect:

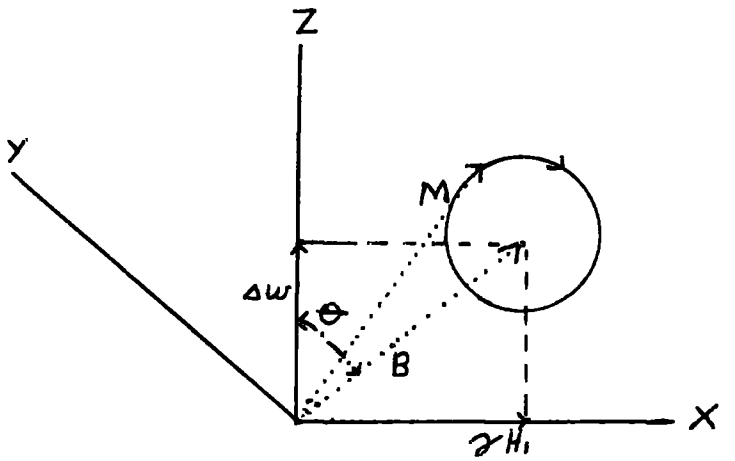

In contrast to the continuous wave techniques of observing nuclear resonance, in which the motion of magnetic nuclei is studied in the presence of an r.f. field, the "Spin Echo" technique studies this motion in the interval or intervals following a sequence of short pulses of r.f. energy.

In the description which follows, the terminology used will be mainly that of Jaynes and Bloom (ref. A.3 and A.4). We shall consider a system of nuclei in a

constant magnetic field H_o which is applied along the Z direction. These nuclei experience an r.f. field of amplitude $2H_1$ which is linearly polarized along the X direction in the laboratory frame.

Let the angular velocity of the r.f. field be w. Then if one transfers the problem to a system rotating about the Z direction with velocity w, the effective field H in the Z direction will now be $\Delta w/\gamma$ where $\Delta w = \gamma H_o - w$

and γ = gyromagnetic ratio of nuclei under investigation.

Jaynes then takes Bloch's equations of motion of the nuclear magnetization

$$\frac{\partial \underline{m}}{\partial t} + \frac{\underline{m} - \chi \underline{H}}{T} + \gamma(H \times m) = 0 \qquad \text{A.2.1}$$

where χ = static nuclear susceptibility and T is the relaxation time. He transforms A.2.1 into matrix form by defining a matrix β such that

$$\beta N = \gamma H \times N$$

A.2.1 then becomes

$$\frac{\partial m}{\partial t} + \left[\frac{1}{T} + \beta(t)\right] m = \frac{\chi H}{T} \qquad \text{A.2.2}$$

The solution to this can be shown to be

$$m(t) = \exp. \left[-\left(\frac{1}{T} + \beta\right)\right] m_o \qquad \text{A.2.3}$$

where m_o is the initial polarization.

The effect of A.2.3 is to produce a rotation of m about the effective field H with exponential damping of the magnitude of m. If the duration of the applied r.f. pulse is sufficiently short that one can ignore relaxation effects during the pulse then the rotation matrix can be defined in terms of the Caylen-Klein (ref. A.5) parameters α and β where

$$\alpha = \text{Cos}\left(\tfrac{1}{2}bt\right) - i \text{ Cos } \theta \text{ sin}\left(\tfrac{1}{2}bt\right)$$

$$\beta = - i \text{ Sin } \theta \text{ Sin}\left(\tfrac{1}{2}bt\right)$$

and

t = duration of pulse

$b = |B| = \left|(\gamma^2 H_1^{\,2} + w^2)\right|^{\frac{1}{2}}$ = resultant field in the rotating system

and

$$\theta = \text{Tan}^{-1} \left(\gamma H_1 / \Delta w\right)$$

Using these parameters the rotation matrix is then

$$R = \begin{bmatrix} \alpha^{*2} & - & \beta^{*2} & - & 2\alpha^{*} & \beta^{*} \\ -\beta^{2} & & \alpha^{2} & - & 2\alpha & \beta \\ \alpha^{*}\beta & & \alpha\beta^{*} & & (\alpha\alpha^{*} - \beta\beta^{*}) & \end{bmatrix} \qquad \text{A.2.4}$$

and $m' = Rm$

between pulses $\alpha = e^{-\frac{1}{2}i\Delta wt}$

$\beta = 0$

Now during the time between pulses relaxation effects cannot be ignored. Hence the rotation matrix R' must be the product of a strict rotation matrix and the relaxation matrix

$$R' = \begin{bmatrix} e^{i\Delta wt - \frac{1}{T_2}} & 0 & 0 \\ 0 & e^{-i\Delta wt - \frac{1}{T_2}} & 0 \\ 0 & 0 & 1 - \frac{1}{T_1} \end{bmatrix} \qquad \text{A.2.5}$$

From this the magnetization m' after the first pulse is $m_1 = R'Rm_o$ where m_o is the initial magnetization, assumed in the Z direction.

In the above we have assumed that Δw is single valued at any particular time and for any particular nucleus. In real samples this is obviously not the case, as any field inhomogeneity within the sample leads to a spread in the value of the resonance frequency and hence in the value of Δw at a given time. Also, as a result of spin-dipolar interactions (Portis 1956, ref. A.6) with characteristic interaction times T_2, nuclei at different positions in the resonance spectrum are able to exchange energy leading to spin diffusion.

This nuclear spin diffusion process leads to a time variation in the resonant frequency of a given nucleus. Hence R' above becomes

$$R' = \begin{bmatrix} e^{i\Delta w(t)}\,e^{-\frac{t}{T_2}} & 0 & 0 \\ 0 & e^{-i\Delta w(t)}\,e^{-\frac{t}{T_2}} & 0 \\ 0 & 0 & 1-\frac{t}{T_1} \end{bmatrix} \qquad \text{A.2.5'}$$

where $\Delta w(t)$ is a function of time.

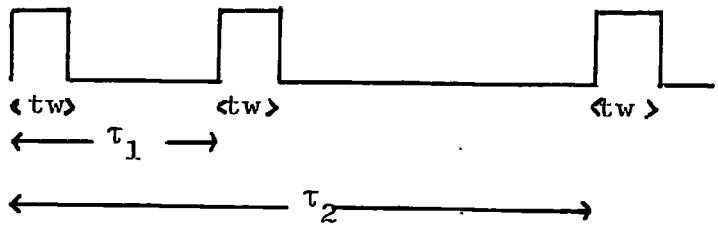

Let us consider a series of three pulses of equal width as indicated above. We can construct a transformation matrix for each of the above time intervals. Let Ri and Ri' be matrices for the i^{th} pulse and the i^{th} interval respectively. Then in order to determine conditions after the application of the third pulse we have

$$m_3 = R_3'R_3R_2'R_2R_1'R_1m_o = R_tm_o \qquad \text{A.2.6}$$

From this we can obtain $m_3(x\text{-}iy)$ which is the observed component of magnetization; that is the matrix element R_t23.

Das and Saha performed this calculation and obtained for the stimulated echo

$$m_3(x-iy) = \frac{\sin^3 btw}{2} \exp\left[-(\tau_2-\tau_1)\left(\frac{1}{T_1}-\frac{1}{T_2}\right)-\frac{t}{T_2}\right]$$

$$x \exp\left[\frac{-t-(\tau_2+\tau_1)}{2T_2^{*2}}\right] \exp\left[-1/3k(t-\tau_2)^3\right.$$

$$\left.-\tau_1^3+3\tau_1(t-\tau_1)^2+3(\tau_2-\tau_1)(t-\tau_2)^2\right] m_o$$

A.2.7

In addition there were three other terms which are of little interest here, and have been neglected.

As can be seen the stimulated echo occurs at time $t = \tau_2+\tau_1$ and decays approximately with time constant $1/T_1$ except for the added diffusion damping term. For the two pulse primary echoes we get

$$m(x-iy) = \sin btw \sin^2\tfrac{1}{2}btw \; x \exp\left[-\frac{t}{\tau_2}-\frac{(t-2\tau_1)^2}{2T_2^{*2}}\right]$$

$$x \exp\left[-\frac{k}{3}(t-\tau_1)^3+\tau_1^3+3\tau_1(t-\tau_1)^2\right] m_o$$

A.2.8

This echo appears at time $t = 2\tau_1$ and is of amplitude proportional to $\exp\left(\frac{-2\tau_1}{T_2}-\frac{5k\tau_1^3}{3}\right)$

Thus it can be seen that the primary echo decays approximately as τ_1^3 in the presence of diffusion processes.

In the above $k = \gamma^2 G^2 D$

where G = Field gradient within the sample, assumed constant.

D = Spin diffusion coefficient.

oOo

-: ACKNOWLEDGEMENTS :-

In looking back over the years which I have spent at Durham, I find that there are many people who have been generous in their help to me. In particular I would like to thank Professor G.D. Rochester, Head of the Department of Physics, for the kind interest he has shown in the progress of my work; Dr. K.N.R. Taylor, my supervisor, for the active help and suggestions he has made in the planning of the research reported above; Dr. P.C. Riedi, * of Southampton University, for the use of his Spin Echo apparatus before my own was built and also for a corroborative search for a gadolinium resonance in the region of both 45 m.c.s. and 80 m.c.s.

In addition I would like to offer my thanks to Mr. M.B. Allenson for many useful hints concerning the construction of the r.f. transmitter and detector; Mr. G.M. Young for the initial aid he gave in the construction of the pulse generator,

*Now at St. Andrews University, Scotland.

Dr. A.R. Piercy for the use of his vibrating sample magnetometer in making the magnetization measurements and to other members of the Rare Earth Research group for all the help they have given me in my stay in Durham.

I would also like to thank the many laboratory technicians and senior technicians who have been of invaluable assistance in the construction of equipment.

Particular thanks must be given to the Association of Commonwealth Universities for financing my course of study at Durham; and to Dr. W.A. Prowse, Master of Van Mildert College, for providing a most congenial atmosphere for life at the college. Last but not least, to my wife Marlene for all the help she has been to me during my studies and for decipering and typing this thesis, my most profound thanks.

-o-

R E F E R E N C E S

1:1 K.A. Gschneider: in "Rare Earth Alloys" published by Van Nostrand. (1961)

1:2 R.J. Elliot: "Theory of Magnetism in Rare Earth Metals" in Magnetism: Vol. IIA edited by Rado and Suhe published by Academic Press 1965.

1:3 A. Stolovy: Phys. Rev. 134, B. 68 (1964) Gd 340 Koe

1:4 R.L. Cohen and J.H. Wernick: Phys. Rev. 134, B 503 (1964) Er 8.4 moe.

1:5 Kalvius et al: Z. Physik, 172, 231 (1963) Tm 7.0 moe.

1:6 S. Ofer, M. Rakavay, E. Segal, B. Khurgin: Phys. Rev. 138, A241 (1965) Dy 6.7 moe.

1:7 J. Itoh, S. Kobayashi, N. Sano: J. Appl. Phys. 39, 1325, 1968 Tb 4.0 moe.

1:8 P.H. Barret and D.A. Shirley: Phys. Rev. 131, 123, (1963) Eu 264 Koe.

1:9 R.E. Gegenwarth, J.I. Budnick, S. Skalski, J.H. Wernick: Phys. Rev. Lett. 18, 9, (1967)

1:10 R.M. Moon, W.C. Kolhler, J. Farrel: J. Appl. Phys. 36, 978, (1965)

1:11 G.K. Wertheim & J.H. Wernick: Phys. Rev. 125, 1937 (1962)

1:12 W.E. Wallace & F.A. Skrabek in "Rare Earth Research" ed. K.S. Vorres, published by Gordon & Breach. New York 1964.

1:13 J. Farrell & W.E. Wallace: Inorg. Chem. 5, 105, (1966)

1:14 A.R. Piercy & K.N.R. Taylor: J. Appl. Phys. 39, 1096 (1968)

1:15 G.J. Bowden, D.St.P. Bunbury, A.P. Guimarães, & R.E. Snyder: Proc. Phys. Soc. (C) Series 2 Vol. 1 p. 1376 (1968)

1:16 E. Fermi: Z. Physik 60, 320 (1930)

1:17 O.V. Lounasmaa: "Nuclear Specific Heats" in "Hyperfine Interactions" edited by A.J. Freeman and R.B. Frankel Academic Press 1967.

1:18 W. Marshall: Phys. Rev. 110, 1280 (1958)

1:19 R.L. Mossbauer: Z. Physik 151, 124 (1958)

1:20 R.V. Pound & G.A. Rebka: Phys. Rev. Lett. 4, 337, 1960.

1:21 A.J.F. Boyle & H.E. Hall: Rep. Prog. Phys. xxv, p. 441, (1962)

1:22 R.L. Mossbauer & M.J. Clauser: "Recoilless Absorption of γ-rays" in "Hyperfine Interactions" edited by Freeman and Frankel Academic Press 1967.

1:23 D. Nagle, H. Fraunfelder, R.D. Taylor, D.R.F. Colhran, B.T. Matthias: Phys. Rev. Lett. 5, 364 (1960)

1:24 L. Grodzins, R. Borchers & G.B. Hagemann: Phys. Lett. 21, 214, (1966)

1:25 I.I. Rabi, S. Millman, P. Kusch, J.R. Zacharias: Phys. Rev. 55, 526, (1939)

1:26 F. Bloch: Phys. Rev. 70, 460 (1946)

1:27 A. Abragam: Principles of Nuclear Magnetism; Oxford University Press (1961)

2:1 E.M. Purcell, H. Torrey and R.V. Pound: Phys. Rev. 69, 37, (1946)

2:2 F. Bloch, W.W. Hansen and M. Packard: Phys. Rev. 69, 680 (1946)

2:3 R.V. Pound & W.D. Knight: Rev. Sci. Inst. 21.219 (1950)

2:4 W.G. Proctor: Phys. Rev. 79, 35 (1950)

2:5 A. Roberts: Rev. Sci. Inst. 18, 845 (1947)

2:6 A. Narath, W.J. O'Sullivan, W.A. Robinson & W.W. Simmons: Rev. Sci. Inst. 35, 476 (1964)

2:7 E.L. Hahn: Phys. Rev. 80, 580, (1950)

2:8 W.G. Clark: Rev. Sci. Inst. 35, 316, (1964)

2:9 W.B. Mims: Rev. Sci. Inst. 36, 1472 (1965)

2:10 R.L. Streever & G.A. Uriano: Phys. Rev. 139, A135 (1965)

2:11 J. Schwarz: Rev. Sci. Inst. 28, 780, (1957)

2:12 T.P. Das & A.K. Saha: Phys. Rev. 93, 749, (1954)

2:13 E.T. Jaynes: Phys. Rev. 98, 1099, (1955)

2:14 A.L. Bloom: Phys. Rev. 98, 1105, (1955)

2:15 A.C. Gossard and A.M. Portis: Phys. Rev. Lett. 3, 164, (1959)

2:16 J. Itoh, K. Asayama, & S. Kobayishi: J. Phys. Soc. Jap. 18, 455, 458 (1963)

2:17 R.C. LaForce: Rev. Sci. Inst. 32, 1387 (1961)

2:18 J.R. Whitehead: "Super-regenerative Receivers" Cambridge University Press. New York 1950.

2:19 D. Grollet: Mullard Technical Communications, p. 238, Vol. 6. No. 56, 1962.

2:20 H.D. Ellis: Ph.D. Thesis Durham University 1967.

2:21 A.R. Piercy: Ph.D. Thesis Durham University 1969.

2:22 J.P. Nelson & D.P. Riley: Proc. Roy. Soc. Lon. 57, 160, 1945.

3:1 M.B. Stearns: Phys. Rev. 162, 496, (1967)

3:2 J.I. Budnick & S. Skalski: in "Hyperfine Interactions" ed. by A.J. Freeman & R.B. Frankel: Acad. Press 1967.

3:3 R.E. Gegenwarth, J.I. Budnick, S.Skalski, & J.H. Wernick: J. Appl. Phys. 37, 1244, (1966)

3:4 A.M. Portis & A.C. Gossard: J. Appl. Phys. 31, 205s, (1960)

3:5 G.K. Wertheim, V.Jaccarino, & J.H. Wernick: Phys. Rev. 135, A151, (1964)

3:6 K.N.R. Taylor, M.I. Darby & H.D. Ellis: Phys. Lett. 20, 327, (1966)

3:7 R. Lemaire: Cobalt 32, 132 (1966).

4:1 See ref. 3.1.

4:2 See ref. 3.2.

4:3 W.B. Mims: Phys. Rev. 141, 499, (1966)

4:4 See ref. 3.4.

4:5 S.S. Hanna, J. Heberle, C. Littlejohn, G.J. Perlow, R.S. Preston, & D.H. Vincent: Phys. Rev. Lett. 4, 177 (1960) and Phys. Rev. Lett. 4, 513, (1960)

4:6 A.C. Gossard, A.M. Portis, M. Rubinstein & R.H. Lindquist: Phys. Rev. 138, A 1415, (1965)

4:7 P.W. Anderson & A.M. Clogston: Bull. Am. Phys. Soc. 2, 124 (1961) also see R.E. Watson, S. Koide, M. Peter & A.J. Freeman in Phys. Rev. 139, A 167 (1965)

4:8 S. Hüfner: Phys. Rev. Lett. 19, 1034 (1967)

4:9 A.R. Piercy & K.N.R. Taylor: J.Phys. Chem. 1, 1112, 1968

4:10 R. Lemaire: Cobalt 32, 132 (1966)

4:11 R.M. Moon, W.C. Koehler, & J. Farrell: J. Appl. Phys. 36, 978 (1965)

4:12 G.K. Wertheim & J.H. Wernick: Phys. Rev. 125, 1937 (1962)

4:13 A.R. Piercy & K.N.R. Taylor: J. Appl. Phys. 39, 1096 (1968)

4:14 N.F. Mott: Advances in Physics 13, 325 (1964)

A:1 Albert Messiah: Quantum Mechanics p. 940. Publishers John Wiley and Sons Inc, 1962.

A:2 R.M. Sternheimer: Phys. Rev. 86, 316 (1952)

A:3 E.T. Jaynes: Phys. Rev. 98, 1099 (1955)

A:4 A.L. Bloom: Phys. Rev. 98, 1105 (1955)

A:5 H. Goldstein: Classical Mechanics Addison-Wesley publishers 1959

A:6 A.M. Portis: Phys. Rev. 104, 584 (1956)

-o-